SUBMITTED TO APJS
Preprint typeset using LaTeX style emulateapj v. 08/22/09

arXiv:1403.7186v1 [astro-ph.GA] 27 Mar 2014

THE BLANCO COSMOLOGY SURVEY: AN OPTICALLY-SELECTED GALAXY CLUSTER CATALOG AND A PUBLIC RELEASE OF OPTICAL DATA PRODUCTS

L. E. BLEEM,[1,2] B. STALDER,[3] M. BRODWIN,[4] M. T. BUSHA,[5,6] M. D. GLADDERS,[2,7] F. W. HIGH, A. REST,[8] R. H. WECHSLER,[5,9,6]

Submitted to ApJS

ABSTRACT

The Blanco Cosmology Survey is 4-band (*griz*) optical-imaging survey that covers $\sim$80 deg^2 of the southern sky. The survey consists of two fields roughly centered at (RA,DEC) = (23h,-55d) and (5h30m,-53d) with imaging designed to reach depths sufficient for the detection of $L_\star$ galaxies out to a redshift of one. In this paper we describe the reduction of the survey data, the creation of calibrated source catalogs and a new method for the separation of stars and galaxies. We search these catalogs for galaxy clusters at $z \leq$0.75 by identifying spatial over-densities of red-sequence galaxies. We report the coordinates, redshift, and optical richness, λ, for 764 detected galaxy clusters at z $\leq$ 0.75. This sample, $>$85% of which are new discoveries, has a median redshift of 0.52 and median richness $\lambda(0.4L_\star)$ of 16.4. Accompanying this paper we also release data products including the reduced images and calibrated source catalogs. These products are available at `http://data.rcc.uchicago.edu/dataset/blanco-cosmology-survey`.

Subject headings: galaxies: clusters: general—surveys—techniques: photometric

1. INTRODUCTION

Multi-band optical surveys provide powerful data sets with which to study cosmology. Technological improvements in CCD imagers over the past two decades have led to a rapid increase in the number of such surveys. Notable examples include the large-area Sloan Digital Sky Survey (SDSS York et al. 2000) and deeper, moderate-area surveys including the Red Sequence Cluster Survey (Gladders & Yee 2005), the Canada-France-Hawaii Telescope Legacy Survey[1], and the NOAO Deep Wide-Field Survey (Jannuzi & Dey 1999). A new generation of both large ($\gtrsim$ 1000 deg^2) and deep surveys including the Panoramic Survey Telescope & Rapid Response System (Kaiser et al. 2010), RCS2 (Gilbank et al. 2011), the Dark Energy Survey[2] and the Subaru Hyper Suprime-Cam project (Takada 2010) highlight further advances in the field.

Such surveys are particularly useful for constraining cosmology with galaxy clusters as large areas are required to obtain statistically useful numbers of these rare, massive objects. The selection of galaxy clusters from optical surveys has a rich history beginning with Abell's visual identification of over-densities of galaxies in the Palomar Sky Survey (Abell 1958) and continuing with modern techniques that identify concentrations of the red, passively-evolving E/S0 galaxies that form the red-sequence in clusters (e.g., Gladders & Yee 2000; Koester et al. 2007a; Hao et al. 2010; see Allen et al. (2011) for a recent review).

The critical challenge for cosmology with clusters is connecting observable cluster properties to the mass of the system. While optical selection does provide a mass proxy — usually in the form of a "richness" parameter related to the number of galaxies in the cluster — complimentary mm-wave or X-ray data sets can greatly improve cluster mass-calibration and provide a cross-check by testing the self-consistency of the respective observable-to-mass scaling relations (Rozo et al. 2012). Indeed, joint optical and mm-wave analyses of the maxBCG cluster sample (Koester et al. 2007a) with data from the *Planck* satellite (Planck Collaboration et al. 2011) and the Atacama Cosmology Telescope (ACT Sehgal et al. 2012) have already revealed tensions between the mm-wave mass and optical richness-mass scaling relations.

The Blanco Cosmology Survey (BCS Desai et al. 2012), an $\sim$80 deg^2 multi-band optical survey, while of moderate depth, is particularly interesting owing to the wealth of multi-wavelength data in the survey region. In addition to being contained within the footprint of both the South Pole Telescope (SPT Carlstrom et al. 2011) and ACT mm-wave surveys, one of the two BCS fields contains the XMM-BCS survey (Šuhada et al. 2012), a subset of a new *XMM* survey, the XXL[3], and is itself contained within the 100 deg^2 SPT Deep Field which features near-infrared imaging from *Spitzer* (Ashby et al. 2013) and has been imaged with *Herschel*'s SPIRE camera at 250, 350 and 500 microns (Holder et al. 2013).

In this paper we present calibrated optical source catalogs from the BCS. We identify galaxy clusters in these data using a cluster-detection technique based upon the methodology of Gladders & Yee (2000), which uses a matched filter in position, color and magnitude space to identify spatial over-densities of red-sequence galaxies. The paper is organized as follows: in §2, we provide a brief overview of the BCS and describe our image reduction pipeline and photometric cali-

[1] Argonne National Laboratory, 9700 S. Cass Avenue, Argonne, IL, USA 60439
[2] Kavli Institute for Cosmological Physics, University of Chicago, 5640 South Ellis Avenue, Chicago, IL, USA 60637
[3] Harvard-Smithsonian Center for Astrophysics, 60 Garden Street, Cambridge, MA, USA 02138
[4] Department of Physics and Astronomy, University of Missouri, 5110 Rockhill Road, Kansas City, MO 64110
[5] Kavli Institute for Particle Astrophysics and Cosmology 452 Lomita Mall, Stanford University, Stanford, CA, 94305
[6] SLAC National Accelerator Laboratory, 2575 Sand Hill Rd., MS 29, Menlo Park, CA, 94025
[7] Department of Astronomy and Astrophysics, University of Chicago, 5640 South Ellis Avenue, Chicago, IL, USA 60637
[8] Space Telescope Science Institute, 3700 San Martin Dr., Baltimore, MD 21218
[9] Department of Physics, Stanford University, Stanford, CA, 94305
[1] http://www.cfht.hawaii.edu/Science/CFHLS/
[2] www.darkenergysurvey.org
[3] http://irfu.cea.fr/xxl/

bration. We describe the galaxy cluster detection algorithm in §3, and measurement of cluster properties in §4. In §5 we discuss tests of our algorithm on simulated catalogs and in §6 compare our results to previous cluster catalogs that overlap the BCS region. Finally, we conclude in §7. Where applicable we assume a flat ΛCDM cosmology with $\Omega_M = 0.27$ and $h = 0.71$. Unless otherwise specified, all masses are reported in terms of M_{200}, where M_{200} is defined as the mass contained within a radius r_{200} at which the average density is 200 times the critical density, and all magnitudes are reported in the AB system.

2. DATA OVERVIEW AND REDUCTION

In this section we provide a brief overview of the Blanco Cosmology Survey and describe our production of calibrated source catalogs from the publicly available imaging data. For a more detailed description of the survey goals and observational strategy readers are referred to previous publications (Menanteau et al. 2009, 2010; Desai et al. 2012).

2.1. *Survey Overview*

The BCS, an NOAO large survey program (2005B-0043), is a 4-band (*griz*) optical-imaging survey that covers ∼80 deg^2 of the southern sky. The survey was designed to reach depths sufficient to detect $L_\star$ galaxies out to a redshift of $z = 1$ (Desai et al. 2012). The survey consists of two fields roughly centered at (RA,DEC) = (23h,-55d) and (5h30m,-53d), and the field locations were coordinated to overlap with the initial mm-wave survey fields of the South Pole Telescope and Atacama Cosmology Telescope.

The data presented here were acquired during 57 nights split over 6 observing runs between November 2005 and November 2008 using the MOSAIC II imager[4] on the 4-m Blanco Telescope at Cerro Tololo Inter-American Observatory, Chile. The MOSAIC II camera is composed of 8 2k × 4k SITe CCDs with a plate scale of 0.27″ per pixel, resulting in a 36′ × 36′ field of view. The camera was operated in 16 channel mode (in which each CCD is read out with 2 amplifiers) throughout the survey.

The two large survey fields were observed in small tiles roughly the size of the MOSAIC II field of view. Here we present reductions of 133 tiles for the 5 h field and 100 tiles for the 23 h field covering ∼ 45 deg^{2}and ∼ 33 deg^2, respectively.[5]. The footprint of the reduced tiles is shown in Figure 1. Each individual tile nominally consists of 2 × 125 s, 2 × 300 s, 3 × 450 s and 3 × 235 s exposures in the *g-,r-,i-* and *z*-bands respectively, though the actual number of exposures can vary owing to variable observing conditions over the course of the survey. Exposures are offset several arc minutes to cover chip gaps and to provide overlap between neighboring tiles.

2.2. *Data Reduction*

The imaging data is reduced with the PHOTPIPE pipeline. This pipeline, initially developed for the SuperMACHO and ESSENCE projects is described in detail in Rest et al. (2005) and Miknaitis et al. (2007). For all images the reduction process includes masking of bad and saturated pixels, crosstalk correction, overscan correction, debiasing, flat fielding, and illumination corrections. The *i*- and *z*-band images are also corrected for fringing. Illumination corrections are determined on a nightly basis by combining all science exposures from a given filter into a master flat. Corrections are applied from nearby nights for nights with insufficient exposures (we find a minimum of 11 images without bright stars is necessary to a create good master flat). Fringe patterns on images from the MOSAIC II camera are quite stable and we obtain good results defringing the *i*- and *z*-band images using fringe frames constructed from all science exposures obtained in the respective filter during an observing run.

Following this processing an initial source finding run is performed using `SExtractor` (Bertin & Arnouts 1996). Astrometric calibration is then tied to the Two Micron All Sky Survey (2MASS) catalog (Skrutskie et al. 2006). The astrometric solution shows residuals of ∼200 milliarcseconds (mas), see Figure 2. This is roughly the same size as the positional uncertainty of the typical 16.3 (Vega) *J*-band 2MASS sources that are associated with the BCS sources.

Next, in preparation for coadding the images, the relative zeropoints of all images for each filter for a given tile are determined using high significance objects from the initial source finding run. The individual images are then reprojected to a common center per tile with a pixel scale of 0.3″ per pixel and coadded using `SWarp` (Bertin et al. 2002). Inverse noise-variance maps used as weight maps during final source detection are also generated at this stage. The distribution of seeing —computed as the average full width at half maximum of the seeing disk in the single epoch images that compose the coadd— for each of the BCS tiles as well as the 5 σ point source depths for the coadded images are shown in Figure 3.

After coaddition, the tiles are visually inspected and areas with significant artifacts (predominately corresponding to halos around the very brightest stars or noisy amplifiers) are identified and weight maps in these areas are set to zero. As the centers of tiles in the different filters are sometimes slightly offset, the coadded images are then slightly trimmed to 36′ × 36′ to help ensure sky coverage in all 4 filters. For ~ 1 deg^2 of survey data (distributed over many tiles) we have excluded *g*-band data owing to excess noise on the CCDs. Finally, as discussed below, we create flag images for use in the source extraction step based on the weight maps, flagging regions with weight less than 10% of the maximum weight.

2.3. *Source Catalog Creation*

Source catalogs are created by running `SExtractor` 2.8.6 in dual image mode using the *i*-band images for detection and extracting *griz* MAG_AUTO and 4″ aperture magnitudes at the locations of detected sources. Detection settings are provided in Table 1.

Following the creation of the source catalog we perform additional steps before photometric calibration. First, we identify regions of roughly uniform coverage in each coadd. As described above, the BCS tiles are nominally composed of 2 or 3 exposures in each filter, with offsets of several arc minutes between exposures. As we are processing the survey on a tile-by-tile basis (as opposed to coadding all images of a given filter into a single monolithic block for each survey field) this naturally leads to shallower regions at the edges of the tiles. Based on the source location in the tile we designate each source as coming from the central (i.e. roughly uniform coverage) or edge region of the tile.

We next apply a correction to the magnitude uncertainties as we find that the default SExtractor uncertainties underestimate the scatter in the data. We estimate a correction factor

[4] http://www.ctio.noao.edu/mosaic/

[5] We have adopted the original field names in the NOAO archive for our tile naming scheme and note that our names can differ from Desai et al. (2012) for the same region of sky.

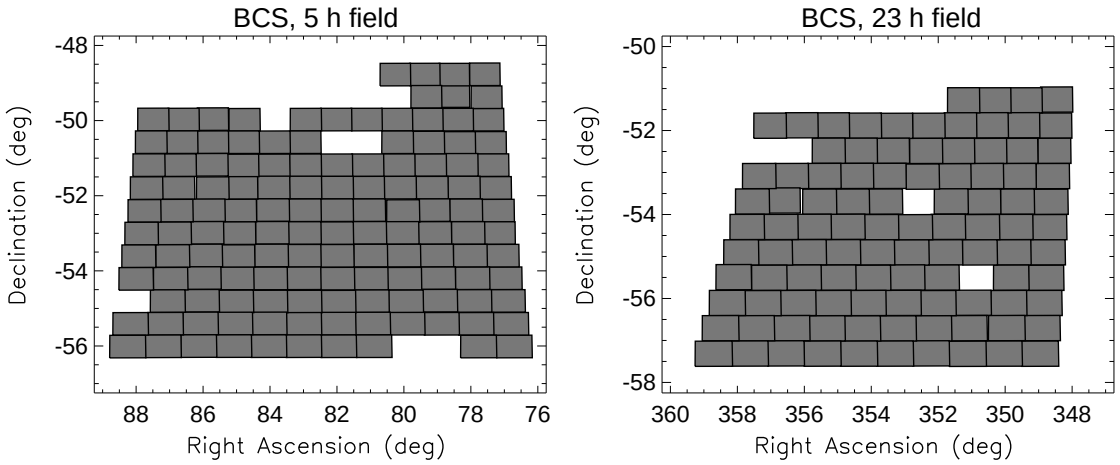

FIG. 1.— Spatial footprint of the imaging data presented in this work. Coadded images and inverse-noise weight maps for each tile are available in the *g*-,*r*-,*i*- and *z*-bands.

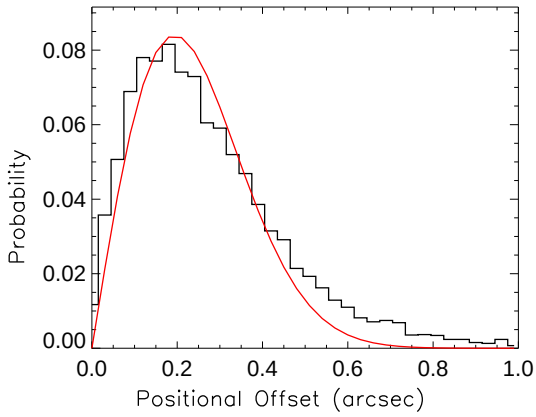

FIG. 2.— Astrometric residuals of BCS sources associated with 2MASS sources. Plotted are the residuals of sources with $16 < J < 16.5$ (Vega) and J-band uncertainty ≤ 0.25. Overplotted is the best fit Gaussian model with 194 mas positional uncertainty. We restrict the magnitude range of the 2MASS data plotted for clarity as the positional scatter is a strong function of magnitude (signal-to-noise) at the faint end of the 2MASS catalog.

TABLE 1
SEXTRACTOR SOURCE DETECTION SETTINGS

DETECT_TYPE	CCD
DETECT_MINAREA	$1.1\pi\times$ (i-band seeing)^2
THRESH_TYPE	RELATIVE
DETECT_THRESH	1.2
ANALYSIS_THRESH	1.2
FILTER	Y
FILTER_NAME	default.conv
DEBLEND_NTHRESH	32
DEBLEND_MINCONT	0.005
BACKPHOTO_TYPE	LOCAL

NOTE. — SExtractor settings used in the extraction of source catalogs. SExtractor was run in dual image mode with the i-band images set as the detection images. The i-band seeing value refers to the average full width at half maximum of the seeing disk in the single epoch images that compose the coadds.

by measuring the sky noise —the dominant contribution to the flux uncertainty for faint sources— utilizing a modified version of the Monte-Carlo based technique described in Ashby et al. (2009). In brief, we perform photometry on the sky in $4''$ apertures at 1500 random positions in the central region of each coadded image. We then fit a Gaussian function to the resulting flux distribution, excluding the bright tail which is biased by real sources in the image. We compare the measured scatter to the median $4''$ flux uncertainty estimated by SExtractor for sources from this same region. We rescale the error bars by this factor which is typically 1.3 to 1.5 times greater the initial uncertainty estimated by SExtractor. We have verified this correction by comparing the distribution of magnitude differences for objects measured in sequential single epoch imaging with the corrected magnitude uncertainties. Our rescaling factor also agrees with the correction determined in Brown et al. (2007) who found a 40% underestimate in the MAG_AUTO magnitude uncertainties. This method works for sources with signal-to-noise $\gtrsim 2.5$, below which there is again extra scatter not reflected by the rescaled error bars. The 5 σ point source depths plotted in Figure 3 are derived from corrected uncertainties on point sources. We find for the detection band, i-band, these depths correspond to the peaks in number counts distributions.

The last step we perform before photometric calibration is identifying sources that may have biased flux measurements owing to their proximity to bright stars. Such stars are often surrounded by "halo-like" features in the image caused by internal reflections in the camera. We find it necessary to flag regions around stars brighter than 14 (Vega) in J-band. At fainter magnitudes default flagging from the weight maps is sufficient. All stars with J-band magnitude brighter than 7 (Vega) are visually inspected in pseudo-*rgb* color images generated from the *z*-,*i*-,*r*-band coadded images and the affected regions are flagged. Fifty stars in the 23 h field and 101 stars in the 5 h field meet this magnitude cut. For the fainter stars flagged regions were automatically generated in circular apertures around each star. The radii of these apertures were conservatively chosen based on inspection of a subset of stars. For these fainter stars the aperture radii ranged from $2'$ at J=7 (Vega) to $0.25'$ at J=14 (Vega). Sources in these flagged regions are excluded when fitting for the photometric calibration parameters for each tile (described below), but are retained in the released catalogs and marked as having potentially biased photometry.

We calibrate the colors of stars and galaxies using Stellar Locus Regression (SLR High et al. 2009). SLR calibrates

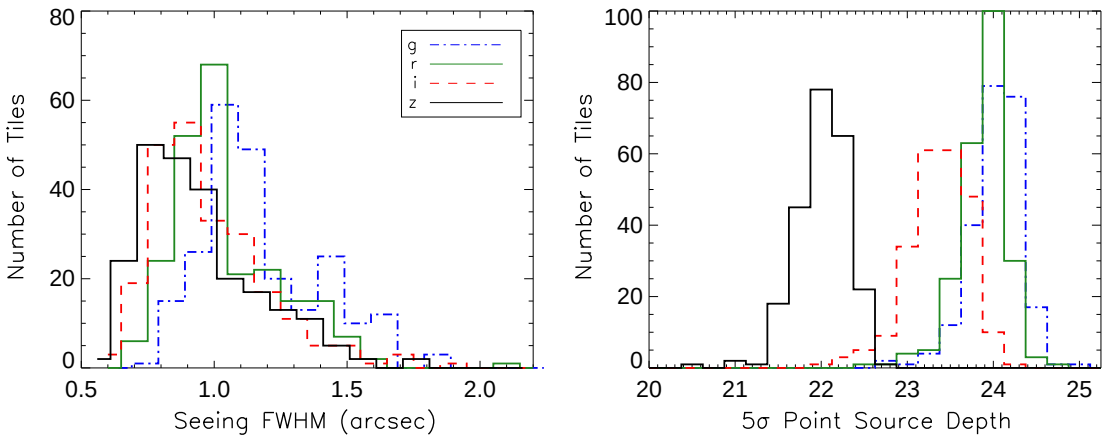

FIG. 3.— Seeing distribution and 5σ corrected MAG_AUTO point source depths for the 233 tiles presented in this work. The plotting scheme is the same in both panels: *g*-band is traced by blue dot-dash, *r*-band is solid green, *i*-band is dashed red and *z*-band is solid black. In the left panel the *g*- and *z*-band distributions are offset slightly to the right and left, respectively, for clarity.

colors by matching the instrumental colors of stars to that of a universal stellar color-color locus as measured by $\sim 10^5$ stars in SDSS (Covey et al. 2007). SLR has previously been used to calibrate the photometry for pointed follow-up of SPT-detected galaxy clusters (e.g., High et al. 2010), an alternate reduction of the BCS (Desai et al. 2012), and similar techniques have been utilized elsewhere in the literature for the photometric calibration of large surveys (Gilbank et al. 2011) and to compliment more standard calibration (Ivezić et al. 2007). As discussed in High et al. (2009), SLR naturally corrects for atmospheric and —as the majority of the stars at BCS survey depths are behind the Galactic dust sheet— Galactic extinction. To determine the necessary calibration terms on a tile-by-tile basis, for each tile we use sources with signal-to-noise greater than 3 in the color combinations of interest, SExtractor CLASS_STAR greater than 0.95 in the *r*- and *i*-bands and require the star to be located in the central region of the coadded images. By using only the central portion of the coadd to determine the photometric calibration, we can use the overlap regions at the edges of the tiles as an independent check of our calibration.

We transform the MOSAIC II magnitudes to the SDSS system using a single set of color terms for all CCDs (Table 2). The color terms were measured by performing a first order fit between MOSAIC II instrumental and SDSS magnitudes in several SDSS-observed star fields. When correcting for extinction and color terms, it is necessary to chose a color multiplier in the transformation from raw to calibrated colors. In general, broad filter combinations (such as *g*-*i*) are beneficial as they provide wide leverage over the range of stellar colors. However, owing to the relatively shallow depth in *g*-band of the BCS catalogs with respect to high-redshift $L_\star$ galaxies (and as these catalogs were constructed for detection of red-sequence cluster galaxies), we chose the color multiplier to always include the *r*-band filter.

The absolute flux scaling is also calibrated using SLR by matching bright stars in the BCS with stars from the 2MASS point source catalog (Skrutskie et al. 2006). Determining robust zeropoints proved to be the most difficult part of the catalog calibration process, so we discuss the process in some detail here. Constraining zeropoints with SLR proceeds analogously to all other color-color calibrations with the stellar locus, only one of the colors is constructed from an instrumental magnitude and 2MASS magnitude. The quality of the

TABLE 2
COLOR TERMS

Filter	Color Term	Color Multiplier
g	-0.1344	*g* - *r*
r	-0.0103	*r* - *i*
i	-0.1148	*r* - *i*
z	0.0028	*r* - *z*

NOTE. — Color terms and color multipliers applied in the calibration of source catalogs from the BCS.

zeropoint fit can be checked by obtaining zeropoints for each of the filters and comparing colors constructed from these absolute magnitudes against colors from the SLR-color calibration. Initial calibration (without flagging generated from the weight maps) revealed large discrepancies between these two sets of calibrated colors. We found that these discrepancies were largest for tiles observed in the best conditions and also noticed that the brighter, bluer stars systematically deviated from the median locus relation — both of these symptoms pointed to saturated stars being included in the zeropoint calibration.

We utilize the SWarp-generated weight maps to identify the non-masked saturated sources (which we note did not exceed the SATURATE keyword in the images' fits headers and so were not masked earlier in the reduction process). The algorithm that creates these weight maps includes a contribution from the Poisson error from bright sources[6], which makes it possible to identify the locations of saturated sources in the map prior to source extraction. We find that flagging objects whose weight is less than 10% of the maximum weight is sufficient to exclude saturated objects. Owing to the long exposures in *i*-band (450 s) a number of tiles had too few non-saturated 2MASS sources in the *i*-band selected catalogs to provide accurate calibration. We instead determine zeropoints for all tiles using the *grz*-band magnitudes of these 2MASS sources. For these bright objects we report only the *grz*-band MAG_AUTO magnitudes and associated colors in the released catalogs.

Zeropoints were calculated using *z*-*J* versus *r*-*z* and *r*-*J* versus *r*-*z*. For many tiles we found *g*-*J* unsuitable as, when the

[6] https://www.astromatic.net/pubsvn/software/swarp/trunk/doc/swarp.pdf

brightest (bluest) objects are saturated, the locus for the remaining fainter objects is essentially vertical and provides little constraining power. Comparison between the *i*-band magnitudes computed using SLR-derived colors and absolute *r*- and *z*-band magnitudes shows good agreement (0.02 magnitude root-mean-square (rms) in the difference). For simplicity, we set the zeropoints of all filters using the *r*-band zeropoint calibration and the SLR-derived colors. In Figure 4 we show an example of the SLR calibration for a typical BCS tile.

2.4. *Photometry Validation*

We perform several tests to check the accuracy of the catalog calibration. First, we compare photometry for objects in the few arc minute overlapping regions between neighboring tiles. As mentioned above, as each tile is calibrated independently and the edge regions are not included in the determination of the calibration solution, we can use these regions to test the quality of our photometric solutions. We note that, as this test is performed on the edges of the image where corrections for flat fielding are generally the poorest, the photometry in the central portion of the tile is potentially better. We report statistics for the median magnitude or color difference of objects in tiles for which this overlap region has $\geq$100 sources with signal-to-noise $\geq$4 in the *r,i,z*-bands (204/233 tiles) or $\geq$75 sources in the *g*-band (188/233 tiles). The results are shown in Figure 5 . We divide the standard deviation measured from these distributions by $\sqrt{2}$ to obtain the uncertainty on the calibration for a single tile. From these tests we measure 2.4% rms variation in *i*-band zeropoints. Checks on the colors show 1.9%, 1.3%, 1.3% rms in the *g-r*, *r-i* and *i-z* calibration, respectively. Investigation of the tile pairs with outlying median-color differences shows that the outliers predominately correspond to tiles with poorer seeing or significantly shallower-than-average data at the tile edges.

As another test, we use the stellar locus to check whether our reported magnitude uncertainties accurately reflect the measurement uncertainty. Using high signal-to-noise stars from the "high-quality" sample described in Covey et al. (2007) we identify low-scatter regions of the stellar locus that are locally linear in various color-color combinations. We then fit for these linear relations. For each tile in the BCS we test the reported uncertainties using these same color combinations. For each color-color pair we use stars where uncertainties in the abscissa color are small but errors in the ordinate color are greater than the locus scatter. This requirement ensures that the measured spread in the distribution around the above-described linear relation is dominated by our measurement uncertainty. To check the *i-z* color uncertainties we use stars with *g-r* $<$1.2, for the *g-r* color we use 0.5 $<$*i-z* $<$0.8 and for *r-z* we use stars with 0.2 $<$*g-i* $<$1.8. This test proved extremely useful —results on preliminary catalogs uncovered a small error in the coaddition process and identified single-epoch images to exclude from the coadds. The final distributions are well behaved, with some excess scatter again observed in filters with poorer seeing (this particularly affects the *g*-band, as this band typically had worse seeing and lower sky noise).

2.5. *Star Galaxy Separation*

As a cross-check of the SExtractor star-galaxy statistic, CLASS_STAR, and to identify the magnitude limit to which this separation is robust, we perform an additional morphological classification of the detected sources. The process to determine this new statistic is simple: we square the *i*-band images, source extract in dual image mode using the original *i*-band image as the detection image and then compute the difference in magnitudes between sources in the original and squared image. Using bright stars identified with CLASS_STAR $\geq$0.98 we fit for and subtract a linear relation between this difference and the calibrated magnitudes. The result of this process is shown in the left panel of Figure 6. As can be seen for bright objects this adjusted difference, Δ, between the "squared" and original magnitudes separates into two populations, with Δ of stars centered around zero.[7] We find the separation between the two populations extends to fainter magnitudes using aperture photometry instead of MAG_AUTO, so we calculate the difference using 3″ aperture magnitudes. As there are few stars brighter than 19.5 *i*-magnitude and CLASS_STAR is robust at this bright end in all tiles, we use the CLASS_STAR statistic for these sources. For sources fainter than 19.5, we fit a double Gaussian model to the sources in sets of 400 ordered by increasing magnitude. The new star-galaxy statistic, *SG*, is defined as:

$$SG = \frac{A_{\rm star}\, e^{\frac{(\Delta-\mu_{\rm star})^2}{2\sigma^2_{\rm star}}}}{A_{\rm star}\, e^{\frac{(\Delta-\mu_{\rm star})^2}{2\sigma^2_{\rm star}}} + A_{\rm galaxy}\, e^{\frac{(\Delta-\mu_{\rm galaxy})^2}{2\sigma^2_{\rm galaxy}}}} \quad (1)$$

where the parameters A, μ, and σ correspond to the amplitude, mean and standard deviation of the Gaussian fits, and —as with CLASS_STAR— a value of 1 corresponds to a high probability of the source being a star. Finally, for the few sources with Δ $<$0 and *SG* $<$0.8 we set *SG* to 2.0 as visual inspection of these objects indicate they are predominately image artifacts.

For each BCS tile, we record this new statistic for each tile up to the magnitude where there is a ratio of 9 stars to each galaxy at the mean of the Gaussian that corresponds to the stellar population. As for any morphological classifier, the magnitude limit to which this classifier is robust is highly seeing and depth dependent. We include this limit as a column in Table 3.

To evaluate the performance of the new star-galaxy statistic we use external optical- and spaced-based imaging from the Extended Groth strip. Using the same SExtractor settings as in the BCS, sources are extracted from deep, "best-seeing" (0.65″ FWHM) *i*-band coadds from the Canada-France-Hawaii Telescope Legacy Survey (Gwyn 2012). Owing to the excellent seeing in these coadds, we compute the *SG* statistic using 1.5″ aperture magnitudes to better demonstrate the power of this statistic as a morphological classifier (while the 3″ aperture-derived statistic proved robust in this test, the limiting magnitude was roughly 0.75 magnitudes shallower as the larger aperture did not fully leverage the available spatial resolution). Using a 1″ association radius, we match this source list with the Advanced Camera for Surveys General Catalog (Griffith et al. 2012) which contains morphological information derived from *HST* imaging. Guided by Gray et al. (2009) (Equation 1), we adopt an *HST*-based morpho-

[7] To motivate this statistic consider the simple case where stars are modeled as 2-dimensional Gaussians. For a Gaussian distribution, the squaring and subsequent differencing procedure described above produces a linear relation between magnitude - magnitude$_{\rm squared_image}$ versus magnitude with a slope of -1. Subtracting off this relation then centers the stellar population around zero. Galaxies, with considerably more extended profiles, form a separate population until noise and limited resolution conspire to wash out morphological information.

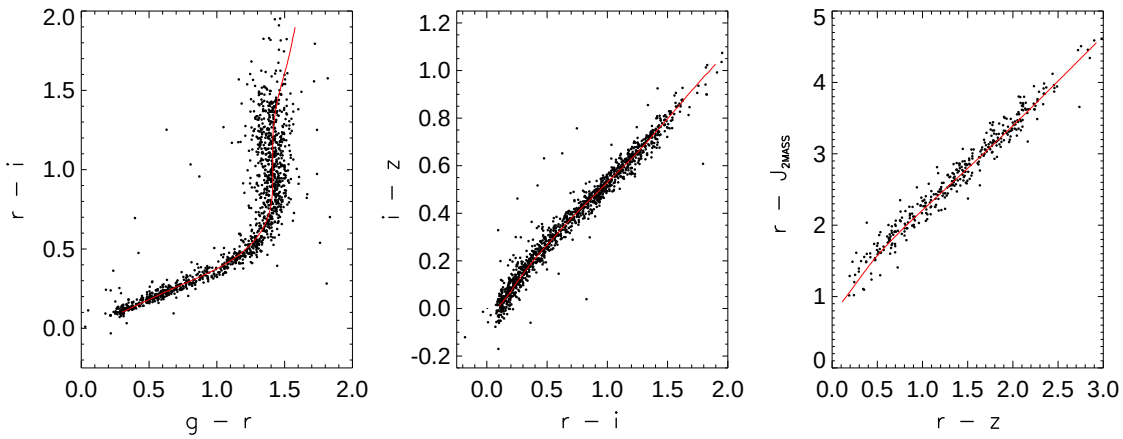

FIG. 4.— Color-color diagram of a subsample of stars with $SG > 0.8$ (see §2.5) and color errors less than 0.25 magnitudes after photometric calibration of BCS tile 0548-5524. Overplotted in red are the median color-color relations of the stellar locus as reported in Covey et al. (2007).

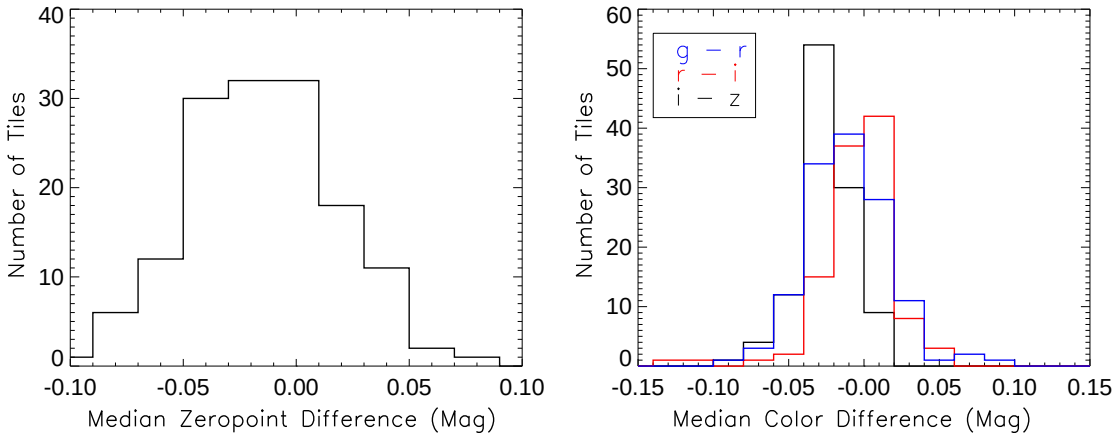

FIG. 5.— Median *i*-band magnitude (*Left*) and *g - r, r - i, i - z* color (*Right*) differences for objects that lie in the overlapping region between neighboring tiles. We report magnitude and color statistics for all tiles with ≥ 100 sources with signal-to-noise ≥ 4 in the *r*-,*i*-,*z*-bands (≥ 75 sources with signal-to-noise ≥ 4 in *g*-band) corresponding to 204 (188) of the 233 survey tiles. We divide the standard deviation measured from these distributions by $\sqrt{2}$ to obtain the uncertainty on the calibration for a single tile. We measure 2.4% rms variation in *i*-band zeropoints and 1.9%, 1.3%, 1.3% rms in the *g-r*, *r-i* and *i-z* calibration, respectively.

logical classification using the SExtractor MAG_BEST and FLUX_RADIUS ($r_{\rm flux}$) parameters derived from the I_{814}-band. We classify as stars sources with i-band < 23 (the *SG*-magnitude limit determined as described above) and

$$\log(r_{\rm flux}) < \max(0.35, 1.50 - 0.05(I_{814} + 1), 8.7 - 0.42I_{814}).$$

The resulting ∼900 sources matching these criterion (out of ∼5,000 total sources brighter than the magnitude cut) are used as the "true" stars in our evaluation of the ground-based morphological classifiers.

We plot comparisons of the CLASS_STAR- and *SG*-classifications to the *HST*-results in the middle and right panels of Figure 6. As demonstrated in these panels, the *SG*-statistic shows significantly fewer galaxies misclassified as stars. In this test, considering only sources brighter than the classification magnitude (*i*-band=23), a catalog generated from $SG < 0.8$ contains 99% of all galaxies and removes 93% of all stars, while a similar catalog from CLASS_STAR < 0.95 includes 94% of all possible galaxies and excludes 95% of all stars.

3. CLUSTER DETECTION

We detect clusters using an algorithm based upon the red-sequence cluster detection algorithm presented in Gladders & Yee (2000, 2005). The algorithm identifies clusters as over-densities of galaxies in position, color and magnitude space. Here we provide a brief overview of the algorithm and note key differences in our implementation as compared to the literature.

Similar to Gladders & Yee (2000, 2005), the algorithm works by assigning each galaxy a weight as a function of redshift where weights are based upon the consistency of the galaxies' magnitudes and colors with a model for the red sequence as a function of redshift. The weighted density of galaxies in a series of redshift slices is computed in $0.25'$ cells and smoothed with a kernel with a core radius of 350 kpc. The galaxies that contribute non-zero weight in each slice are then bootstrap resampled and new density maps are created to estimate the background distribution that is used to map the density values to Gaussian significance. The significance maps at each redshift are then stacked into a 3 dimensional datacube in which peaks greater than a significance threshold of 3.1σ and with at least five galaxies contributing any amount of weight to the detection are identified as clusters (the additional constraint is necessary to reduce spurious detections at

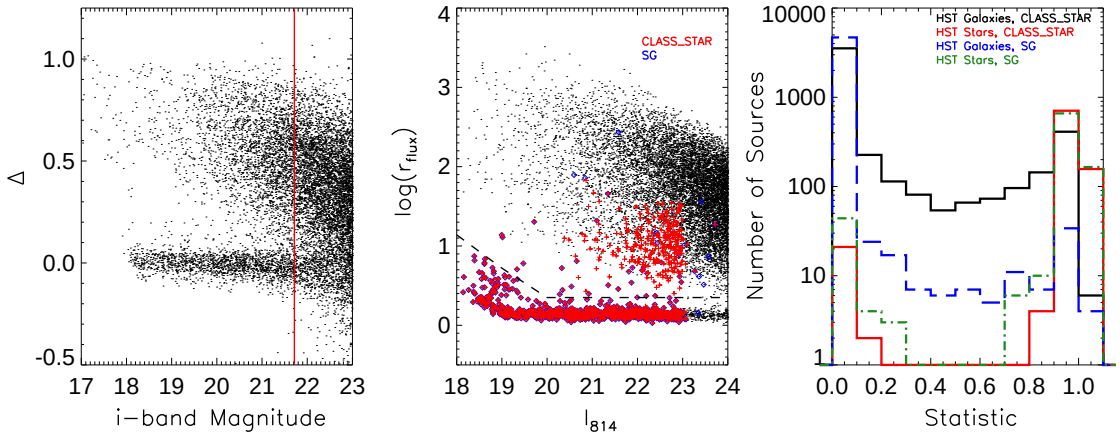

FIG. 6.— (*Left*) Example of the new star-galaxy separation process discussed in §2.5 as applied to BCS tile 0511-5448. Plotted is morphological parameter, Δ, versus magnitude. The stellar population forms a narrow band centered around 0. The solid red line corresponds to the *i*-band magnitude (21.7 for this tile) at which there is a ratio of 9 stars to each galaxy at the center of this band. (*Middle*) Test of the new star-galaxy statistic using *HST*-classified sources in the Extended Groth strip. We classify sources below the black dashed-line in the I_{814}-log(r_{flux}) plane as stars in the HST catalog. Overplotted in red are sources with CLASS_STAR ≥ 0.95 and in blue are sources with $SG \geq 0.8$. The limiting classification magnitude (in *i*-band from the ground-based optical data) is determined as in the previous panel. (*Right*) Distribution of CLASS_STAR and *SG* parameters for *HST*-classified galaxies (solid black and dashed-blue, respectively) and *HST*-classified stars (solid red and dot-dashed green). The last two panels demonstrate that significantly fewer galaxies are erroneously removed from a galaxy catalog generated from a cut on the star-galaxy statistic using *SG* compared to CLASS_STAR.

high-redshift). This threshold, determined using mock catalogs (described in §5), was chosen to limit catalog impurity (including the failure mode of selecting small clumps of large clusters as separate systems) while maximizing completeness.

The largest change in our implementation of the cluster-finding algorithm lies in the procedure for placing the small 0.33 deg^2 tiles into larger blocks for the creation of the background estimates that define the detection significance. As the BCS survey is somewhat heterogeneous (Figure 3) , it is difficult to apply the rigorous image matching technique of Gladders & Yee (2005) and still obtain blocks of sufficiently large area for robust background estimation. Instead, we simplify the problem by restricting our cluster search to lower redshifts and brighter magnitudes where the differences in photometric errors between tiles are reduced. As part of this process we restrict the magnitude weighting applied during the assignment of galaxy weights to magnitudes brighter than $m_\star + 1.5$ in each redshift slice.

To define the regions for the cluster search we begin by excluding tiles with *i*- or *r*-band seeing in excess of 1.6″. In the 5 h field we also exclude 6 tiles (BCS0532-5412, BCS0532-5448, BCS0536-5448, BCS0536-5412, BCS0540-5412 and BCS0540-5524) owing to prominent Galactic cirrus visible in the tiles. We then group the tiles based upon their noise properties in the *r-, i-* and *z*-bands. For each field we produce three different catalogs – a large catalog used in a "low-redshift" cluster search to $z = 0.5$ and two smaller catalogs for a higher redshift cluster search extending to $z = 0.84$ (above our nominal redshift upper limit of 0.75). For each catalog we ensure roughly uniform completeness levels at $m_\star + 1.5$ (*i*-band) at the highest redshift of interest by excluding tiles that have *i*-band 5 σ point source depths less than $m_\star + 1.75$ at this redshift.

The "low-redshift" catalogs for each field are created by merging source catalogs from tiles satisfying the above constraints and the additional requirement that a typical $m_\star + 1.5$ galaxy at z = 0.5 have a *r*-*z* color uncertainty less than 0.16 (80/100 tiles 23 h field, 115/133 tiles in the 5 h field). We run two searches on these catalogs – first using the *g-, r-, i*-band magnitudes we detect clusters between redshifts 0.15 and 0.35. We then extend the search to redshift 0.5 using the *r-, i-, z*-band magnitudes. The two higher redshift catalogs for each field are created by merging the source catalogs of the tiles that have *r*-*z* color uncertainty of a red-sequence $m_\star$ + 1.5 galaxy at z = 0.7 less than 0.33 (32/100 tiles 23 h, 62/133 5 h) and between 0.33 and 0.4 (31/100 tiles and 34/133 tiles in the 23 h and 5 h fields respectively). In Table 3 we flag the tiles searched for clusters.

As the tile boundaries can overlap at the edges, when creating the merged catalogs we check for and remove duplicate sources. We identify the sources for a given tile which have a counterpart within an adjacent tile using a 1″ association radius. When duplicates are found, we use the photometry with the smaller *r-i* color uncertainty in the final merged catalog.

Once the tiles are chosen, we use the new star-galaxy statistic, *SG*, to separate stars and galaxies for sources brighter than *i*=20.5 (corresponding to $m_\star$ at z = 0.55), classifying sources as stars when $SG \geq 0.8$. We choose this conservative magnitude for separation to mitigate spatial variations in source density induced by seeing variations in the stellar-excised source catalogs.

We next identify regions to utilize for background estimation — these regions are slightly more restrictive than the actual area used for the cluster search. Regions for inclusion are identified in a two step process: first, using the weight maps produced by SWarp for each tile during the coaddition process, we mark as 'good' the 0.3″ pixels that have greater than one-third of the median weight, lie inside the nominal central region of the tile, and are not in a region previously flagged during the cataloging process (see Section §2.3). We next rebin these small pixels into the 0.25′ -scale pixels that are used by the cluster detection algorithm and mask the 0.25′ pixels for which less than 75% of the pixel area is marked for inclusion. Density values are drawn from unmasked pixels during the bootstrap resampling step. We include the edge regions of the tiles in the cluster search as they provide a natural taper at the edge of each tile but exclude them from the bootstrapping process as the coverage at the edges of tiles is significantly more variable than in the central regions. As a consequence the detectability of clusters in these edge regions is lessened

owing to both the higher photometric scatter of sources in these regions and as they are less well-matched to the estimated background drawn from the less noisy central regions.

Finally, the red sequence models used in this analysis were created using the GALAXEV routines provided in conjunction with Bruzual & Charlot (2003). The models consist of a passively-evolved single stellar population generated with the Salpeter initial mass function, the Padova 1994 tracks and an instantaneous star burst at redshift z = 3. Metallicites are chosen based upon analytical fits to RCS2 cluster data (Koester, *private communication*). Cubic splines are used to interpolate the discrete output of the code to arbitrary redshifts. Assuming passive evolution, we tie our $m_\star(z)$ model to the analytical function valid $0.05 < z < 0.35$ for the maxBCG cluster sample as reported in equation 11 in Rykoff et al. (2012).

We calibrate three color-magnitude relations as a function of redshift: *g - r* vs. *i*, *r - i* vs. *i* and *r - z* vs. *i* using 47 clusters with spectroscopic redshifts ($0.05 < z < 0.9$) selected from the SPT-SZ survey (Reichardt et al. 2012; Ruel et al. 2013) and processed in a similar fashion to the BCS survey data. For each cluster we first identify an excess of galaxies in color-magnitude space around the SPT position. We compare the colors and magnitudes of these galaxies against our red-sequence model as a function of redshift. To avoid the redshift determination being influenced by outliers or dominated by a few galaxies with small photometric uncertainties we bootstrap resample the galaxies and clip galaxies with colors further than three sigma from the median offset from the red-sequence color-magnitude relation under consideration. For each bootstrap, the estimated redshift is the redshift at which the χ^2 statistic:

$$\chi^2 = \sum_{\rm galaxies} \frac{[Model(magnitude,\ color,\ z) - \mathbf{g}]^2}{color\ error^2 + {\sigma_{\rm rs}}^2}$$

(where **g** encodes the color and magnitude of the galaxies and $\sigma_{\rm rs}$ = 0.05 (Koester et al. 2007b; Mei et al. 2009) is the intrinsic spread of the red sequence) is minimized. We report the redshift as the median redshift of 100 bootstrap resamples.

We find a simple linear fit of model redshifts z_{model} to spectroscopic redshifts, z_{spec},

$$z_{\rm spec} = A z_{\rm model} + B$$

is sufficient for tuning the *g - r vs. i* relation over the redshift range 0.05 to 0.35. However, when extending the redshift range to 0.75 (*r-i vs. i*) and 0.9 (*r-z vs. i*), structure is apparent in the residuals from the linear fits. We instead calibrate these two relations as follows. As we do not, *a priori*, have a model for how to map the raw-model redshifts into the measured spectroscopic redshifts (only the expectation that such a mapping should be smoothly varying and monotonic),we use non-linear least squares minimization to fit the z_{model} and z_{spec} relation to a monotonic function generated using the methodology of Ramsay (1998) where we have chosen sines and cosines as the basis functions and include these functions to the 4th order. In Figure 7 we plot the results of our model calibration.

We estimate the uncertainty in our model calibration by determining the quantity δz such that the reduced chi-squared statistic, $\chi^2_{\rm red}$:

$$\chi^2_{\rm red} = \frac{1}{\nu} \sum \frac{(z_{\rm estimated} - z_{\rm spec})^2}{(\delta z (1+z))^2} = 1$$

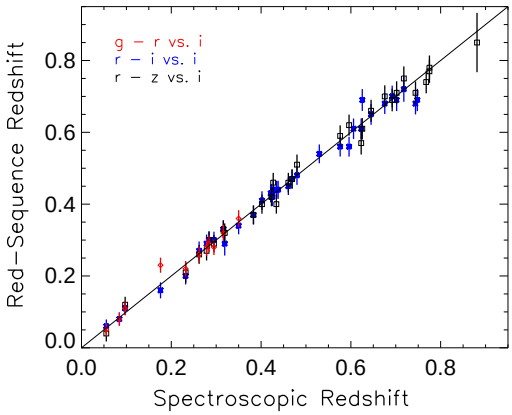

FIG. 7.— Results of red-sequence model training with a sample of spectroscopic clusters from the SPT-SZ survey. Plotted is the estimated versus spectroscopic redshift for *g-r vs. i*-band (red diamonds), *r-i vs. i*-band (blue crosses) and *r-z vs. i*-band (black boxes). The typical scatter, accounting for the degrees of freedom removed by the model fitting, is $\delta_z/(1+z) \sim 0.018$.

where $z_{\rm estimated}$ is our calibrated model redshift and ν is the number of degrees of freedom. Here the total degrees of freedom are reduced by 2 by the linear fit in the *g - r vs. i* calibration and by 10 for the *r -i vs. i* and *r -z vs. i* calibration. We find uncertainties of $\delta_z/(1+z) \sim$ 0.015-0.018 for all of the redshift models.

As an illustration of the cluster-detection process, a redshift slice of the 3d significance data cube from the 23 h field and a pair of identified clusters is shown in Figure 8.

4. CLUSTER CHARACTERIZATION

Following the initial cluster extraction we determine several properties for each cluster: its redshift, brightest cluster galaxy (BCG), and optical richness. For our richness measure we utilize the λ statistic introduced in Rozo et al. (2009) and explored further in Rykoff et al. (2012).

4.1. *Redshift Remeasurement*

We first remeasure the redshift of each cluster. To determine the redshift we select all galaxies that contribute to the cluster detection and then compute the cluster redshift as described in §3. We use the average of *r-i vs i* and *r-z vs i* red-sequence redshifts to determine the redshift for all systems. When this estimated redshift is $\leq$0.35 we further refine the estimate using the *g-r vs i* red-sequence model. The redshift uncertainty is reported as the rms of 100 bootstrap–estimated redshifts added in quadrature with a minimum scatter determined during both our spectroscopic tuning and catalog merging process (see below) of $\delta_z/(1+z) = 0.02$. In general we find good agreement with the initial redshift estimate from the cluster finder itself except at the boundaries of the searched redshift-range, or, for systems selected during of the *g-r vs. i* cluster search, where initial redshifts were misestimated owing to color-redshift degeneracies.

4.2. *BCG Selection*

Following measurement of the cluster redshift, we next determine the BCG of each system. For the BCG we pick the brightest galaxy within a box in color-magnitude plane such that its *i*-band magnitude, *m*, is -3 + $m_\star < m < m_\star$, its *r-z* color is greater than 2.5 σ redward of the red-sequence model and less than 3.5 σ or 0.3 mags (whichever is larger) blueward, and require the galaxy to be located within 350 kpc of

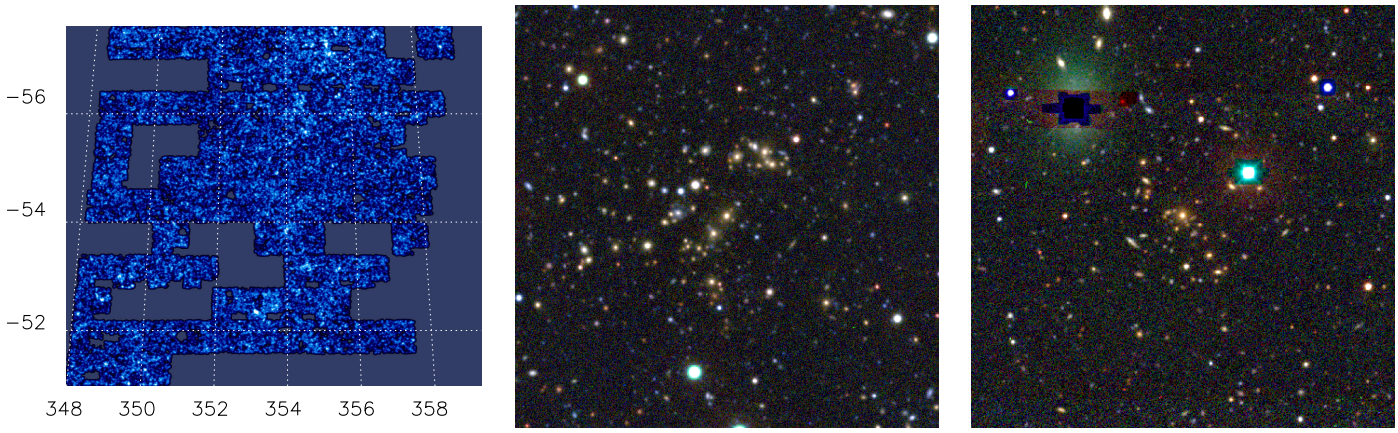

FIG. 8.— *(Left)* Example red-sequence significance map at z=0.47 from the low-z cluster search in the 23 h field. Masked stars and amplifiers create the holes in the map. The color scale ranges from -2.5 to 3.3 σ. *(Middle)* LCS-CLJ231509-5233.6 (SCSO-J231511-523322), a rich cluster from this redshift slice at z=0.47 with richness, $\lambda(0.4L_\star)$, of 27. *(Right)* A more typical cluster, LCS-CLJ233818-5238.1, at z=0.54 and richness $\lambda(0.4L_\star)$=10.5.

the cluster-finder determined location. If no such galaxy exists, we expand the search radius to 450 kpc. If no galaxy is located in this expanded search, we report the cluster location at the cluster-finder determined location and flag the system. Otherwise we report the BCG position as the location of the cluster. After this automated selection we visually inspect all chosen BCGs and manually select an alternative BCG for $\sim$ 30 systems where the BCG was misidentified owing to artifacts, deblending issues in the cluster core or lack of inclusion in the catalog owing the the presence of bright stars.

The search radii was chosen based upon a coarse optimization in simulations as well as visual inspection of the selected centers in image cutouts around the clusters. We chose a fixed radius independent of cluster size as, while 350 kpc is a large fraction of r_{500} for smaller clusters, the searched area is small enough that there are few bright galaxies to misidentify as the BCG. This optimization may be too simplistic and further data is required to test the fidelity of our centering algorithm.

4.3. *Richness*

After BCG selection we determine the optical richness of each cluster. For our richness measure we use λ, a statistic optimized to minimize the scatter in the Mass-richness relation (Rykoff et al. 2012). Much like the red-sequence cluster finder developed in Gladders & Yee (2000), the λ statistic includes spatial, magnitude and color weighting to optimize the contrast of cluster galaxies against the background (Rozo et al. 2009; Rykoff et al. 2012). Simple Monte Carlo tests, as well as tests with mock catalogs, show that for BCS-depths accurate richnesses can be determined out to redshift z=0.75 counting galaxies to 0.4L$_\star$ and to z=0.55 counting to 0.2L$_\star$. As the *i*-band data is significantly deeper than the other bands for red-sequence objects, the relatively larger photometric uncertainties in the *r*-band determine these limits rather than incompleteness in the catalogs.

To compute λ we modify the code provided for the SDSS dataset by Rykoff et al. (2012)[8] to utilize our red-sequence model and measurements of the background source density in color-magnitude space. We estimate two backgrounds for the BCS, one for each field, as the fields are centered at different galactic latitudes (-33 latitude for the 5 h field and -58 latitude for the 23 h field) and our star-galaxy separation does not extend to the faint limits of the BCS catalogs. We report λ using the *r-i* vs. *i* red-sequence relation as this color-magnitude combination has the smallest photometric errors in the BCS. For each cluster, we use the best fit *r-i* vs *i* red-sequence model, but enforce L$_\star$ limits using the best-fit redshifts as determined above.

[8] http://kipac.stanford.edu/maxbcg/lambda_richness.pro

4.4. *Stellar Contamination of the Cluster Catalog*

With the fairly conservative bright star cut of *i*-band = 20.5, the excision of stars from the source catalogs is not complete to the magnitude limit used for the cluster search. While the ratio of stars to galaxies falls at fainter magnitudes, the presence of stars (especially class-M stars which have similar colors and magnitudes as high-redshift cluster galaxies) can add scatter to richness estimates and, because of the steeply rising number density of clusters with decreasing richness, can artificially boost the number of systems above a fixed richness threshold. We explore the effect of stellar contamination using the 90% (96%) of the tiles searched for clusters (high-redshift clusters) for which the star separation was robust to *i*=21.5 (sufficient to excise stars to $m_\star$+1.0 at $z = 0.55$ compared to $z = 0.38$ for the conservative cut). We test for the effect separately in the 23 h and 5 h fields as we expect the effect to be more pronounced in the lower galactic latitude 5 h field.

While some differences in richness may be caused by the removal of actual cluster galaxies with this stricter cut (as this is at the faint limit of the star-galaxy separation), our tests in the Extended Groth Strip show that this leakage should be small. We can empirically test for the removal of cluster galaxies at the fainter magnitudes of the cut using a sample of 11 moderately rich clusters $\lambda(0.4L_{star}) > 20$ at $0.38 < z < 0.43$. At these redshifts the deeper star-galaxy limiting magnitude reaches $0.2L_\star$ at z=0.43 but only $0.4L_\star$ for the shallower cut, so, by comparing the difference in richness measures between $\lambda(0.2L_\star)$ and $\lambda(0.4L_\star)$ for the two cuts we can estimate the fraction of cluster galaxies erroneously removed by the deeper cut. The observed effect is small: from this test we find the mean difference in richness is -0.17 $\pm$ 1 counts or 0.3%.

Comparing the numbers of clusters at $\lambda(0.4L_\star) > 10$ and $0.55 < z < 0.75$ in the 5 h field we find 272 systems in the deeper star-cut catalogs opposed to 282 in the shallow. Similarly in the 23 h field we find 135/138 clusters in the shallower/deeper-cut catalogs. While the fixed magnitude cuts affect a declining fraction of the source population

as the redshift increases, (i.e., with a fixed magnitude limit we can excise stars to a magnitude comparable to an $m_\star + 1$ galaxy at $z = 0.55$ but only to $\sim m_\star$ at $z = 0.75$), this test shows that *on average* the background correction is sufficient. However, to reduce scatter and mitigate the effects of stellar-contamination we estimate λ with deeper stellar-excised catalogs where possible.

After the λ computation, we merge the catalogs from the low- and high-z cluster searches. For every candidate we search for other candidates within the aperture determined by the λ algorithm (see Equation 4 of Rykoff et al. (2012)), and within Δz =0.05 in redshift. For all matched pairs of candidates we robustly estimate the scatter in the redshift differences between the pairs, finding a spread of $\delta_z/(1 + z) = 0.011$ in the difference. As many of the member galaxies are in common, we consider this extra scatter to be added by the cluster-finding process and so add it in quadrature with the model uncertainty determined during the spectroscopic tuning process. This produces a floor in the redshift uncertainty of $\delta_z/(1 + z) = 0.02$[9]. We next match clusters within the richness aperture and 3 σ of the redshift scatter from the matched pairs. As this merger procedure is designed to both merge separate cluster catalogs and to remove sub-clumps of rich clusters from the final catalog, we select the richer of the two systems when duplicates occur. Finally, we make a final visual inspection of the $\sim$20 clusters with potential counterparts within $1'$ but outside the redshift cut. We exclude the few systems which are clearly composed of a small subset of galaxies from a richer lower-redshift system or clearly mismeasured at the boundary redshift of the low-z search.

4.5. *Compensating for Masked Regions*

As a last step, we compensate for the systematic reduction in richness owing to masked regions around the clusters. For every cluster we compute the fraction of area masked around the BCG in 100 kpc-wide rings out to 2 Mpc. Using the galaxy weights provided by the λ-algorithm we then compute an area-corrected richness-per-radial bin for each cluster for both $\lambda(0.4L_\star)$- and $\lambda(0.2L_\star)$-richnesses. Combining the cluster catalog from both fields to improve statistics and excluding the most heavily masked systems, we use clusters between $0.3 < z < 0.75$ (0.55 for $\lambda(0.2L_\star)$) to compute an "average" richness-per-radial bin as a function of richness. This average is derived from hundreds of systems at the low-richness end down to $\sim$10 clusters for the richest systems. Based upon an individual cluster's masking we then compute a correction to its richness. If this richness correction pushes the system into a higher-richness bin, we iterate the correction process until the correction converges. We report the corrected richnesses as well as the value of the richness-correction as entries in the cluster tables.

5. TESTS ON SIMULATED CATALOGS

We characterize the completeness and purity of the cluster-detection algorithm using simulated galaxy catalogs. As we have not incorporated the complex masking required for the BCS into these tests we consider these results to be an idealized scenario.

The mock galaxy sample is drawn from a 220 degree lightcone populated with galaxies in the redshift range $0 < z < 1.3$ down to a flux limit $m_i \sim 25$. The underlying dark matter distribution is based on a cosmological simulation of 1 h^{-1}Gpc; this simulation is a single 'Carmen' simulation from the Large Suite of Dark Matter Simulations project (LASDAMAS McBride et al. 2011)[10]. The lightcone was created by pasting together 34 separate snapshots. The Adding Density Determined GAlaxies to Lightcone Simulations (ADDGALS) algorithm is run to assign galaxies to the dark matter particles in a way that reproduces the known luminosities and two-point function. SEDs are then added using a training set of low-redshift spectroscopic galaxies from SDSS DR5 in such a way as to reproduce the observed magnitude-color-environment relation. These simulated catalogs produce realistic distributions of galaxies and their colors, including a well defined cluster red sequence. Because of these properties, the catalogs have previously been used for tests of cluster finding (Koester et al. 2007b; Hao et al. 2010; Soares-Santos et al. 2011; Rykoff et al. 2013), photometric redshifts (Gerdes et al. 2010), and spectroscopic followup (Cunha et al. 2012). The technique was previously presented in Wechsler (2004); Busha & Wechsler (2008), and a full description of the algorithm and the simulated sky catalogs it produces will be presented in Wechsler et al. (in preparation) and Busha et al. (in preparation).

We degrade the mocks to BCS depths by adding to the model fluxes a random deviate drawn from the normal distribution, N(0,$\sigma_{\rm BCS}$), where $\sigma_{\rm BCS}$ is the typical source flux uncertainty in each optical band: 0.19, 0.21, 0.35, and 1.3 uJy in the *g-,r-,i-,* and *z*-bands respectively:

$$flux = flux_{\rm true} + N(0, \sigma_{\rm BCS}). \quad (2)$$

The fluxes are converted to magnitudes and sources with *i*-band magnitude uncertainty > 0.3 or *r-, z*-band uncertainties > 0.5 are excluded. In this simplified degradation of the mocks, we do not attempt to include the effects of incompleteness beyond these uncertainty constraints.

We tune our synthetic red-sequence model to the simulations in an analogous procedure to that used to connect these models to the real cluster observations. We select 30 halos with redshift, z_{halo}, $0.09 > z_{halo} > 0.9$ and $M_{200} > 3 \times 10^{14} M_\odot$ from the mock catalogs.

As in §2.3 we identify an excess of red-sequence galaxies around these systems and use a monotonic remapping of our synthetic redshift z_{model} to the halo redshifts. Using these red sequence models we run the cluster-finding algorithm on the simulations, where we have split the simulated catalog into ten patches of 22 deg^2 (or roughly the scale of each patch used in the BCS cluster-search).

We make the same cuts on the recovered cluster catalog as were used in constructing the BCS cluster catalogs — namely signal-to-noise > 3.1 and $\lambda(0.4L_\star) > 10$. To check the purity of this catalog we cross-match against the simulation halo catalog. Here we adopt a similar matching criterion to Dong et al. (2008) and consider a cluster to match a halo if the projected distance between the cluster and halo center is less than r_{200} and the redshift difference, Δz, is $< 0.035 \times (1 + z_{halo})$. The results of these checks are shown in Figure 9. We find an accuracy in the recovered redshifts on the simulations to have scatter of $\delta_z/(1 + z) = 0.014$.

We find $> 85\%$ purity for systems with $\lambda > 10$ out to redshift 0.75. Expanding the redshift scaling to $0.05 \times (1 + z_{halo})$

[9] We find similar scatter in the mock catalogs (§5), where the initial tuning with 30 rich systems showed a scatter of $\delta_z/(1 + z) = 0.007$ and the final catalog showed a net scatter of $\delta_z/(1 + z) = 0.014$ around the true redshifts, an extra scatter of $0.012 \times (1+z)$.

[10] http://lss.phy.vanderbilt.edu/lasdamas

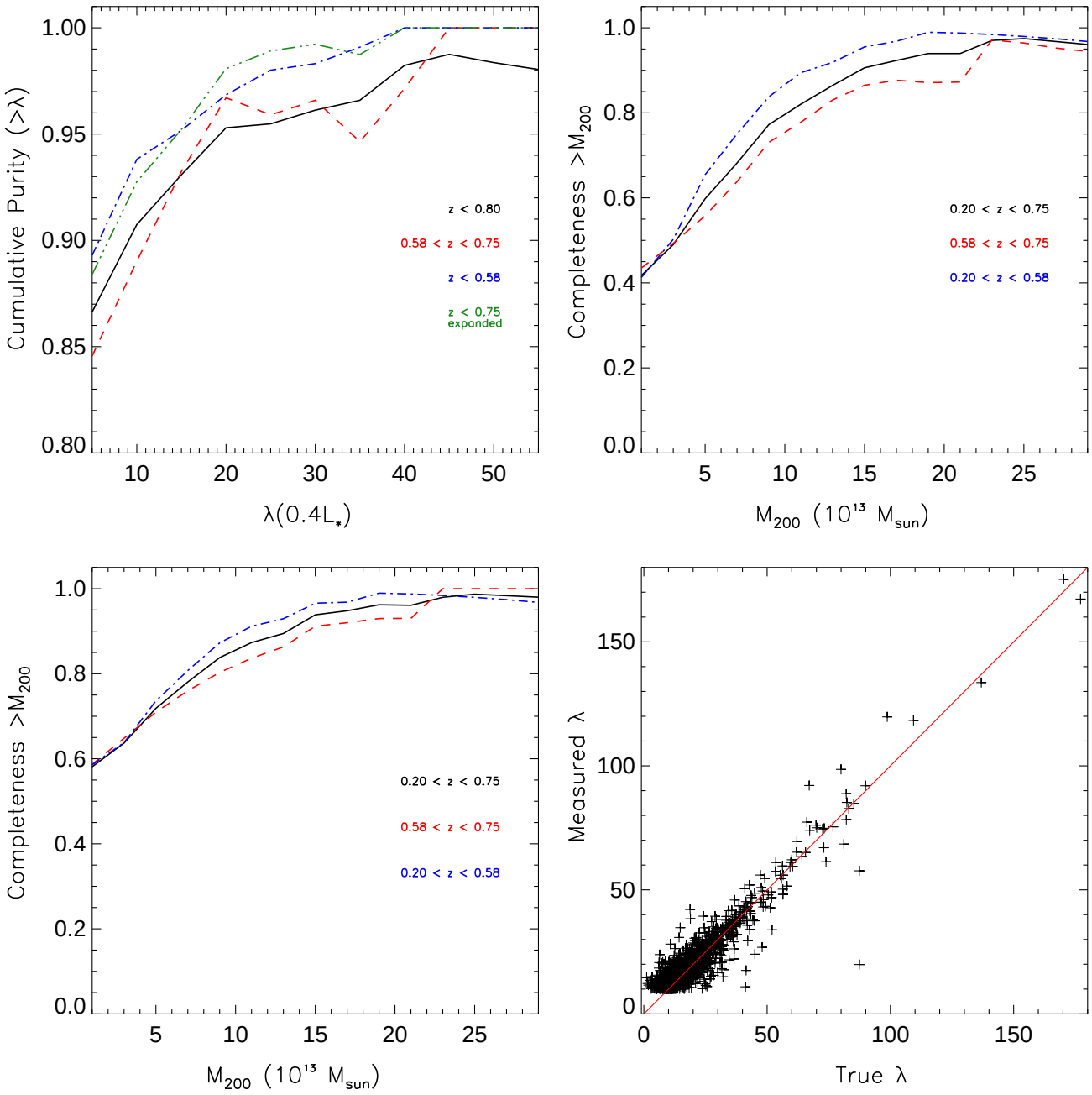

FIG. 9.— Purity and completeness tests of the cluster-detection algorithm on mock catalogs (§5). (*Top Left*) Fraction of systems matched to halos within r_{200} and $\Delta z < 0.035 \times (1 + z_{halo})$ for 3 redshift ranges: $z < 0.8$ (solid-black), $0.58 < z < 0.75$ (dashed-red), $z < 0.58$ (dot-dashed blue) where 0.58 is the median redshift of the extracted cluster catalog. Expanding the redshift matching criterion to $\Delta z < 0.05 \times (1 + z_{halo})$ produces the green dashed-triple dotted line. (*Top Right*) Fraction of halos recovered with > 10 members (both red and blue) where matched clusters are centered within r_{200} of the halo and $\Delta z < 0.035 \times (1 + z_{halo})$. (*Bottom Left*) Identical to top right panel except plotting fraction of recovered halos with $\lambda_{true} > 10$ where λ_{true} is measured to $0.4L_\star$ centered on the halo center and using the true magnitudes for both the lambda measurement and background estimation. (*Bottom Right*) λ_{true} versus measured λ for matched systems at $z < 0.75$ for halos with $M_{200} > 2 \times 10^{13} M_\odot$.

to account for outliers, the purity exceeds 90%. Beyond z=0.75 the purity falls off, primarily due to increasing discrepancies between the model redshift and the simulation red-sequence. As the photometric uncertainties in the BCS preclude accurate richness measurements above z=0.75, we reserve exploration of the cluster-finder at higher redshifts for future work.

Next, considering halos with more than 10 members of any magnitude and color (ie both blue and red members), the catalog is 90% complete above $2\times10^{14}M_{\odot}$. Finally, cutting the halo catalogs at $\lambda_{true} > 10$ (where λ_{true} is measured for all halos to $0.4L_{\star}$ by centering on the halo's central galaxy and using the true galaxy magnitudes and redshifts) the cluster catalogs are 90% complete at $1\times10^{14}M_{\odot}$. Exploring the missing halos above this mass we find 75% of the missing systems exceed our cluster extraction threshold in the cluster-finder datacube. As such, these systems are either falling outside our redshift search, below the richness threshold or being merged with a nearby system.

6. FINAL CATALOG

The final cluster catalog extracted from the BCS consists of 764 clusters (415 and 349 clusters in the 5 and 23 h fields, respectively) at $\lambda \geq 10$ and at z $\leq$ 0.75. The median redshift of the sample is 0.52 and the median richness is 16.4. More than 85% of the sample is newly discovered. We plot the redshift and richness distribution of this catalog in Figure 10. We denote these systems by the acronym "LCS", for Little Cluster Survey, in light of the ongoing Dark Energy Survey[11] which is in the midst of a 5 year survey that will image 5000 deg^2 of the southern sky (including the BCS region). In Tables 5–6 we report the locations, redshifts, and richnesses of the systems as well as previous identifications in the literature.

6.1. *Comparisons to Other Cluster Catalogs*

Here we compare our cluster catalog with other catalogs of galaxy clusters which contain systems within the BCS footprint. In this section we specifically consider systems from the SPT and ACT mm-wave surveys (Vanderlinde et al. 2010; Reichardt et al. 2012; Marriage et al. 2011), the optical Southern Cosmology Survey (SCS) (Menanteau et al. 2009, 2010), and the X-ray XMM-BCS survey (Šuhada et al. 2012). (For a more thorough cross-check in tables 5— 6, we also query the SIMBAD[12] database and check for counterparts within 3′ of each system). The SZ-selected clusters are massive, with SZ-determined masses $M_{500} > 2.8\times10^{14}M_{\odot}$ (Reichardt et al. 2012; Marriage et al. 2011), the SCS-systems are selected based upon their galaxy content to have masses $M_{200} > 3\times10^{14}M_{\odot}$ (with respect to the mean density of the universe) (Menanteau et al. 2010), and –as is typical for a flux-limited X-ray survey– the XMM-BCS systems span a broad range in mass, with a median mass of $M_{500} \approx 1\times10^{14}M_{\odot}$ as derived from the X-ray luminosities (Šuhada et al. 2012).

For this comparison we only consider systems within the redshift range searched for a given BCS tile—e.g., we do not consider a high-redshift system to be "missed" in our search if the cluster-finding algorithm was only run at significantly lower-redshifts. Taking into account possible differences in redshift-estimation accuracy we use cuts of $0.15 < z < 0.55$ for tiles used in the low-redshift cluster search and extend this to $z < 0.9$ for regions included in the higher-redshift search. We consider systems to be a "match" if they are within $|\delta z| < 0.2$ and within the richness algorithm cutoff radius (typically 900 kpc). We adopt the large redshift matching-criterion to avoid missing systems due to differences in estimated redshifts (in particular, for the SCS systems we find discrepancies between our redshifts and the redshifts reported in Menanteau et al. (2010) similar to those reported in Šuhada et al. (2012)). As expanded upon below, the results proceed as expected: we recover all non-masked, massive systems from the SZ-surveys, the majority of the optically-selected clusters from SCS catalog, and a significant fraction of the XMM-BCS catalog with the non-matched systems generally residing at lower masses.

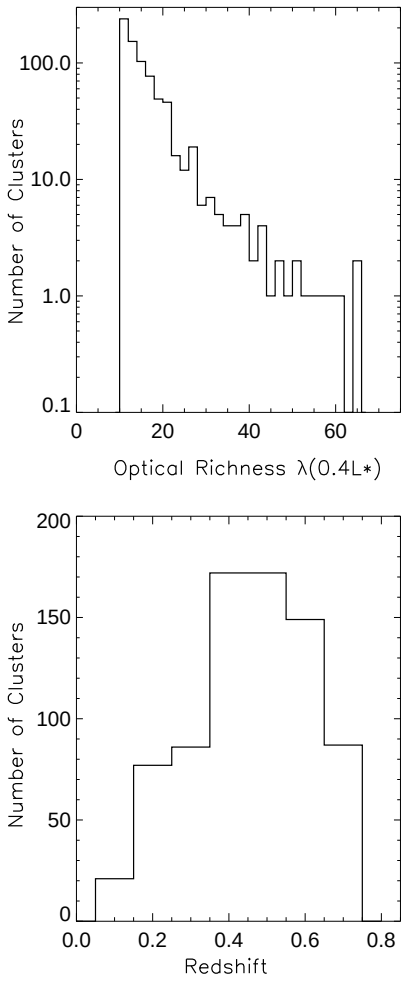

FIG. 10.— *(Top)* Distribution in optical richness, λ, measured to $0.4L_{\star}$ for the 764 clusters at z $\leq$ 0.75. *(Bottom)* Redshift distribution of the entire cluster catalog.

The SCS catalog provides the largest catalog of clusters for comparison — 65 systems lie within the redshift range and footprint searched. Of these 65 clusters, 54 have counterparts in our catalogs. Of the remaining 11 systems, 4 are matched by clusters detected by our cluster-finder but at richnesses below our cutoff threshold, 2 were significantly masked within 1′ around the SCS-BCG by our automated masking procedure, and for 2 clusters both algorithms identified the same cluster but selected significantly separated BCGs. One cluster

[11] www.darkenergysurvey.org
[12] http://simbad.u-strasbg.fr/simbad

was not detected in our search and the two remaining SCS-detected clusters were not found as their redshifts (as measured by our algorithms) lie outside of the range searched. Inverting the question, for tiles the catalogs share in common and using $\lambda(0.4L_\star)$ as the richness metric, we find SCS counterparts for 20/25 (32/50) of the richest systems in these regions.

From the XMM-BCS catalog there are 40 systems in this comparison (we include the "lower-quality" detections in this check). Of these, 23 systems have counterparts in our catalog while an additional 7 were detected by the cluster-finder but have richnesses below the cut-off threshold. For the matched systems we find the redshifts to be on average consistent within the quoted uncertainties. The outstanding 10 non-recovered systems (ID 69,70,81,94,156,355,357,536,540) have estimated masses ranging from $M_{200} \sim 4 - 25 \times 10^{13} M_\odot$. Three of these systems (355, 536, 540) are termed "lower-quality" detections in the X-ray data (Šuhada et al. 2012) and have masses $M_{200} < 10 \times 10^{13} M_\odot$ and five of these systems (94,156,357,430,540) lie on the edges of BCS tiles where coverage is less uniform.

Of the 10 possible mm-wave selected-systems (one of which is also a REFLEX cluster (Böhringer et al. 2004)), 8 have counterparts in our catalogs while the remaining 2 unmatched systems have greater than 50% of the area within $1'$ of the reported center masked owing to the presence of bright stars. Not surprisingly (as some of these systems were used in our red-sequence model training), there is good agreement between our estimated redshifts and the literature redshifts for these systems.

7. SUMMARY AND FUTURE WORK

In this paper we have presented our reductions of optical imaging data from the Blanco Cosmology Survey, including our methodology for creating calibrated source catalogs, for correcting underestimated photometric errors returned by SExtractor, and our implementation of a new, easily-coded morphological star-galaxy separation statistic. Using a red-sequence-based cluster finding algorithm, we have searched the BCS for galaxy clusters. We report the coordinates, redshifts, and optical richnesses for 764 clusters at z $\leq$0.75, of which greater than $>$85% are new detections. This sample has a median redshift of 0.52 and median optical richness, λ, of 16.4. Based upon tests with realistic mock catalogs, the catalog is expected to be $> 85\%$ pure at z < 0.75.

One of the strengths of the Blanco Cosmology Survey is its overlap with other multi-wavelength data. The optical catalogs presented here have been used to confirm cluster candidates and estimate redshifts for SZ-selected clusters in the SPT-SZ survey (Reichardt et al. 2012; Song et al. 2012), as well as to make the first measurement of galaxy bias from the gravitational lensing of the Cosmic Microwave Background (Bleem et al. 2012). As these reductions might be of broader utility, we release the reduced *g*-, *r*-, *i*-, *z*-band images and weight maps as well as the calibrated source catalogs for this $\sim$80 deg^2 survey. These products are available at `http://data.rcc.uchicago.edu/dataset/blanco-cosmology-survey`.

The authors wish to thank Michael Huff for assistance with flagging spurious objects in the source catalogs and Doug Rudd for his assistance setting up the online data access. LB would like to thank Tom Crawford for useful discussions. LB acknowledges support by the U.S. Department of Energy, Basic Energy Sciences, Office of Science, under contract No. DE-AC02-06CH11357, the NSF Physics Frontier Center award PHY-0551142 and the NSF OPP award ANT-0638937. Galaxy cluster research at SAO is supported in part by NSF grants AST-1009649 and MRI-0723073. This research draws upon data provided by NOAO PI 2005B-0043 as distributed by the NOAO Science Archive. NOAO is operated by the Association of Universities for Research in Astronomy (AURA), Inc. under a cooperative agreement with the National Science Foundation. Characterization of the new star-galaxy classifier was based upon both data from both AEGIS (a multi-wavelength sky survey conducted with the Chandra, GALEX, Hubble, Keck, CFHT, MMT, Subaru, Palomar, Spitzer, VLA, and other telescopes and supported in part by the NSF, NASA, and the STFC) and upon observations obtained with MegaPrime/MegaCam, a joint project of CFHT and CEA/DAPNIA, at the Canada-France-Hawaii Telescope (CFHT) which is operated by the National Research Council (NRC) of Canada, the Institut National des Science de l'Univers of the Centre National de la Recherche Scientifique (CNRS) of France, and the University of Hawaii. This work is based in part on data products produced at the Canadian Astronomy Data Centre as part of the Canada-France-Hawaii Telescope Legacy Survey, a collaborative project of NRC and CNRS. Additionally, this research has made use of the SIMBAD database, operated at CDS, Strasbourg, France. Finally, the authors acknowledge the University of Chicago Research Computing Center for hosting the data products presented in this work.

Facilities: Blanco (MOSAIC II)

REFERENCES

Abell, G. O. 1958, ApJS, 3, 211
Abell, G. O., Corwin, Jr., H. G., & Olowin, R. P. 1989, ApJS, 70, 1
Allen, S. W., Evrard, A. E., & Mantz, A. B. 2011, ARA&A, 49, 409
Ashby, M. L. N., et al. 2013, ApJS, 209, 22
——. 2009, ApJ,, 701, 428
Bertin, E., & Arnouts, S. 1996, A&AS, 117, 393
Bertin, E., Mellier, Y., Radovich, M., Missonnier, G., Didelon, P., & Morin, B. 2002, in Astronomical Society of the Pacific Conference Series, Vol. 281, Astronomical Data Analysis Software and Systems XI, ed. D. A. Bohlender, D. Durand, & T. H. Handley, 228–+
Bleem, L. E., et al. 2012, ApJ, 753, L9
Böhringer, H., et al. 2004, A&A, 425, 367
Brown, M. J. I., Dey, A., Jannuzi, B. T., Brand, K., Benson, A. J., Brodwin, M., Croton, D. J., & Eisenhardt, P. R. 2007, ApJ, 654, 858
Bruzual, G., & Charlot, S. 2003, MNRAS, 344, 1000
Buckley-Geer, E. J., et al. 2011, ApJ, 742, 48
Busha, M. T., & Wechsler, R. H. 2008, in 43rd Rencontres de Moriond
Carlstrom, J. E., et al. 2011, PASP, 123, 568
Covey, K. R., et al. 2007, AJ, 134, 2398
Cunha, C. E., Huterer, D., Busha, M. T., & Wechsler, R. H. 2012, MNRAS, 423, 909
Desai, S., et al. 2012, ApJ, 757, 83
Dong, F., Pierpaoli, E., Gunn, J. E., & Wechsler, R. H. 2008, ApJ, 676, 868
Gerdes, D. W., Sypniewski, A. J., McKay, T. A., Hao, J., Weis, M. R., Wechsler, R. H., & Busha, M. T. 2010, The Astrophysical Journal, 715, 823
Gilbank, D. G., Gladders, M. D., Yee, H. K. C., & Hsieh, B. C. 2011, AJ, 141, 94
Gladders, M. D., & Yee, H. K. C. 2000, AJ, 120, 2148
Gladders, M. D., & Yee, H. K. C. 2005, ApJS, 157, 1
Gray, M. E., et al. 2009, MNRAS, 393, 1275
Griffith, R. L., et al. 2012, ApJS, 200, 9

Gwyn, S. D. J. 2012, AJ, 143, 38
Hao, J., et al. 2010, ApJS, 191, 254
High, F. W., et al. 2010, ApJ, 723, 1736
High, F. W., Stubbs, C. W., Rest, A., Stalder, B., & Challis, P. 2009, AJ, 138, 110
Holder, G. P., et al. 2013, ApJ, 771, L16
Ivezić, Ž., et al. 2007, AJ, 134, 973
Jannuzi, B. T., & Dey, A. 1999, in ASP Conf. Ser. 191: Photometric Redshifts and the Detection of High Redshift Galaxies, 111–+
Kaiser, N., et al. 2010, in Society of Photo-Optical Instrumentation Engineers (SPIE) Conference Series, Vol. 7733, Society of Photo-Optical Instrumentation Engineers (SPIE) Conference Series
Koester, B. P., et al. 2007a, ApJ, 660, 239
——. 2007b, ApJ, 660, 221
Marriage, T. A., et al. 2011, ApJ, 737, 61
McBride, C., et al. 2011, in Bulletin of the American Astronomical Society, Vol. 43, American Astronomical Society Meeting Abstracts 217, 249.07
Mei, S., et al. 2009, ApJ, 690, 42
Menanteau, F., et al. 2010, ApJS, 191, 340
——. 2009, ApJ, 698, 1221
Miknaitis, G., et al. 2007, ApJ, 666, 674
Planck Collaboration, et al. 2013, ArXiv e-prints, 1303.5089
——. 2011, A&A, 536, A12
Ramsay, J. O. 1998, Journal of the Royal Statistical Society: Series B (Statistical Methodology), 60, 365
Reichardt, C. L., et al. 2012, ArXiv:1203.5775
Rest, A., et al. 2005, ApJ, 634, 1103
Rozo, E., Bartlett, J. G., Evrard, A. E., & Rykoff, E. S. 2012, ArXiv e-prints, 1204.6305
Rozo, E., et al. 2009, ApJ, 699, 768
Ruel, J., et al. 2013, ArXiv e-prints, 1311.4953
Rykoff, E. S., et al. 2012, ApJ, 746, 178
——. 2013, ArXiv e-prints, 1303.3562
Sehgal, N., et al. 2012, ArXiv e-prints, 1205.2369
Skrutskie, M. F., et al. 2006, AJ, 131, 1163
Soares-Santos, M., et al. 2011, ApJ, 727, 45
Song, J., et al. 2012, ArXiv e-prints, 1207.4369
Takada, M. 2010, in American Institute of Physics Conference Series, Vol. 1279, American Institute of Physics Conference Series, ed. N. Kawai & S. Nagataki, 120–127
Šuhada, R., et al. 2012, A&A, 537, A39
Vanderlinde, K., et al. 2010, ApJ, 722, 1180
Vikhlinin, A., McNamara, B. R., Forman, W., Jones, C., Quintana, H., & Hornstrup, A. 1998, ApJ, 502, 558
Wechsler, R. H. 2004, Clusters of Galaxies: Probes of Cosmological Structure and Galaxy Evolution
York, D. G., et al. 2000, AJ, 120, 1579

APPENDIX

BCS TILE INFORMATION

Summary information for reduced BCS tiles. Images and calibrated catalogs are available at `http://data.rcc.uchicago.edu/dataset/blanco-cosmology-survey`.

TABLE 3
SUMMARY INFORMATION FOR BCS DATA PRESENTED IN THIS WORK.

ID & coordinates:			**Seeing (arcsec)**				**5σ Point Source Depth**				**Star Limit**	**Comments**
BCS ID	RA	DEC	*g*	*r*	*i*	*z*	*g*	*r*	*i*	*z*		
BCS0506-5601	76.708	−56.015	1.33	1.23	1.11	0.99	24.19	23.88	23.35	21.65	21.78	-
BCS0507-5412	76.985	−54.199	0.91	1.01	0.75	0.68	24.35	24.47	23.89	22.34	22.21	L,H
BCS0507-5448	76.897	−54.803	0.95	0.92	0.78	0.76	24.38	24.30	23.80	22.26	22.23	L,H
BCS0507-5524	76.804	−55.411	1.07	1.10	0.90	0.96	24.28	24.24	23.60	22.05	22.24	L,H
BCS0508-5223	77.195	−52.398	1.10	0.93	0.91	0.89	24.17	24.10	23.97	22.37	22.09	L,H
BCS0508-5300	77.174	−52.995	1.12	1.10	0.88	0.79	23.89	24.15	23.78	22.20	22.02	L,H
BCS0508-5336	77.067	−53.597	0.88	0.98	0.91	0.82	24.15	24.19	23.69	22.13	21.98	L,H
BCS0509-4959	77.482	−49.977	1.46	1.49	0.83	0.76	24.27	23.95	23.94	22.32	21.71	L,H
BCS0509-5035	77.414	−50.594	1.07	1.01	1.40	1.27	23.84	23.61	23.03	21.76	21.17	-
BCS0509-5111	77.345	−51.188	0.86	0.75	0.89	0.99	24.24	24.31	23.69	21.98	21.98	L,H
BCS0509-5147	77.274	−51.793	0.96	0.90	0.86	0.82	24.19	24.17	23.97	22.56	22.31	L,H
BCS0510-4846	77.584	−48.769	0.95	0.82	0.76	0.80	24.43	24.41	23.77	22.30	22.30	L,H
BCS0510-4922	77.530	−49.380	1.10	1.02	0.81	0.76	24.66	24.44	23.84	22.21	22.05	L,H
BCS0511-5412	77.947	−54.197	1.49	1.27	0.92	0.94	24.15	24.22	23.88	22.31	22.24	L,H
BCS0511-5448	77.897	−54.802	1.47	1.23	0.96	0.92	24.09	24.07	23.77	22.34	21.72	L,H
BCS0511-5524	77.844	−55.411	1.09	1.00	1.00	0.91	24.21	24.13	23.65	22.11	21.89	L,H
BCS0511-5601	77.768	−56.016	1.04	1.00	1.06	0.90	24.18	24.04	23.38	21.92	21.84	L,H
BCS0512-5147	78.206	−51.783	1.21	1.01	0.70	0.97	24.30	24.43	24.07	22.57	22.00	L,H
BCS0512-5223	78.143	−52.390	1.41	1.07	0.74	0.96	24.45	24.44	24.13	22.62	22.22	L,H
BCS0512-5300	78.081	−52.993	1.44	1.25	0.81	1.13	24.33	24.23	24.00	22.65	22.32	L,H
BCS0512-5336	78.016	−53.596	1.47	1.26	0.82	1.25	24.31	24.24	24.04	22.61	22.24	L,H
BCS0513-4922	78.496	−49.349	0.87	0.80	0.68	0.70	24.36	24.10	23.89	22.32	22.21	L,H
BCS0513-4959	78.390	−49.975	1.54	1.38	0.83	0.84	24.02	24.04	23.92	22.46	22.18	L,H
BCS0513-5035	78.334	−50.595	0.97	0.91	1.10	1.03	24.36	23.90	23.25	21.81	21.53	L
BCS0513-5111	78.264	−51.178	1.28	1.01	0.71	0.78	24.37	24.38	23.88	22.62	22.10	L,H
BCS0514-4846	78.495	−48.778	1.16	1.10	1.12	1.12	23.99	23.92	23.53	22.08	21.35	L,H
BCS0515-5412	78.973	−54.194	1.29	1.12	1.18	1.48	24.09	24.01	23.35	22.01	21.30	L,H
BCS0515-5448	78.919	−54.795	1.21	1.08	1.16	1.09	24.03	24.05	23.47	21.88	21.95	L,H
BCS0515-5524	78.876	−55.409	1.36	1.24	1.14	1.06	24.01	23.69	23.02	21.99	21.58	L
BCS0516-5111	79.208	−51.182	1.41	1.28	0.97	1.12	24.42	24.29	23.63	22.23	22.18	L,H
BCS0516-5147	79.162	−51.787	1.64	1.49	1.18	1.36	24.23	24.07	23.38	21.98	21.58	L,H
BCS0516-5223	79.115	−52.386	1.63	1.49	1.25	1.42	24.06	23.81	23.18	21.95	21.42	L

TABLE 3 — *Continued*

ID & coordinates:			Seeing (arcsec)				5σ Point Source Depth				Star Limit	Comments
BCS ID	RA	DEC	g	r	i	z	g	r	i	z		
BCS0516-5300	79.075	−52.992	1.35	1.15	1.07	1.40	24.07	24.01	23.37	21.95	21.33	L,H
BCS0516-5336	79.025	−53.593	1.22	1.05	1.30	1.38	24.08	23.99	23.25	21.76	21.31	L
BCS0517-4846	79.377	−48.776	1.38	1.27	1.12	1.16	24.05	23.97	23.41	22.07	21.84	L,H
BCS0517-4922	79.329	−49.367	0.86	0.73	0.66	0.68	24.46	24.41	24.00	22.55	22.29	L,H
BCS0517-4959	79.297	−49.975	1.16	1.20	0.84	0.77	24.26	24.17	23.98	22.48	21.88	L,H
BCS0517-5035	79.259	−50.586	0.98	0.94	1.19	1.21	24.03	23.83	23.23	21.83	21.83	L
BCS0519-5412	79.984	−54.210	1.02	1.08	0.85	0.76	24.60	24.23	23.98	22.54	22.23	L,H
BCS0519-5448	79.939	−54.813	0.89	0.93	1.23	1.09	23.61	23.95	23.61	22.81	21.57	L,H
BCS0519-5524	79.902	−55.408	1.44	1.31	1.19	1.30	24.04	23.87	23.81	21.97	22.03	L
BCS0520-4959	80.206	−49.974	1.39	1.24	0.83	0.80	24.14	24.06	23.76	22.44	22.23	L,H
BCS0520-5035	80.187	−50.579	1.01	0.99	0.98	0.90	24.13	24.04	23.43	22.06	21.82	L,H
BCS0520-5111	80.147	−51.189	0.88	1.09	0.82	0.86	24.69	24.47	23.79	22.39	21.87	L,H
BCS0520-5147	80.113	−51.785	0.96	0.81	0.73	0.70	24.32	24.42	24.10	22.58	22.18	L,H
BCS0520-5223	80.023	−52.409	1.16	1.04	0.87	1.02	24.09	23.84	23.47	22.16	21.82	L,H
BCS0520-5300	80.050	−52.990	1.13	1.11	0.95	0.93	24.36	24.04	23.42	22.74	21.94	L,H
BCS0520-5336	80.005	−53.594	1.16	1.05	0.94	0.99	24.16	24.13	23.63	22.28	22.07	L,H
BCS0521-4846	80.255	−48.777	1.46	1.35	1.04	1.04	23.98	23.97	23.49	21.82	21.65	L
BCS0523-5412	80.985	−54.209	1.09	1.06	0.81	0.85	24.55	24.31	23.76	22.28	22.20	L,H
BCS0523-5448	80.962	−54.810	1.08	0.96	0.94	0.94	23.73	23.83	24.26	22.72	21.97	L,H
BCS0523-5524	80.930	−55.404	1.63	1.48	1.12	1.02	24.00	23.79	23.26	21.88	22.06	L
BCS0523-5601	80.897	−56.008	1.00	1.15	1.39	1.32	23.86	23.47	22.61	21.99	21.44	L
BCS0524-4959	81.115	−49.974	1.04	1.03	0.81	0.80	24.26	24.18	23.71	22.24	22.11	L,H
BCS0524-5111	81.079	−51.189	0.89	0.97	0.98	0.88	24.74	24.28	23.69	22.13	22.00	L,H
BCS0524-5147	81.065	−51.786	0.91	0.81	0.76	0.83	24.34	24.39	24.00	22.48	22.30	L,H
BCS0524-5223	81.041	−52.387	1.06	1.26	0.77	0.93	24.47	24.56	23.41	22.06	22.21	L,H
BCS0524-5300	81.017	−52.990	1.02	1.16	0.83	0.92	24.24	24.19	23.58	22.18	22.36	L,H
BCS0524-5336	80.993	−53.593	1.11	1.11	0.90	1.00	24.07	24.14	23.66	22.16	22.10	L,H
BCS0527-5412	81.985	−54.209	1.16	1.04	0.80	0.88	24.54	24.15	23.60	22.37	22.05	L,H
BCS0527-5448	81.958	−54.821	1.21	1.08	1.02	1.04	24.21	24.12	23.58	22.37	22.09	L,H
BCS0527-5524	81.963	−55.406	1.68	1.39	1.06	0.93	24.26	23.95	23.29	22.13	22.15	L,H
BCS0527-5601	81.952	−56.009	1.28	1.14	1.28	1.54	23.93	23.76	23.20	21.76	21.59	-
BCS0528-4959	82.023	−49.974	1.13	1.01	0.93	1.06	24.18	24.02	23.59	22.14	21.99	L,H
BCS0528-5111	82.011	−51.190	1.12	0.91	1.05	0.94	24.43	24.37	23.49	22.21	22.00	L,H
BCS0528-5147	81.993	−51.784	1.00	1.00	0.88	0.85	24.17	24.12	24.00	22.60	22.16	L,H
BCS0528-5223	82.002	−52.387	1.07	1.07	0.80	0.86	24.48	24.30	23.59	22.27	22.27	L,H
BCS0528-5300	82.005	−52.998	1.05	0.91	0.85	0.88	24.24	24.19	23.62	22.41	22.15	L,H
BCS0528-5336	81.997	−53.600	1.00	0.97	0.82	1.04	23.97	24.22	23.91	22.53	22.13	L,H
BCS0531-4959	82.929	−49.976	1.01	0.92	0.90	0.97	24.13	24.12	23.57	22.19	22.06	L,H
BCS0531-5035	82.949	−50.577	0.85	0.79	0.97	0.95	24.38	24.23	23.46	22.23	21.84	L,H
BCS0531-5111	82.943	−51.191	1.16	1.01	1.07	0.93	24.53	24.22	23.66	22.22	21.60	L,H
BCS0531-5147	82.942	−51.782	1.01	0.97	0.91	0.82	24.35	24.28	23.89	22.21	22.10	L,H
BCS0531-5223	82.963	−52.389	1.00	0.98	0.89	1.05	24.21	24.12	23.36	22.28	21.98	L,H
BCS0531-5300	82.971	−52.994	1.03	1.01	0.85	0.99	24.37	24.17	23.56	22.11	22.12	L,H
BCS0531-5336	82.981	−53.598	1.08	0.99	0.86	0.95	24.25	24.06	23.62	22.12	22.46	L,H
BCS0532-5412	82.991	−54.200	1.00	1.04	1.01	0.89	24.41	24.16	23.42	22.24	21.90	Galactic Cirrus
BCS0532-5448	82.975	−54.820	1.08	1.04	1.07	1.02	23.99	23.90	23.26	22.68	21.53	Galactic Cirrus
BCS0532-5524	82.988	−55.411	1.52	1.23	0.83	0.73	24.03	24.12	23.74	22.26	22.17	L,H
BCS0532-5601	82.995	−56.007	1.11	1.02	1.54	1.50	23.82	23.63	22.93	21.73	21.12	-
BCS0535-5035	83.868	−50.578	0.81	0.78	0.92	1.05	24.31	24.25	23.76	22.31	21.75	L,H
BCS0535-5111	83.884	−51.194	1.15	0.87	0.93	0.85	24.51	24.20	24.09	22.31	21.88	L,H
BCS0535-5147	83.891	−51.781	1.10	0.97	0.95	0.85	24.12	24.00	23.67	22.30	21.70	L,H
BCS0535-5223	83.911	−52.384	1.09	1.08	0.93	0.95	23.95	24.07	23.54	22.35	22.02	L,H
BCS0535-5300	83.933	−52.988	1.05	1.02	0.85	0.89	24.10	24.11	23.81	22.59	22.11	L,H
BCS0535-5336	83.956	−53.592	1.14	1.02	0.87	0.93	24.31	24.09	23.73	22.44	22.05	L,H
BCS0536-5412	83.993	−54.203	1.20	1.09	1.05	0.96	24.26	24.09	23.38	22.00	21.98	Galactic Cirrus
BCS0536-5448	83.994	−54.818	1.08	0.99	0.95	0.85	24.05	23.93	23.58	22.55	21.85	Galactic Cirrus
BCS0536-5524	84.026	−55.400	1.48	1.68	0.80	0.74	24.17	23.87	23.59	22.09	22.29	-
BCS0536-5601	84.041	−56.006	1.17	1.07	1.05	1.04	23.88	23.84	23.09	21.72	21.72	-
BCS0539-4959	84.762	−49.979	0.98	0.85	0.92	0.87	24.21	24.07	23.48	21.99	21.71	L,H
BCS0539-5035	84.789	−50.577	0.87	0.80	0.74	0.71	24.31	24.31	23.81	22.47	21.77	L,H
BCS0539-5111	84.814	−51.196	0.95	0.93	0.93	0.83	24.57	24.33	23.96	22.43	22.15	L,H
BCS0539-5147	84.851	−51.793	1.40	0.94	0.87	0.81	24.71	24.50	23.78	22.39	22.16	L,H

TABLE 3 — *Continued*

ID & coordinates:			Seeing (arcsec)				5σ Point Source Depth				Star Limit	Comments
BCS ID	RA	DEC	*g*	*r*	*i*	*z*	*g*	*r*	*i*	*z*		
BCS0539-5223	84.895	−52.395	1.18	0.86	0.88	0.74	24.55	24.25	23.71	22.21	21.96	L,H
BCS0539-5300	84.926	−52.998	1.16	0.84	1.10	0.72	24.36	24.09	23.41	22.48	21.67	L,H
BCS0539-5336	84.960	−53.609	1.12	0.99	0.94	1.04	24.56	24.05	23.73	22.23	21.81	L,H
BCS0540-5412	84.993	−54.203	1.14	0.89	1.08	1.07	24.17	24.08	23.46	22.19	21.73	Galactic Cirrus
BCS0540-5448	85.012	−54.816	1.13	0.91	0.91	0.86	24.27	24.07	23.91	22.30	22.39	L,H
BCS0540-5524	85.046	−55.402	1.49	1.21	0.86	0.94	23.90	23.90	23.54	21.93	21.98	Galactic Cirrus
BCS0540-5601	85.085	−56.005	1.28	1.07	1.15	1.35	23.83	23.68	23.09	21.80	22.11	-
BCS0542-4959	85.706	−49.962	1.02	0.96	0.97	1.00	23.89	23.76	23.17	22.13	21.82	L
BCS0542-5035	85.709	−50.577	0.96	0.90	0.77	0.75	24.38	24.15	23.69	22.27	22.06	L,H
BCS0543-5111	85.731	−51.178	1.09	1.00	1.02	1.19	24.03	23.98	23.65	22.08	21.63	L,H
BCS0543-5147	85.711	−51.800	1.01	0.96	1.02	1.20	24.13	23.59	23.50	22.07	21.75	L
BCS0543-5223	85.833	−52.390	1.57	1.25	1.10	1.10	24.30	23.99	23.22	22.21	22.09	L,H
BCS0543-5300	85.880	−52.989	1.63	1.49	1.00	1.03	24.45	24.17	23.56	22.14	21.95	L,H
BCS0543-5336	85.926	−53.592	1.65	1.43	1.00	1.03	24.26	24.14	23.60	22.15	21.87	L,H
BCS0544-5412	85.974	−54.194	1.49	1.33	0.96	1.11	24.36	24.18	23.69	22.29	22.25	L,H
BCS0544-5448	86.034	−54.798	1.44	1.31	0.94	1.12	24.26	24.08	23.78	22.33	22.14	L,H
BCS0544-5524	86.073	−55.401	1.43	1.23	0.93	1.06	23.85	23.73	23.45	21.89	21.99	-
BCS0544-5601	86.130	−56.004	1.09	0.94	1.38	1.43	23.72	23.70	22.79	21.54	21.07	-
BCS0546-4959	86.581	−49.973	1.02	1.07	0.99	0.88	24.11	24.02	23.76	22.13	21.74	L,H
BCS0546-5035	86.628	−50.576	1.02	1.09	0.75	0.75	24.30	24.18	23.97	22.29	22.23	L,H
BCS0546-5111	86.681	−51.188	1.01	0.96	1.03	0.95	23.94	23.91	23.31	22.07	21.62	L,H
BCS0547-5147	86.734	−51.794	1.17	1.04	0.98	0.97	24.00	24.08	23.48	21.95	22.06	L,H
BCS0547-5223	86.791	−52.398	1.09	1.08	1.03	0.99	24.11	23.97	23.41	21.91	21.78	L
BCS0547-5300	86.848	−53.003	1.13	1.09	1.04	0.96	23.91	23.96	23.32	21.91	22.12	L
BCS0547-5336	86.907	−53.607	1.12	1.00	1.24	0.95	23.82	23.88	23.06	21.89	21.46	L
BCS0548-5412	86.968	−54.210	1.03	0.94	1.12	1.07	23.93	23.90	23.18	22.05	21.82	L,H
BCS0548-5448	87.054	−54.806	1.05	1.00	1.20	1.09	23.81	23.71	23.36	22.05	21.88	L
BCS0548-5524	87.121	−55.408	0.98	0.97	1.40	1.16	23.70	23.78	23.09	22.02	20.19	L
BCS0548-5601	87.191	−56.010	1.06	0.94	0.90	0.96	23.70	23.98	23.46	22.18	21.68	L,H
BCS0550-4959	87.485	−49.970	0.94	0.81	0.90	0.88	24.14	24.33	23.78	22.28	21.78	L,H
BCS0550-5035	87.548	−50.576	1.25	1.07	0.75	0.71	24.07	24.07	23.92	22.40	22.02	L,H
BCS0550-5111	87.615	−51.187	1.14	1.12	1.09	1.05	24.08	23.51	23.14	21.74	21.59	-
BCS0550-5147	87.687	−51.798	1.22	1.03	1.11	0.98	23.94	23.84	23.14	22.08	21.62	L
BCS0551-5223	87.750	−52.405	1.13	1.01	1.11	1.07	24.00	23.87	23.33	22.13	21.96	L,H
BCS0551-5300	87.836	−53.008	1.68	1.37	1.75	1.59	23.56	23.33	22.83	21.59	20.73	-
BCS0551-5336	87.920	−53.612	1.47	1.34	1.30	1.13	23.75	23.56	23.08	21.63	21.66	-
BCS0552-5412	87.999	−54.214	1.34	1.01	1.10	1.23	22.93	22.72	22.58	21.18	21.21	-
BCS0552-5524	88.164	−55.412	1.30	1.11	1.55	1.59	23.51	23.18	23.03	22.17	21.57	L
BCS0553-5601	88.251	−56.017	1.10	1.07	1.54	1.34	23.40	23.31	23.07	22.00	21.86	L
BCS2313-5116	348.463	−51.263	1.10	1.05	0.84	0.81	24.08	24.25	23.62	22.24	21.92	L,H
BCS2314-5152	348.496	−51.884	1.18	1.05	0.87	0.89	24.22	24.14	23.69	22.28	21.85	L,H
BCS2314-5229	348.530	−52.485	1.65	1.48	1.21	1.46	24.35	24.03	23.18	22.11	21.57	L,H
BCS2314-5305	348.578	−53.086	0.96	1.15	0.98	0.89	24.26	24.13	23.71	22.28	21.96	L,H
BCS2314-5341	348.628	−53.699	1.40	1.36	1.05	1.10	23.42	23.32	22.91	21.66	21.91	-
BCS2314-5417	348.673	−54.303	1.22	1.17	1.01	1.04	24.17	23.78	23.65	22.32	21.89	L,H
BCS2315-5453	348.726	−54.903	1.22	1.21	0.92	0.94	23.90	23.83	23.87	22.50	22.10	L,H
BCS2315-5530	348.777	−55.510	1.16	1.18	1.14	1.10	24.73	24.19	23.43	22.31	21.75	L,H
BCS2315-5606	348.840	−56.109	1.16	1.02	1.13	1.03	24.76	24.68	23.39	22.31	21.74	L,H
BCS2315-5642	348.902	−56.707	1.28	1.04	1.10	1.05	24.01	23.05	22.85	21.65	21.41	-
BCS2315-5718	348.960	−57.317	1.15	1.01	0.86	0.73	24.17	24.02	23.65	22.08	21.76	L,H
BCS2317-5116	349.373	−51.282	1.05	1.01	0.91	0.91	24.25	24.16	23.64	22.10	21.95	L,H
BCS2317-5152	349.453	−51.875	1.49	1.38	1.14	1.08	23.94	23.83	23.28	22.05	21.90	L,H
BCS2318-5229	349.516	−52.487	1.48	1.23	1.36	1.45	24.19	23.83	22.13	21.69	20.87	-
BCS2318-5305	349.574	−53.085	1.01	1.43	0.91	0.85	24.26	24.03	23.80	22.41	22.05	L,H
BCS2318-5341	349.632	−53.695	1.44	1.52	1.32	1.29	23.46	23.13	22.83	21.64	21.74	-
BCS2318-5417	349.683	−54.299	1.05	1.06	1.50	1.47	24.27	23.83	23.12	21.84	21.68	L
BCS2319-5453	349.750	−54.903	1.17	1.16	1.75	1.51	24.09	23.80	22.95	21.82	20.74	-
BCS2319-5530	349.819	−55.506	1.20	1.18	1.96	1.88	23.55	23.63	22.94	21.59	20.58	-
BCS2319-5606	349.892	−56.110	1.14	1.20	1.25	1.16	23.96	23.98	23.22	22.05	21.25	L,H
BCS2319-5642	349.951	−56.706	0.99	0.92	0.92	0.95	23.73	23.97	23.44	21.83	21.71	-
BCS2320-5718	350.046	−57.315	0.89	0.87	0.79	0.72	24.32	24.25	23.94	22.54	21.86	L,H
BCS2321-5116	350.306	−51.282	1.27	1.19	1.30	1.23	23.92	23.76	23.39	21.84	21.68	L

TABLE 3 — *Continued*

ID & coordinates:			Seeing (arcsec)				5σ Point Source Depth				Star Limit	Comments
BCS ID	RA	DEC	g	r	i	z	g	r	i	z		
BCS2321-5152	350.392	−51.876	1.16	1.04	0.88	0.88	24.18	24.01	23.76	22.17	21.74	L,H
BCS2321-5229	350.446	−52.487	1.47	1.35	1.27	1.30	24.03	23.66	22.33	20.70	21.23	-
BCS2322-5305	350.546	−53.086	1.82	1.60	0.90	0.83	24.46	24.15	23.86	22.25	21.83	L,H
BCS2322-5341	350.639	−53.696	1.50	1.40	1.37	1.32	23.66	23.61	23.22	22.00	21.39	L
BCS2322-5417	350.679	−54.302	1.01	1.01	1.05	1.19	24.16	23.97	23.66	22.46	21.60	L,H
BCS2323-5453	350.756	−54.904	0.99	1.06	0.89	1.23	24.18	23.90	23.71	22.67	22.11	L,H
BCS2323-5606	350.954	−56.104	1.18	1.12	0.88	0.90	24.47	24.00	23.46	22.22	22.43	L,H
BCS2324-5642	351.082	−56.708	1.84	1.51	1.55	1.69	23.37	23.28	23.01	21.62	20.97	-
BCS2324-5718	351.120	−57.319	0.95	0.86	0.78	0.74	24.35	24.29	23.99	22.42	22.19	L,H
BCS2325-5116	351.241	−51.281	1.58	1.30	1.15	1.16	23.88	23.77	23.26	21.68	21.97	-
BCS2325-5152	351.336	−51.878	1.18	1.14	0.94	0.93	24.10	23.79	23.45	22.05	21.34	L
BCS2325-5229	351.404	−52.487	1.43	1.29	1.23	1.27	24.37	23.75	22.33	21.66	21.24	-
BCS2326-5305	351.518	−53.092	1.00	1.02	0.91	0.85	23.97	23.92	23.69	22.25	21.88	L,H
BCS2326-5341	351.611	−53.690	1.84	2.16	1.17	1.22	23.82	23.54	23.15	21.83	21.72	-
BCS2326-5417	351.699	−54.296	0.79	1.00	0.98	0.95	24.31	24.06	23.16	21.86	21.84	L
BCS2327-5453	351.792	−54.904	0.88	0.82	0.85	0.92	24.29	24.07	23.50	22.07	21.75	L,H
BCS2327-5530	351.901	−55.504	0.87	1.02	0.95	1.03	24.42	24.21	23.27	22.28	22.09	L,H
BCS2328-5606	352.004	−56.111	0.94	0.90	0.88	1.03	24.34	24.24	23.56	22.18	21.96	L,H
BCS2328-5642	352.143	−56.714	1.70	1.54	1.30	1.23	23.83	23.82	23.46	22.25	21.57	L,H
BCS2328-5718	352.219	−57.309	0.89	0.83	0.81	0.81	24.43	24.18	23.82	22.35	22.18	L,H
BCS2329-5152	352.283	−51.888	0.96	0.92	0.84	0.88	24.31	24.14	23.80	22.15	22.11	L,H
BCS2329-5229	352.361	−52.487	1.60	1.52	1.17	1.11	24.24	23.70	22.52	21.82	21.19	L
BCS2330-5305	352.466	−53.099	1.06	1.04	1.44	1.35	24.20	23.69	22.97	21.63	20.56	-
BCS2330-5417	352.682	−54.304	1.11	0.93	1.00	0.82	24.49	24.12	23.26	21.99	22.03	L,H
BCS2331-5453	352.795	−54.906	1.08	0.90	0.84	0.90	24.26	24.11	24.04	22.22	22.08	L,H
BCS2331-5530	352.929	−55.501	1.18	0.89	0.96	0.88	24.33	24.21	23.73	22.34	21.87	L,H
BCS2332-5606	353.047	−56.107	1.10	0.97	0.94	0.86	24.44	24.18	23.79	22.28	21.86	L,H
BCS2332-5642	353.201	−56.715	1.53	1.26	1.40	1.37	23.98	23.85	23.18	22.05	21.47	L,H
BCS2333-5152	353.246	−51.889	1.00	0.90	0.91	0.85	24.36	24.23	23.68	22.05	21.83	L,H
BCS2333-5229	353.351	−52.484	0.95	0.84	1.03	1.06	24.24	24.10	23.46	22.50	21.62	L,H
BCS2333-5305	353.458	−53.082	1.19	1.08	1.74	1.42	23.93	23.59	22.63	21.47	20.50	-
BCS2333-5718	353.294	−57.314	1.01	0.92	0.78	0.84	24.50	24.38	23.90	22.41	22.26	L,H
BCS2334-5341	353.571	−53.694	1.47	1.41	0.90	0.88	24.17	23.99	23.32	21.91	21.99	L
BCS2334-5417	353.694	−54.302	0.92	0.94	0.89	0.89	24.32	24.11	23.47	22.23	22.02	L,H
BCS2335-5453	353.824	−54.903	1.08	0.97	1.02	0.98	24.17	24.10	23.46	22.31	21.82	L,H
BCS2335-5530	353.949	−55.509	0.98	0.98	1.20	1.20	24.05	24.11	23.82	22.65	21.53	L,H
BCS2336-5152	354.181	−51.885	1.10	1.06	1.05	1.14	24.20	23.71	23.42	21.94	21.09	L
BCS2336-5606	354.094	−56.109	0.96	0.94	0.90	0.81	24.28	24.16	23.52	22.13	21.79	L,H
BCS2337-5229	354.310	−52.483	0.89	0.82	0.81	0.85	24.49	24.22	23.96	22.47	21.80	L,H
BCS2337-5305	354.430	−53.082	1.27	1.21	1.08	1.08	24.11	23.98	23.28	22.01	21.97	L,H
BCS2337-5642	354.268	−56.716	1.68	1.27	1.45	1.87	23.90	23.67	23.13	21.84	21.46	L
BCS2337-5718	354.367	−57.315	1.12	1.10	0.98	1.00	24.13	24.07	23.54	22.07	22.04	L,H
BCS2338-5341	354.560	−53.695	1.55	1.53	0.97	1.06	23.80	23.59	23.82	22.74	21.59	L
BCS2338-5417	354.700	−54.294	1.15	0.90	0.85	0.99	24.68	24.23	23.47	22.58	22.07	L,H
BCS2339-5453	354.841	−54.900	1.06	0.99	0.82	0.80	24.28	24.14	23.52	22.18	22.06	L,H
BCS2340-5152	355.136	−51.878	1.19	1.01	0.96	0.93	24.21	23.73	23.58	22.11	22.10	L
BCS2340-5530	354.985	−55.505	1.05	1.07	0.88	0.84	24.26	24.16	23.43	22.08	22.25	L,H
BCS2340-5606	355.135	−56.110	1.00	1.00	1.28	1.30	23.91	23.81	23.39	21.88	21.56	L
BCS2341-5229	355.270	−52.482	0.94	0.84	0.77	0.83	24.45	24.26	24.08	22.39	21.93	L,H
BCS2341-5305	355.403	−53.083	1.55	1.36	1.17	1.40	24.38	24.03	23.23	21.98	21.60	L,H
BCS2341-5642	355.327	−56.714	1.57	1.57	1.29	1.40	24.01	23.88	23.45	22.30	21.49	L,H
BCS2341-5718	355.459	−57.315	1.11	1.05	0.83	0.88	24.22	24.10	23.66	22.06	21.88	L,H
BCS2342-5341	355.542	−53.696	1.40	1.41	1.26	1.38	22.97	22.84	23.53	22.30	21.71	-
BCS2342-5417	355.707	−54.294	1.07	0.87	1.22	1.20	24.10	23.96	23.35	22.23	22.01	L,H
BCS2343-5453	355.862	−54.900	1.04	0.86	1.05	1.00	24.19	24.05	23.44	22.21	21.62	L,H
BCS2344-5152	356.075	−51.876	1.14	0.98	0.80	0.80	24.25	24.05	23.62	22.26	22.45	L,H
BCS2344-5530	356.022	−55.504	1.10	0.91	1.07	0.97	24.37	24.05	23.47	22.19	21.92	L,H
BCS2344-5606	356.189	−56.109	1.05	0.87	0.91	0.81	24.34	24.26	23.82	22.38	21.76	L,H
BCS2345-5305	356.373	−53.085	1.47	1.48	1.43	1.50	24.16	23.78	23.03	21.78	21.68	L
BCS2345-5642	356.380	−56.708	1.35	1.32	1.18	1.25	24.11	23.97	23.36	22.27	21.47	L,H
BCS2346-5341	356.628	−53.668	1.15	1.15	1.62	1.64	23.55	23.53	23.03	22.10	20.50	-
BCS2346-5417	356.700	−54.298	1.01	0.89	1.00	0.99	24.49	24.16	23.63	22.37	22.11	L,H

TABLE 3 — *Continued*

ID & coordinates:			**Seeing (arcsec)**				**5σ Point Source Depth**				**Star Limit**	**Comments**
BCS ID	RA	DEC	*g*	*r*	*i*	*z*	*g*	*r*	*i*	*z*		
BCS2346-5718	356.556	−57.310	1.17	1.05	1.06	1.04	23.72	23.94	23.40	21.96	21.04	L
BCS2347-5453	356.876	−54.906	1.25	1.12	0.96	0.94	24.62	24.25	23.74	22.46	21.91	L,H
BCS2348-5152	357.022	−51.886	1.02	0.84	0.78	0.77	24.56	24.46	24.01	22.52	22.06	L,H
BCS2348-5530	357.046	−55.508	1.28	1.01	0.97	0.96	24.47	24.46	23.52	22.20	21.85	L,H
BCS2349-5305	357.347	−53.085	1.65	1.68	1.32	1.35	24.40	23.92	22.67	21.67	21.27	-
BCS2349-5606	357.234	−56.112	1.08	0.97	0.97	1.02	25.02	24.84	23.63	22.36	21.92	L,H
BCS2349-5642	357.437	−56.710	1.32	1.46	1.22	1.27	24.05	23.86	23.63	22.15	21.51	L,H
BCS2350-5341	357.549	−53.692	1.13	1.02	1.52	1.44	23.89	23.67	23.07	21.92	21.38	L
BCS2350-5417	357.707	−54.298	1.39	1.10	0.97	1.10	24.35	24.21	23.67	22.48	21.67	L,H
BCS2350-5718	357.632	−57.313	1.35	1.24	1.19	1.15	23.94	23.71	23.12	21.73	21.74	-
BCS2351-5453	357.885	−54.903	1.21	1.05	1.06	1.05	24.67	24.50	23.52	22.28	21.60	L,H
BCS2352-5530	358.109	−55.494	1.46	1.40	1.36	1.43	23.20	23.13	22.32	21.05	21.26	-
BCS2353-5606	358.299	−56.108	1.66	1.46	1.31	1.22	23.94	23.83	23.32	22.00	21.55	L
BCS2354-5642	358.502	−56.709	1.27	1.09	0.95	1.10	23.85	23.52	23.24	21.95	21.66	-
BCS2354-5718	358.705	−57.317	1.42	1.36	1.15	1.19	24.06	23.76	23.17	21.88	21.73	L

NOTE. — Summary information for the BCS imaging data presented in this work. Coordinate positions are given for the center of the $36' \times 36'$ tiles. The reported seeing is the average full width at half maximum of the seeing disk of the single epoch images that contribute to the coadded images. The point source depths are calculated as in Section §2.3 and the Star Limit corresponds to the faintest *i*-band magnitude for which we find robust morphological separation of stars and galaxies as described in Section §2.5. In the "Comments" field , "L" corresponds to tiles utilized in the low-redshift cluster search while "H" denotes tiles searched for higher-redshift systems (see §3).

TABLE 4
DESCRIPTION OF CATALOG COLUMNS

FIELDNAME	-	BCS tile name
OBJ_ID	-	Object Identification Number (unique per tile)
RA	degree	Right Ascension (J2000)
DEC	degree	Declination (J2000)
G	AB Magnitude	*g*-band MAG_AUTO
GERR	AB Magnitude	*g*-band corrected magnitude uncertainty (See §2.3)
G_SEX	-	*g*-band Source Extractor Flags + Bright Star proximity flag[(a)]
G_CLASSSTAR	-	*g*-band Source Extractor Class Star
R	AB Magnitude	*r*-band MAG_AUTO
RERR	AB Magnitude	*r*-band corrected magnitude uncertainty (See §2.3)
R_SEX	-	*r*-band Source Extractor Flags + Bright star proximity flag[(a)]
R_CLASSSTAR	-	*r*-band Source Extractor Class Star
I	AB Magnitude	*i*-band MAG_AUTO
IERR	AB Magnitude	*i*-band corrected magnitude uncertainty (See §2.3)
I_SEX	-	*i*-band Source Extractor Flags + Bright star proximity flag[(a)]
I_CLASSSTAR	-	*i*-band Source Extractor Class Star
Z	AB Magnitude	*z*-band MAG_AUTO
ZERR	AB Magnitude	*z*-band corrected magnitude uncertainty (See §2.3)
Z_SEX	-	*z*-band Source Extractor Flags + Bright star proximity flag[(a)]
Z_CLASSTAR	-	*z*-band Source Extractor Class Star
JTMASS	Vega Magnitude	2MASS *J*-band
JTMASS_ERR	Vega Magnitude	2MASS *J*-band uncertainty
GAUTO_ERR	AB Magnitude	Uncorrected *g*-band MAG_AUTO Uncertainty
RAUTO_ERR	AB Magnitude	Uncorrected *r*-band MAG_AUTO Uncertainty
IAUTO_ERR	AB Magnitude	Uncorrected *i*-band MAG_AUTO Uncertainty
ZAUTO_ERR	AB Magnitude	Uncorrected *z*-band MAG_AUTO Uncertainty
X_IMAGE	pixel units	Horizontal source location on tile
Y_IMAGE	pixel units	Vertical source location on tile
UNIFORM	-	Binary Flag, set to 1 if source is in nominal uniform-coverage region for the tile (See §2.3)
G4	AB Magnitude	Aperture-corrected $4''$ *g*-band magnitude
R4	AB Magnitude	Aperture-corrected $4''$ *r*-band magnitude
I4	AB Magnitude	Aperture-corrected $4''$ *i*-band magnitude
Z4	AB Magnitude	Aperture-corrected $4''$ *z*-band magnitude
G4_ERR	AB Magnitude	Aperture-corrected $4''$ *g*-band magnitude uncertainty
R4_ERR	AB Magnitude	Aperture-corrected $4''$ *r*-band magnitude uncertainty
I4_ERR	AB Magnitude	Aperture-corrected $4''$ *i*-band magnitude uncertainty
Z4_ERR	AB Magnitude	Aperture-corrected $4''$ *z*-band magnitude uncertainty
SG	-	New Star-galaxy classification statistic (See §2.5)
DELTA_SQ	-	New Star-galaxy statistic (Sec §2.5)

NOTE. — [(a)] Reported flags are the sum of all possible extraction flags (as is standard in SExtractor output).
0 — 124 Standard SExtractor flags
256 Missing data
512 Corrupted *i*-band (i.e. bright source that saturated in *i*-band, but not *r*- or *z*-band)
1024 Photometry potentially corrupted owing to proximity to bright star

TABLE 5
OPTICALLY-SELECTED GALAXY CLUSTERS LOCATED IN THE 23 H BCS FIELD

ID	R.A.	Dec	z	δz	Sigma	λ	$\delta\lambda$	$\Delta\lambda$	$\lambda(0.2L_\star)$	$\delta\lambda(0.2L_\star)$	$\Delta\lambda(0.2L_\star)$	Mask 200 kpc	Mask 500 kpc	Edge of Tile	Previous ID
LCS-CL J231218-5109.2	348.0766	−51.1548	0.32	0.025	3.21	14.4	2	1.3	23.8	3	2.6	0.00	0.05	1	-
LCS-CL J231224-5115.3	348.1009	−51.2560	0.75	0.040	3.27	14.0	3	0.0	–	–	–	0.00	0.01	–	-
LCS-CL J231230-5214.0	348.1262	−52.2335	0.28	0.024	4.14	14.1	2	1.3	18.3	3	1.9	0.00	0.03	1	-
LCS-CL J231235-5218.6	348.1469	−52.3114	0.42	0.031	4.11	16.3	2	0.9	34.0	4	2.2	0.00	0.03	–	-
LCS-CL J231240-5201.3	348.1674	−52.0220	0.49	0.033	3.65	11.7	2	0.4	17.2	3	0.6	0.00	0.04	–	-
LCS-CL J231253-5203.4	348.2222	−52.0570	0.69	0.040	3.51	12.1	2	0.1	–	–	–	0.00	0.00	–	-
LCS-CL J231305-5259.0	348.2729	−52.9843	0.65	0.037	3.93	11.0	2	0.5	–	–	–	0.01	0.01	–	-
LCS-CL J231309-5101.5	348.2886	−51.0254	0.33	0.024	4.67	21.0	2	1.1	37.1	4	2.7	0.04	0.03	–	-
LCS-CL J231313-5405.1	348.3052	−54.0859	0.20	0.021	3.43	13.0	2	1.5	17.0	3	2.1	0.16	0.05	1	-
LCS-CL J231321-5435.2	348.3404	−54.5878	0.56	0.035	3.37	14.2	3	4.3	–	–	–	0.28	0.32	1	-
LCS-CL J231322-5249.7	348.3457	−52.8286	0.70	0.039	3.85	20.2	3	0.3	–	–	–	0.00	0.01	–	-
LCS-CL J231323-5401.5	348.3497	−54.0260	0.53	0.036	3.59	12.4	3	3.0	17.0	3	4.3	0.00	0.30	1	-
LCS-CL J231325-5423.4	348.3544	−54.3914	0.62	0.037	3.83	12.4	2	0.2	–	–	–	0.00	0.00	–	-
LCS-CL J231325-5215.3	348.3575	−52.2554	0.27	0.023	4.76	46.4	4	2.5	80.4	5	4.0	0.08	0.05	–	0,2
LCS-CL J231333-5452.3	348.3880	−54.8730	0.55	0.037	3.45	10.3	2	0.6	13.3	3	0.8	0.00	0.10	–	-
LCS-CL J231338-5442.5	348.4111	−54.7086	0.65	0.037	3.74	11.6	2	0.5	–	–	–	0.00	0.01	–	-
LCS-CL J231345-5728.1	348.4376	−57.4685	0.71	0.040	3.45	14.5	3	1.9	–	–	–	0.00	0.03	1	-
LCS-CL J231345-5428.9	348.4410	−54.4829	0.30	0.024	4.62	17.8	2	2.8	31.3	3	4.8	0.23	0.12	–	-
LCS-CL J231351-5154.7	348.4634	−51.9123	0.73	0.038	3.44	15.8	2	0.0	–	–	–	0.00	0.00	–	-
LCS-CL J231352-5420.9	348.4688	−54.3484	0.20	0.023	4.93	16.7	2	1.5	19.5	3	1.7	0.00	0.11	–	-
LCS-CL J231402-5735.3	348.5096	−57.5890	0.43	0.047	3.38	10.2	2	1.7	12.5	3	2.0	0.00	0.12	–	-
LCS-CL J231403-5545.5	348.5147	−55.7587	0.60	0.036	3.92	10.6	2	0.8	–	–	–	0.06	0.13	–	-
LCS-CL J231409-5554.1	348.5401	−55.9032	0.75	0.039	3.96	17.1	3	0.4	–	–	–	0.00	0.01	–	-
LCS-CL J231411-5716.9	348.5468	−57.2823	0.73	0.039	3.59	17.8	3	1.8	–	–	–	0.00	0.04	–	-
LCS-CL J231411-5443.6	348.5500	−54.7274	0.37	0.033	3.74	13.5	3	2.2	24.0	4	3.8	0.20	0.17	–	-
LCS-CL J231419-5425.3	348.5803	−54.4233	0.32	0.023	4.04	13.5	2	0.9	24.2	3	1.9	0.00	0.04	–	-
LCS-CL J231422-5424.0	348.5936	−54.4010	0.74	0.039	4.29	29.3	3	2.3	–	–	–	0.00	0.05	–	-
LCS-CL J231430-5306.8	348.6271	−53.1144	0.32	0.024	4.24	12.0	2	1.0	20.0	3	1.8	0.00	0.10	–	-
LCS-CL J231434-5237.7	348.6421	−52.6288	0.47	0.033	3.33	13.3	2	0.7	19.7	3	1.3	0.00	0.02	–	-
LCS-CL J231434-5449.8	348.6453	−54.8303	0.34	0.024	4.71	13.6	2	0.6	32.3	4	2.0	0.00	0.05	–	-
LCS-CL J231442-5503.8	348.6757	−55.0648	0.52	0.034	4.07	10.7	2	1.0	19.1	3	1.8	0.00	0.08	–	-
LCS-CL J231448-5437.1	348.7010	−54.6193	0.60	0.037	4.52	10.8	2	2.1	–	–	–	0.09	0.15	1	-
LCS-CL J231452-5451.5	348.7188	−54.8598	0.60	0.036	3.93	16.8	2	1.0	–	–	–	0.00	0.01	–	-
LCS-CL J231455-5553.1	348.7310	−55.8863	0.25	0.023	3.79	25.4	3	1.4	51.6	4	3.0	0.00	0.08	–	2
LCS-CL J231505-5721.0	348.7733	−57.3501	0.58	0.035	3.45	10.7	2	0.7	–	–	–	0.00	0.08	–	-
LCS-CL J231509-5233.6	348.7891	−52.5612	0.47	0.033	3.92	27.4	3	0.4	43.4	4	0.7	0.00	0.00	–	2
LCS-CL J231516-5406.8	348.8172	−54.1143	0.54	0.034	3.34	10.7	2	0.4	13.0	2	0.5	0.00	0.08	–	-
LCS-CL J231519-5547.7	348.8301	−55.7964	0.25	0.024	3.21	15.5	2	1.0	25.7	4	1.9	0.00	0.10	1	-
LCS-CL J231520-5420.6	348.8343	−54.3441	0.20	0.022	3.53	10.7	2	0.9	19.4	3	1.5	0.06	0.10	–	-
LCS-CL J231527-5236.0	348.8627	−52.6001	0.63	0.037	4.74	14.2	2	0.5	–	–	–	0.00	0.00	–	-
LCS-CL J231528-5729.4	348.8687	−57.4912	0.47	0.033	3.98	11.2	2	0.1	20.4	3	0.1	0.00	0.00	–	-
LCS-CL J231532-5719.9	348.8837	−57.3330	0.44	0.033	3.38	10.5	2	0.1	11.2	2	0.1	0.00	0.01	–	-
LCS-CL J231601-5122.4	349.0072	−51.3741	0.48	0.033	4.16	18.1	3	1.2	35.3	4	2.6	0.00	0.03	–	-
LCS-CL J231602-5111.2	349.0107	−51.1883	0.56	0.035	3.93	12.8	2	0.6	–	–	–	0.00	0.07	–	-
LCS-CL J231605-5307.9	349.0222	−53.1329	0.61	0.037	4.07	15.3	2	0.1	–	–	–	0.00	0.01	1	-
LCS-CL J231605-5622.3	349.0229	−56.3728	0.41	0.031	4.04	22.0	3	4.8	28.4	4	6.2	0.05	0.22	–	-
LCS-CL J231614-5415.8	349.0624	−54.2641	0.32	0.024	4.57	11.0	2	2.1	25.3	3	6.4	0.00	0.14	–	-
LCS-CL J231619-5544.2	349.0797	−55.7372	0.50	0.033	3.48	13.8	2	0.7	23.7	3	1.3	0.00	0.03	–	2

TABLE 5 — *Continued*

ID	R.A.	Dec	z	δz	Sigma	λ	$\delta\lambda$	$\Delta\lambda$	$\lambda(0.2L_\star)$	$\delta\lambda(0.2L_\star)$	$\Delta\lambda(0.2L_\star)$	Mask 200 kpc	Mask 500 kpc	Edge of Tile	Previous ID
LCS-CL J231622-5717.7	349.0925	−57.2963	0.69	0.037	4.34	20.0	3	1.0	–	–	–	0.00	0.01	–	-
LCS-CL J231624-5707.8	349.1009	−57.1313	0.70	0.039	4.11	14.4	2	0.6	–	–	–	0.02	0.02	–	-
LCS-CL J231632-5714.6	349.1374	−57.2438	0.70	0.040	4.05	15.2	3	1.6	–	–	–	0.00	0.03	–	-
LCS-CL J231635-5308.0	349.1462	−53.1335	0.18	0.022	4.29	16.2	2	0.5	28.4	3	0.9	0.00	0.03	1	-
LCS-CL J231646-5125.3	349.1923	−51.4220	0.32	0.023	4.21	10.2	2	0.5	19.6	3	1.0	0.00	0.06	–	-
LCS-CL J231651-5453.9	349.2160	−54.8991	0.38	0.031	4.07	43.4	4	5.2	91.9	6	8.9	0.00	0.10	1	2,5
LCS-CL J231701-5518.0	349.2549	−55.3005	0.31	0.023	4.34	14.1	2	3.0	29.0	4	6.2	0.16	0.28	1	-
LCS-CL J231703-5300.2	349.2627	−53.0050	0.49	0.033	5.30	22.8	2	0.5	48.7	4	1.1	0.00	0.04	–	-
LCS-CL J231706-5423.8	349.2753	−54.3971	0.31	0.024	3.50	10.4	2	0.1	13.5	2	0.2	0.00	0.01	1	-
LCS-CL J231717-5256.2	349.3220	−52.9382	0.42	0.035	3.27	14.5	3	0.8	22.5	3	1.1	0.09	0.03	–	-
LCS-CL J231724-5728.0	349.3527	−57.4668	0.25	0.023	4.26	14.0	2	0.8	23.4	3	1.3	0.00	0.06	–	-
LCS-CL J231728-5321.6	349.3691	−53.3607	0.68	0.040	3.98	11.7	2	1.7	–	–	–	0.06	0.13	1	-
LCS-CL J231735-5146.3	349.3974	−51.7724	0.30	0.023	4.91	21.5	2	0.8	40.0	4	2.6	0.00	0.00	–	0
LCS-CL J231755-5619.1	349.4823	−56.3185	0.58	0.035	4.25	24.5	3	0.8	–	–	–	0.02	0.01	–	-
LCS-CL J231800-5555.0	349.5038	−55.9173	0.57	0.035	3.56	13.0	2	1.5	–	–	–	0.00	0.10	–	-
LCS-CL J231808-5713.0	349.5335	−57.2179	0.70	0.040	3.34	13.7	3	1.0	–	–	–	0.00	0.01	1	-
LCS-CL J231809-5247.3	349.5397	−52.7884	0.45	0.034	3.41	12.4	2	1.3	24.3	4	3.1	0.06	0.07	1	-
LCS-CL J231815-5059.4	349.5654	−50.9904	0.33	0.024	4.05	11.5	3	4.3	16.4	3	6.5	0.18	0.44	1	-
LCS-CL J231819-5300.0	349.5817	−53.0006	0.45	0.032	3.56	10.4	2	0.1	20.9	3	0.2	0.00	0.00	–	-
LCS-CL J231821-5615.1	349.5914	−56.2524	0.70	0.043	3.52	11.3	2	0.1	–	–	–	0.00	0.01	–	-
LCS-CL J231822-5550.0	349.5932	−55.8349	0.24	0.023	4.24	11.1	2	0.6	19.9	3	1.3	0.09	0.07	1	-
LCS-CL J231830-5719.3	349.6254	−57.3231	0.26	0.024	4.34	15.1	2	0.8	40.4	4	2.7	0.00	0.05	–	-
LCS-CL J231830-5249.6	349.6264	−52.8275	0.44	0.033	3.69	22.0	3	4.7	34.3	4	8.3	0.00	0.11	–	-
LCS-CL J231839-5313.4	349.6641	−53.2249	0.43	0.034	3.50	13.3	2	0.3	25.2	3	0.6	0.00	0.00	–	-
LCS-CL J231842-5101.3	349.6781	−51.0231	0.48	0.033	4.20	21.1	3	2.0	32.9	4	3.7	0.00	0.01	1	-
LCS-CL J231843-5612.2	349.6818	−56.2035	0.29	0.024	4.28	17.0	2	1.0	32.3	3	1.8	0.11	0.06	–	-
LCS-CL J231845-5730.0	349.6894	−57.5013	0.26	0.023	4.18	31.8	3	0.9	61.5	5	2.1	0.00	0.03	–	-
LCS-CL J231845-5714.2	349.6902	−57.2378	0.28	0.024	3.55	12.9	2	0.7	16.7	3	0.9	0.00	0.06	–	-
LCS-CL J231848-5617.1	349.7038	−56.2866	0.56	0.034	6.37	39.8	3	0.3	–	–	–	0.00	0.01	–	2
LCS-CL J231905-5126.1	349.7745	−51.4359	0.50	0.033	3.85	13.0	2	0.7	17.1	3	0.9	0.00	0.02	–	-
LCS-CL J231911-5153.1	349.7991	−51.8851	0.49	0.033	3.72	10.7	2	0.0	23.2	3	0.2	0.00	0.00	–	-
LCS-CL J231912-5404.8	349.8038	−54.0815	0.27	0.023	5.16	33.2	2	1.4	57.1	4	2.8	0.00	0.03	–	0
LCS-CL J231917-5707.4	349.8235	−57.1240	0.26	0.022	4.01	13.7	2	0.6	18.8	3	0.8	0.00	0.06	–	-
LCS-CL J231922-5727.0	349.8454	−57.4502	0.44	0.034	3.44	13.4	2	0.1	23.3	3	0.2	0.00	0.00	–	-
LCS-CL J231943-5125.0	349.9311	−51.4167	0.49	0.034	3.57	11.8	2	0.2	23.6	3	0.8	0.00	0.00	–	-
LCS-CL J231947-5703.2	349.9488	−57.0546	0.61	0.038	3.48	11.2	2	0.8	–	–	–	0.05	0.11	–	-
LCS-CL J232001-5147.3	350.0051	−51.7884	0.62	0.037	4.20	17.1	2	0.0	–	–	–	0.00	0.00	–	-
LCS-CL J232003-5611.1	350.0155	−56.1860	0.64	0.037	3.58	10.1	2	0.2	–	–	–	0.02	0.01	–	-
LCS-CL J232010-5620.4	350.0446	−56.3408	0.56	0.035	4.57	27.1	3	1.3	–	–	–	0.00	0.04	–	-
LCS-CL J232011-5202.1	350.0494	−52.0356	0.28	0.024	4.03	11.2	2	0.3	15.9	3	0.5	0.00	0.04	–	-
LCS-CL J232024-5116.5	350.1029	−51.2762	0.45	0.032	4.00	17.6	2	0.3	31.1	3	0.5	0.00	0.01	–	-
LCS-CL J232026-5321.5	350.1089	−53.3589	0.68	0.039	3.43	11.3	2	0.7	–	–	–	0.00	0.05	1	-
LCS-CL J232031-5153.8	350.1297	−51.8978	0.75	0.039	4.10	10.2	2	1.2	–	–	–	0.17	0.07	–	-
LCS-CL J232031-5151.3	350.1304	−51.8565	0.57	0.037	3.78	13.2	2	0.3	–	–	–	0.02	0.00	–	-
LCS-CL J232044-5205.7	350.1859	−52.0959	0.73	0.038	3.68	32.6	4	1.0	–	–	–	0.01	0.00	–	-
LCS-CL J232105-5550.7	350.2716	−55.8465	0.65	0.038	3.25	13.5	3	1.9	–	–	–	0.02	0.15	1	-
LCS-CL J232115-5128.4	350.3162	−51.4739	0.49	0.034	3.11	12.9	2	0.9	17.9	3	1.1	0.03	0.01	–	-
LCS-CL J232116-5319.4	350.3202	−53.3237	0.40	0.032	3.59	14.9	3	4.0	21.4	3	5.0	0.47	0.28	–	-
LCS-CL J232120-5616.4	350.3352	−56.2738	0.61	0.036	4.21	12.8	2	0.7	–	–	–	0.02	0.01	–	-

TABLE 5 — *Continued*

ID	R.A.	Dec	z	δz	Sigma	λ	$\delta\lambda$	$\Delta\lambda$	$\lambda(0.2L_\star)$	$\delta\lambda(0.2L_\star)$	$\Delta\lambda(0.2L_\star)$	Mask 200 kpc	Mask 500 kpc	Edge of Tile	Previous ID
LCS-CL J232136-5059.7	350.4010	−50.9960	0.47	0.033	3.61	15.0	2	3.6	20.3	3	5.3	0.08	0.22	1	-
LCS-CL J232159-5611.3	350.4958	−56.1896	0.62	0.038	3.43	11.7	2	0.2	–	–	–	0.01	0.00	1	-
LCS-CL J232200-5445.0	350.5019	−54.7500	0.33	0.024	5.68	26.0	2	1.3	44.8	4	2.3	0.07	0.03	–	0,5
LCS-CL J232201-5419.1	350.5042	−54.3200	0.66	0.038	3.91	10.2	2	0.7	–	–	–	0.00	0.05	–	5
LCS-CL J232211-5618.7	350.5460	−56.3132	0.69	0.042	3.22	21.4	3	0.5	–	–	–	0.00	0.00	–	5
LCS-CL J232212-5105.9	350.5524	−51.0985	0.50	0.033	3.27	11.1	2	0.2	16.8	3	0.3	0.00	0.00	–	-
LCS-CL J232216-5428.2	350.5695	−54.4711	0.26	0.022	3.90	14.6	2	0.7	23.6	3	1.2	0.00	0.08	–	-
LCS-CL J232227-5148.4	350.6166	−51.8074	0.20	0.025	4.25	34.7	3	3.3	56.0	5	5.3	0.00	0.11	–	0
LCS-CL J232232-5415.6	350.6345	−54.2609	0.41	0.034	3.32	11.8	2	0.5	17.5	3	0.7	0.01	0.01	–	-
LCS-CL J232233-5207.5	350.6394	−52.1250	0.68	0.038	3.93	20.0	3	0.8	–	–	–	0.01	0.07	–	-
LCS-CL J232238-5549.6	350.6590	−55.8271	0.61	0.037	4.56	14.8	2	2.0	–	–	–	0.00	0.05	1	-
LCS-CL J232251-5358.9	350.7125	−53.9823	0.49	0.033	3.95	11.8	2	1.6	20.5	3	2.8	0.00	0.17	1	-
LCS-CL J232315-5141.6	350.8140	−51.6939	0.75	0.040	3.61	11.9	2	0.5	–	–	–	0.00	0.03	1	-
LCS-CL J232350-5301.7	350.9604	−53.0291	0.43	0.034	3.43	11.5	2	0.3	21.0	3	0.6	0.02	0.01	–	-
LCS-CL J232354-5622.5	350.9779	−56.3757	0.33	0.024	3.71	10.9	2	2.1	11.3	2	2.0	0.00	0.16	–	-
LCS-CL J232401-5502.2	351.0058	−55.0382	0.60	0.035	3.81	13.6	2	0.1	–	–	–	0.00	0.00	–	5
LCS-CL J232402-5338.2	351.0086	−53.6376	0.39	0.033	3.25	11.0	2	1.5	18.8	3	2.5	0.24	0.20	–	-
LCS-CL J232418-5140.1	351.0772	−51.6690	0.33	0.025	3.92	11.0	2	0.2	17.4	3	0.3	0.00	0.00	–	-
LCS-CL J232420-5420.0	351.0850	−54.3341	0.50	0.033	4.29	10.5	1	0.1	13.8	2	0.2	0.00	0.01	–	-
LCS-CL J232454-5510.4	351.2267	−55.1744	0.61	0.035	4.57	15.2	2	2.4	–	–	–	0.00	0.15	1	-
LCS-CL J232458-5255.6	351.2417	−52.9275	0.41	0.032	3.28	10.6	2	1.4	14.1	3	1.7	0.13	0.15	–	-
LCS-CL J232518-5708.9	351.3259	−57.1486	0.33	0.024	4.36	26.9	3	4.7	43.4	4	8.3	0.01	0.06	–	-
LCS-CL J232529-5442.1	351.3722	−54.7021	0.18	0.022	3.78	10.3	2	0.4	22.0	3	1.5	0.00	0.02	–	7,5
LCS-CL J232540-5154.1	351.4176	−51.9030	0.17	0.022	3.22	11.5	2	0.8	13.7	2	0.9	0.07	0.08	–	-
LCS-CL J232541-5316.6	351.4240	−53.2774	0.31	0.024	3.69	18.2	3	1.0	37.2	4	2.5	0.00	0.03	–	-
LCS-CL J232549-5135.5	351.4572	−51.5920	0.31	0.027	3.62	12.6	2	0.7	17.0	3	1.0	0.11	0.07	1	-
LCS-CL J232550-5522.7	351.4593	−55.3798	0.62	0.037	4.08	20.5	3	1.7	–	–	–	0.02	0.05	1	-
LCS-CL J232612-5318.9	351.5538	−53.3162	0.18	0.022	4.95	58.0	5	13.3	94.0	6	21.0	0.17	0.30	–	0,2
LCS-CL J232619-5523.1	351.5825	−55.3858	0.65	0.037	4.40	36.2	3	1.6	–	–	–	0.05	0.02	–	5
LCS-CL J232630-5159.8	351.6270	−51.9975	0.20	0.022	3.43	10.4	2	0.1	11.0	2	0.2	0.00	0.01	–	-
LCS-CL J232634-5501.9	351.6452	−55.0323	0.41	0.032	4.33	28.0	3	2.2	35.1	4	2.7	0.00	0.05	–	5
LCS-CL J232641-5721.4	351.6709	−57.3575	0.39	0.033	3.54	12.3	2	0.8	16.3	3	1.1	0.00	0.05	1	-
LCS-CL J232706-5446.8	351.7752	−54.7815	0.63	0.037	4.29	12.4	2	0.3	–	–	–	0.00	0.05	–	-
LCS-CL J232708-5137.5	351.7844	−51.6267	0.37	0.032	5.20	64.3	4	4.4	82.1	5	7.7	0.00	0.05	1	-
LCS-CL J232714-5702.6	351.8114	−57.0447	0.75	0.040	3.52	11.6	2	0.0	–	–	–	0.00	0.01	–	-
LCS-CL J232732-5616.6	351.8845	−56.2779	0.40	0.035	3.90	15.0	2	0.7	18.3	3	0.8	0.00	0.08	–	-
LCS-CL J232748-5148.9	351.9523	−51.8157	0.59	0.036	3.56	11.6	2	0.3	–	–	–	0.02	0.00	–	-
LCS-CL J232804-5630.0	352.0196	−56.5014	0.18	0.021	3.70	12.5	2	2.1	17.1	3	3.0	0.00	0.19	–	-
LCS-CL J232805-5220.3	352.0243	−52.3391	0.26	0.023	3.94	12.0	2	1.3	20.4	3	2.1	0.01	0.12	–	-
LCS-CL J232810-5238.5	352.0422	−52.6420	0.24	0.022	4.45	15.3	2	0.5	25.0	3	1.0	0.00	0.03	–	-
LCS-CL J232816-5140.9	352.0703	−51.6817	0.31	0.024	4.38	10.4	2	1.3	12.2	2	1.5	0.20	0.11	–	-
LCS-CL J232854-5236.6	352.2271	−52.6102	0.34	0.024	3.95	12.3	2	0.5	22.0	3	1.3	0.00	0.00	–	-
LCS-CL J232856-5524.4	352.2369	−55.4079	0.60	0.035	3.82	17.2	3	0.3	–	–	–	0.00	0.01	–	2,5
LCS-CL J232915-5659.1	352.3140	−56.9859	0.18	0.021	3.49	10.2	2	0.3	19.1	3	0.8	0.00	0.05	–	-
LCS-CL J232923-5649.7	352.3468	−56.8297	0.42	0.033	3.21	13.8	2	0.2	22.6	3	0.3	0.00	0.01	–	-
LCS-CL J232955-5608.1	352.4831	−56.1356	0.41	0.031	3.96	24.1	2	1.3	42.4	4	2.3	0.00	0.06	1	5
LCS-CL J232959-5637.4	352.4998	−56.6236	0.48	0.033	3.99	14.9	2	1.5	17.9	3	2.0	0.01	0.04	–	-
LCS-CL J233000-5437.3	352.5018	−54.6224	0.18	0.021	3.47	13.1	2	1.5	22.3	3	2.6	0.07	0.11	1	5
LCS-CL J233003-5414.2	352.5158	−54.2374	0.37	0.031	3.72	16.7	2	0.5	34.7	3	1.2	0.01	0.01	–	5

TABLE 5 — *Continued*

ID	R.A.	Dec	z	δz	Sigma	λ	$\delta\lambda$	$\Delta\lambda$	$\lambda(0.2L_\star)$	$\delta\lambda(0.2L_\star)$	$\Delta\lambda(0.2L_\star)$	Mask 200 kpc	Mask 500 kpc	Edge of Tile	Previous ID
LCS-CL J233021-5235.2	352.5882	−52.5871	0.45	0.033	3.59	10.9	2	0.9	13.0	2	1.0	0.00	0.11	–	-
LCS-CL J233022-5232.1	352.5955	−52.5360	0.27	0.026	3.43	11.3	2	1.2	13.4	2	1.5	0.12	0.17	–	-
LCS-CL J233035-5659.6	352.6470	−56.9938	0.69	0.043	3.58	11.5	2	0.5	–	–	–	0.00	0.01	1	-
LCS-CL J233037-5543.6	352.6545	−55.7274	0.26	0.024	4.19	15.9	2	0.5	29.0	3	1.0	0.00	0.02	–	5
LCS-CL J233052-5520.3	352.7178	−55.3394	0.75	0.039	4.29	17.2	3	1.1	–	–	–	0.00	0.03	–	-
LCS-CL J233111-5552.2	352.7964	−55.8705	0.39	0.033	3.68	13.3	2	1.2	18.7	3	1.7	0.06	0.15	–	-
LCS-CL J233121-5441.8	352.8417	−54.6969	0.56	0.035	3.94	10.8	2	0.5	–	–	–	0.07	0.05	–	-
LCS-CL J233125-5149.7	352.8561	−51.8295	0.62	0.037	3.42	12.1	2	0.2	–	–	–	0.02	0.00	1	-
LCS-CL J233130-5236.3	352.8761	−52.6061	0.59	0.035	3.78	12.8	2	2.4	–	–	–	0.11	0.22	1	-
LCS-CL J233130-5221.7	352.8774	−52.3623	0.55	0.034	3.42	12.9	3	4.1	14.2	3	4.3	0.16	0.38	1	-
LCS-CL J233143-5229.0	352.9316	−52.4840	0.60	0.035	6.52	22.3	3	2.5	–	–	–	0.09	0.10	1	-
LCS-CL J233145-5205.6	352.9382	−52.0935	0.56	0.035	4.76	34.5	3	0.1	–	–	–	0.00	0.00	–	-
LCS-CL J233147-5240.1	352.9477	−52.6696	0.42	0.032	3.80	14.6	2	1.4	35.4	4	3.5	0.15	0.07	1	-
LCS-CL J233148-5225.5	352.9532	−52.4252	0.57	0.035	3.41	12.7	2	1.8	–	–	–	0.21	0.14	1	-
LCS-CL J233151-5736.2	352.9648	−57.6045	0.27	0.024	3.46	20.1	3	7.1	36.4	5	13.4	0.13	0.34	1	-
LCS-CL J233215-5442.1	353.0638	−54.7032	0.24	0.022	4.21	24.7	2	0.6	40.1	4	1.1	0.00	0.02	–	5
LCS-CL J233224-5215.4	353.1020	−52.2582	0.57	0.035	4.79	18.8	3	1.9	–	–	–	0.00	0.11	–	-
LCS-CL J233227-5358.4	353.1145	−53.9745	0.42	0.032	3.93	53.0	5	17.3	84.9	7	27.5	0.00	0.26	1	2,3
LCS-CL J233232-5220.2	353.1351	−52.3379	0.47	0.032	5.28	47.5	3	1.4	81.5	5	2.2	0.01	0.03	–	2
LCS-CL J233236-5413.4	353.1513	−54.2240	0.44	0.034	3.34	11.7	2	0.2	13.4	2	0.2	0.00	0.01	1	-
LCS-CL J233236-5427.5	353.1537	−54.4594	0.52	0.034	3.31	10.0	2	2.3	11.9	3	2.7	0.23	0.21	1	-
LCS-CL J233306-5236.8	353.2776	−52.6139	0.75	0.039	3.64	11.9	3	3.9	–	–	–	0.27	0.35	–	-
LCS-CL J233313-5239.9	353.3055	−52.6654	0.69	0.038	3.42	10.0	2	0.2	–	–	–	0.00	0.02	–	-
LCS-CL J233313-5223.6	353.3081	−52.3947	0.56	0.035	3.80	19.4	3	0.5	–	–	–	0.00	0.01	–	-
LCS-CL J233320-5237.8	353.3359	−52.6303	0.50	0.033	3.60	13.8	3	2.5	25.9	4	4.9	0.00	0.19	–	-
LCS-CL J233326-5350.0	353.3596	−53.8341	0.41	0.037	3.91	11.3	2	1.1	14.0	2	1.4	0.16	0.06	–	-
LCS-CL J233328-5622.8	353.3676	−56.3813	0.50	0.036	3.36	10.9	2	1.0	17.7	3	2.0	0.00	0.05	–	-
LCS-CL J233329-5215.2	353.3732	−52.2537	0.58	0.035	3.89	44.0	5	22.1	–	–	–	0.45	0.49	–	2
LCS-CL J233336-5240.7	353.4025	−52.6799	0.52	0.033	4.16	17.8	2	0.4	33.3	4	1.1	0.02	0.01	–	-
LCS-CL J233337-5432.7	353.4045	−54.5465	0.38	0.043	3.36	10.6	2	0.1	14.5	3	0.2	0.00	0.00	–	-
LCS-CL J233338-5538.1	353.4097	−55.6362	0.69	0.038	3.71	21.7	3	2.6	–	–	–	0.13	0.07	1	5
LCS-CL J233344-5517.6	353.4335	−55.2940	0.64	0.037	3.78	13.0	2	2.0	–	–	–	0.00	0.11	1	-
LCS-CL J233353-5416.0	353.4717	−54.2670	0.53	0.034	3.67	15.1	2	1.5	25.3	3	2.7	0.01	0.05	–	-
LCS-CL J233354-5209.1	353.4771	−52.1522	0.50	0.033	4.04	12.4	2	0.2	18.2	3	0.5	0.00	0.00	–	-
LCS-CL J233355-5508.7	353.4816	−55.1456	0.44	0.032	3.67	21.3	3	4.0	28.4	4	5.2	0.08	0.25	–	-
LCS-CL J233357-5651.1	353.4909	−56.8530	0.61	0.037	4.00	12.0	2	0.2	–	–	–	0.00	0.02	–	-
LCS-CL J233359-5222.9	353.4960	−52.3824	0.43	0.034	3.56	26.7	3	2.8	41.6	4	5.1	0.07	0.16	–	-
LCS-CL J233359-5658.7	353.4962	−56.9790	0.58	0.035	4.36	13.0	2	1.1	–	–	–	0.00	0.02	–	-
LCS-CL J233402-5522.9	353.5102	−55.3821	0.62	0.038	3.56	10.2	2	1.1	–	–	–	0.00	0.11	1	-
LCS-CL J233406-5547.1	353.5257	−55.7854	0.70	0.040	4.00	18.4	3	5.7	–	–	–	0.00	0.32	1	5
LCS-CL J233407-5205.2	353.5315	−52.0882	0.71	0.040	3.20	10.3	2	0.0	–	–	–	0.00	0.00	–	-
LCS-CL J233421-5410.7	353.5876	−54.1788	0.36	0.032	3.69	14.1	2	0.5	31.9	3	1.2	0.00	0.03	–	-
LCS-CL J233421-5147.2	353.5888	−51.7877	0.75	0.039	3.60	11.1	2	0.0	–	–	–	0.00	0.00	–	-
LCS-CL J233423-5540.7	353.5986	−55.6789	0.75	0.038	5.27	37.2	3	0.4	–	–	–	0.00	0.00	–	-
LCS-CL J233425-5427.2	353.6069	−54.4550	0.56	0.035	4.24	32.6	3	1.0	–	–	–	0.00	0.01	–	2,5
LCS-CL J233428-5221.5	353.6171	−52.3594	0.29	0.024	3.84	14.1	2	2.6	27.3	4	5.6	0.04	0.13	–	-
LCS-CL J233430-5224.4	353.6253	−52.4081	0.69	0.040	4.25	18.3	2	0.6	–	–	–	0.05	0.04	–	-
LCS-CL J233434-5442.7	353.6441	−54.7121	0.37	0.032	3.47	13.4	2	0.2	19.1	3	0.4	0.00	0.01	–	-
LCS-CL J233438-5227.1	353.6619	−52.4530	0.72	0.039	3.24	11.5	2	0.3	–	–	–	0.02	0.01	–	-

TABLE 5 — *Continued*

ID	R.A.	Dec	z	δz	Sigma	λ	$\delta\lambda$	$\Delta\lambda$	$\lambda(0.2L_\star)$	$\delta\lambda(0.2L_\star)$	$\Delta\lambda(0.2L_\star)$	Mask 200 kpc	Mask 500 kpc	Edge of Tile	Previous ID
LCS-CL J233444-5702.2	353.6834	−57.0368	0.49	0.034	3.94	14.7	2	1.3	20.8	3	1.9	0.00	0.01	1	-
LCS-CL J233447-5208.0	353.6991	−52.1349	0.30	0.030	3.80	12.9	2	1.9	15.0	2	2.4	0.23	0.19	1	-
LCS-CL J233448-5715.0	353.7015	−57.2510	0.50	0.034	4.10	13.9	2	1.1	19.4	3	1.8	0.00	0.07	–	-
LCS-CL J233450-5226.1	353.7118	−52.4356	0.39	0.042	4.04	20.9	3	0.6	33.2	4	0.9	0.00	0.03	–	-
LCS-CL J233454-5533.7	353.7283	−55.5626	0.41	0.031	3.74	13.0	2	0.8	23.3	3	1.6	0.10	0.08	–	-
LCS-CL J233455-5454.4	353.7321	−54.9082	0.46	0.033	3.12	16.2	2	0.1	25.4	3	0.2	0.00	0.00	–	5
LCS-CL J233459-5455.6	353.7497	−54.9271	0.63	0.037	4.08	20.6	3	0.1	–	–	–	0.00	0.00	–	5
LCS-CL J233502-5222.9	353.7603	−52.3822	0.57	0.035	3.64	10.0	2	0.1	–	–	–	0.00	0.01	–	-
LCS-CL J233516-5638.2	353.8185	−56.6372	0.51	0.035	3.37	14.4	2	0.2	23.2	3	0.3	0.00	0.00	1	-
LCS-CL J233522-5726.4	353.8454	−57.4410	0.54	0.035	3.76	12.3	2	1.2	17.8	3	2.0	0.00	0.03	1	-
LCS-CL J233530-5535.5	353.8761	−55.5927	0.42	0.032	4.18	15.2	2	0.6	18.5	3	0.8	0.00	0.07	–	-
LCS-CL J233539-5719.2	353.9140	−57.3207	0.51	0.033	3.97	19.7	3	1.2	25.7	3	1.7	0.00	0.03	1	-
LCS-CL J233542-5230.1	353.9274	−52.5029	0.75	0.039	3.94	14.1	2	0.6	–	–	–	0.00	0.01	1	-
LCS-CL J233545-5225.2	353.9395	−52.4208	0.64	0.037	4.33	30.0	3	1.0	–	–	–	0.00	0.04	–	-
LCS-CL J233547-5357.2	353.9462	−53.9549	0.31	0.025	3.60	11.6	2	0.9	14.5	2	1.0	0.00	0.01	–	-
LCS-CL J233551-5329.4	353.9648	−53.4915	0.51	0.034	4.15	10.8	2	0.4	16.4	3	0.6	0.00	0.03	–	-
LCS-CL J233551-5152.2	353.9664	−51.8716	0.52	0.034	3.55	27.7	3	0.5	51.9	5	1.0	0.00	0.01	–	-
LCS-CL J233556-5606.0	353.9869	−56.1006	0.57	0.035	4.55	22.7	3	1.0	–	–	–	0.02	0.00	–	2,5
LCS-CL J233558-5637.7	353.9923	−56.6292	0.50	0.033	3.63	11.3	2	0.2	19.3	3	0.4	0.01	0.00	–	-
LCS-CL J233601-5257.0	354.0081	−52.9510	0.54	0.034	4.20	21.2	3	7.0	29.4	4	9.3	0.41	0.43	1	-
LCS-CL J233603-5603.0	354.0133	−56.0510	0.43	0.032	3.69	11.1	2	0.7	20.9	3	1.4	0.01	0.05	–	-
LCS-CL J233607-5352.5	354.0298	−53.8767	0.51	0.034	3.86	54.9	4	3.4	102.3	6	5.5	0.00	0.00	1	2
LCS-CL J233614-5713.1	354.0593	−57.2192	0.64	0.037	4.38	19.6	2	0.2	–	–	–	0.00	0.00	–	-
LCS-CL J233614-5722.1	354.0610	−57.3691	0.49	0.034	3.57	11.2	2	0.8	20.4	3	1.5	0.00	0.13	–	-
LCS-CL J233622-5527.5	354.0937	−55.4586	0.47	0.032	3.34	11.0	2	0.2	22.4	3	0.5	0.00	0.01	–	-
LCS-CL J233629-5342.3	354.1235	−53.7066	0.49	0.035	3.52	10.9	2	1.9	16.7	3	2.9	0.17	0.23	1	-
LCS-CL J233630-5553.9	354.1277	−55.8992	0.49	0.034	3.13	21.8	3	5.7	31.0	4	7.8	0.35	0.40	–	-
LCS-CL J233632-5645.6	354.1373	−56.7602	0.49	0.033	3.72	12.2	2	0.6	18.2	3	1.1	0.00	0.00	–	-
LCS-CL J233637-5244.2	354.1544	−52.7375	0.56	0.035	4.12	15.0	2	0.1	–	–	–	0.00	0.00	–	-
LCS-CL J233639-5434.5	354.1635	−54.5763	0.53	0.035	3.32	10.5	2	4.1	16.8	3	6.2	0.63	0.30	1	-
LCS-CL J233643-5254.5	354.1815	−52.9085	0.54	0.034	4.20	20.8	2	0.3	26.4	3	0.4	0.00	0.02	–	-
LCS-CL J233644-5347.7	354.1835	−53.7959	0.32	0.023	4.49	14.3	2	0.2	35.6	4	0.8	0.00	0.01	–	-
LCS-CL J233646-5146.2	354.1945	−51.7700	0.18	0.022	3.37	15.2	2	1.0	20.4	3	1.6	0.00	0.03	–	-
LCS-CL J233649-5619.4	354.2063	−56.3247	0.66	0.037	3.23	14.8	3	0.2	–	–	–	0.00	0.00	–	-
LCS-CL J233649-5518.0	354.2080	−55.3005	0.57	0.035	4.10	15.0	3	3.9	–	–	–	0.30	0.36	–	5
LCS-CL J233656-5424.7	354.2349	−54.4120	0.53	0.036	3.34	10.2	2	0.8	10.6	2	0.9	0.02	0.09	1	-
LCS-CL J233658-5722.3	354.2417	−57.3730	0.51	0.034	3.71	17.7	2	0.4	24.5	3	0.6	0.00	0.00	–	-
LCS-CL J233702-5604.7	354.2586	−56.0788	0.49	0.033	3.77	17.4	3	3.7	29.1	4	6.5	0.20	0.23	–	-
LCS-CL J233702-5707.5	354.2622	−57.1255	0.23	0.022	4.81	12.4	2	0.7	24.8	3	1.6	0.00	0.05	–	-
LCS-CL J233703-5717.5	354.2658	−57.2929	0.40	0.031	3.63	10.3	2	1.3	17.2	3	2.4	0.00	0.15	–	-
LCS-CL J233708-5239.4	354.2846	−52.6568	0.53	0.034	4.13	16.1	2	0.1	36.4	4	0.3	0.00	0.02	–	-
LCS-CL J233714-5544.6	354.3098	−55.7434	0.75	0.039	3.59	12.0	2	0.5	–	–	–	0.00	0.01	–	-
LCS-CL J233715-5244.0	354.3159	−52.7344	0.40	0.032	3.32	11.1	2	0.3	23.1	3	0.8	0.00	0.00	–	-
LCS-CL J233717-5416.4	354.3248	−54.2741	0.63	0.037	3.94	10.4	2	0.2	–	–	–	0.00	0.04	–	-
LCS-CL J233722-5548.0	354.3417	−55.8012	0.52	0.036	3.15	12.3	3	5.0	18.4	4	7.2	0.70	0.38	1	-
LCS-CL J233728-5603.6	354.3696	−56.0612	0.67	0.038	5.26	41.5	4	9.4	–	–	–	0.11	0.24	–	-
LCS-CL J233740-5223.8	354.4177	−52.3980	0.74	0.038	3.38	11.3	2	0.1	–	–	–	0.00	0.01	–	-
LCS-CL J233753-5611.7	354.4740	−56.1966	0.47	0.032	3.82	14.3	2	0.3	24.9	3	0.6	0.00	0.00	–	-
LCS-CL J233802-5553.3	354.5104	−55.8890	0.60	0.036	3.79	15.9	2	0.1	–	–	–	0.00	0.01	–	-

TABLE 5 — *Continued*

ID	R.A.	Dec	z	δz	Sigma	λ	$\delta\lambda$	$\Delta\lambda$	$\lambda(0.2L_\star)$	$\delta\lambda(0.2L_\star)$	$\Delta\lambda(0.2L_\star)$	Mask 200 kpc	Mask 500 kpc	Edge of Tile	Previous ID
LCS-CL J233805-5617.3	354.5209	−56.2891	0.39	0.030	3.41	21.0	3	0.7	32.4	4	1.1	0.03	0.01	–	-
LCS-CL J233808-5312.3	354.5372	−53.2052	0.51	0.033	4.45	37.7	3	2.9	78.6	5	5.6	0.00	0.11	–	2
LCS-CL J233812-5603.9	354.5526	−56.0652	0.68	0.038	3.41	14.0	3	1.3	–	–	–	0.02	0.08	1	-
LCS-CL J233812-5604.6	354.5527	−56.0769	0.33	0.025	3.73	12.2	2	0.9	27.2	3	2.2	0.00	0.12	–	-
LCS-CL J233814-5726.9	354.5603	−57.4499	0.60	0.038	3.32	10.2	2	0.4	–	–	–	0.00	0.04	–	-
LCS-CL J233818-5238.1	354.5756	−52.6350	0.53	0.035	4.09	10.5	2	0.6	20.0	3	1.2	0.09	0.09	–	-
LCS-CL J233818-5539.5	354.5757	−55.6591	0.47	0.033	3.85	22.0	3	1.0	32.8	4	1.5	0.02	0.02	–	-
LCS-CL J233826-5204.3	354.6088	−52.0727	0.38	0.034	3.16	12.4	2	0.7	16.7	3	1.1	0.00	0.05	1	-
LCS-CL J233829-5221.6	354.6215	−52.3607	0.68	0.038	3.75	18.5	3	0.8	–	–	–	0.00	0.04	–	-
LCS-CL J233832-5716.3	354.6338	−57.2720	0.48	0.033	3.65	13.3	2	0.2	21.1	3	0.3	0.00	0.00	–	-
LCS-CL J233835-5437.4	354.6478	−54.6242	0.30	0.025	3.84	14.8	2	1.5	24.5	3	2.5	0.07	0.12	1	-
LCS-CL J233837-5307.6	354.6571	−53.1276	0.47	0.033	3.54	17.4	2	0.6	32.4	4	1.1	0.02	0.05	–	-
LCS-CL J233905-5722.3	354.7718	−57.3732	0.75	0.039	3.20	11.6	2	0.3	–	–	–	0.00	0.03	–	-
LCS-CL J233908-5722.1	354.7870	−57.3698	0.51	0.034	3.66	11.6	2	0.5	23.9	3	0.9	0.00	0.07	–	-
LCS-CL J233911-5728.4	354.7982	−57.4745	0.51	0.034	3.61	16.0	2	1.9	24.8	4	3.1	0.00	0.15	–	-
LCS-CL J233915-5714.6	354.8154	−57.2441	0.49	0.033	3.49	19.3	3	2.4	37.0	4	5.6	0.00	0.01	–	-
LCS-CL J233917-5231.8	354.8217	−52.5312	0.19	0.022	3.57	11.2	2	0.5	22.6	3	1.1	0.08	0.05	1	-
LCS-CL J233922-5543.7	354.8446	−55.7297	0.75	0.038	3.58	14.4	2	0.5	–	–	–	0.00	0.03	–	-
LCS-CL J233923-5649.0	354.8486	−56.8174	0.41	0.032	3.61	11.4	2	0.2	16.4	3	0.3	0.00	0.00	1	-
LCS-CL J233928-5550.0	354.8677	−55.8350	0.41	0.031	3.70	26.4	3	5.5	41.7	4	9.2	0.10	0.09	1	-
LCS-CL J233931-5138.8	354.8797	−51.6479	0.26	0.024	3.64	12.4	2	1.0	22.2	3	2.2	0.05	0.05	–	-
LCS-CL J233937-5418.5	354.9050	−54.3100	0.54	0.034	4.25	11.9	2	0.0	19.5	3	0.1	0.00	0.01	–	-
LCS-CL J233938-5707.4	354.9097	−57.1241	0.49	0.033	3.56	12.1	2	0.9	30.4	4	2.4	0.00	0.07	1	-
LCS-CL J233939-5215.1	354.9162	−52.2522	0.32	0.024	3.82	11.2	2	0.7	21.6	3	1.3	0.01	0.05	–	-
LCS-CL J233944-5559.0	354.9334	−55.9843	0.41	0.032	3.53	12.7	2	1.4	15.1	3	1.6	0.00	0.08	–	-
LCS-CL J233957-5246.4	354.9905	−52.7735	0.57	0.035	3.89	16.0	3	3.0	–	–	–	0.00	0.25	1	-
LCS-CL J234000-5243.0	355.0039	−52.7172	0.56	0.035	4.85	13.8	2	1.6	–	–	–	0.11	0.12	–	-
LCS-CL J234008-5653.7	355.0373	−56.8951	0.48	0.033	3.83	12.9	2	1.2	20.0	3	1.8	0.02	0.11	–	-
LCS-CL J234009-5731.3	355.0412	−57.5232	0.75	0.039	3.40	17.9	3	1.1	–	–	–	0.00	0.00	–	-
LCS-CL J234012-5419.1	355.0524	−54.3187	0.56	0.035	4.10	19.9	2	0.2	–	–	–	0.00	0.01	–	2
LCS-CL J234018-5139.8	355.0781	−51.6636	0.47	0.033	3.86	14.4	2	2.4	32.9	4	6.2	0.08	0.21	–	-
LCS-CL J234021-5307.7	355.0905	−53.1298	0.55	0.035	3.62	14.7	2	0.6	24.2	3	0.9	0.02	0.00	–	-
LCS-CL J234022-5239.0	355.0955	−52.6514	0.55	0.034	4.55	10.7	2	0.4	20.1	3	0.9	0.00	0.06	–	-
LCS-CL J234023-5559.8	355.0986	−55.9982	0.41	0.034	3.87	19.2	3	3.4	33.3	4	6.3	0.00	0.18	–	-
LCS-CL J234025-5150.0	355.1072	−51.8347	0.25	0.022	3.85	12.0	2	1.0	15.2	2	1.3	0.21	0.05	–	-
LCS-CL J234030-5243.8	355.1270	−52.7310	0.53	0.035	3.51	12.0	2	0.7	12.7	2	0.7	0.00	0.07	–	-
LCS-CL J234035-5440.6	355.1483	−54.6776	0.61	0.036	4.40	14.5	2	0.0	–	–	–	0.00	0.00	–	-
LCS-CL J234037-5647.2	355.1556	−56.7882	0.47	0.032	3.18	10.9	2	0.1	14.7	2	0.1	0.00	0.01	–	-
LCS-CL J234048-5230.3	355.2001	−52.5051	0.58	0.036	3.95	12.4	2	0.6	–	–	–	0.00	0.09	–	-
LCS-CL J234053-5235.0	355.2237	−52.5837	0.53	0.034	3.76	19.4	2	0.2	32.0	4	0.3	0.02	0.00	–	-
LCS-CL J234055-5726.8	355.2321	−57.4478	0.48	0.033	3.84	10.7	2	0.2	15.7	3	0.3	0.00	0.01	–	-
LCS-CL J234103-5720.6	355.2635	−57.3442	0.47	0.035	3.12	21.5	3	1.1	51.8	5	2.9	0.00	0.06	–	-
LCS-CL J234105-5716.0	355.2728	−57.2678	0.46	0.032	4.78	51.2	3	2.5	82.2	5	3.9	0.00	0.02	–	-
LCS-CL J234115-5225.3	355.3133	−52.4227	0.59	0.037	3.44	10.9	2	0.9	–	–	–	0.00	0.11	–	-
LCS-CL J234115-5309.0	355.3159	−53.1515	0.60	0.035	4.58	13.1	2	0.6	–	–	–	0.00	0.10	–	-
LCS-CL J234127-5706.5	355.3632	−57.1095	0.47	0.033	4.54	27.0	3	0.7	52.0	5	1.6	0.00	0.00	–	-
LCS-CL J234128-5502.1	355.3698	−55.0352	0.48	0.033	3.56	11.1	2	0.5	15.2	3	0.7	0.00	0.01	1	-
LCS-CL J234135-5723.3	355.3970	−57.3885	0.75	0.039	4.11	19.8	3	0.1	–	–	–	0.00	0.01	–	-
LCS-CL J234136-5305.6	355.4012	−53.0935	0.51	0.034	3.77	19.4	2	0.7	31.6	4	1.4	0.00	0.07	–	-

TABLE 5 — *Continued*

ID	R.A.	Dec	z	δz	Sigma	λ	$\delta\lambda$	$\Delta\lambda$	$\lambda(0.2L_\star)$	$\delta\lambda(0.2L_\star)$	$\Delta\lambda(0.2L_\star)$	Mask 200 kpc	Mask 500 kpc	Edge of Tile	Previous ID
LCS-CL J234137-5452.1	355.4081	−54.8696	0.58	0.035	4.10	17.1	3	1.0	–	–	–	0.02	0.02	1	2
LCS-CL J234143-5557.8	355.4330	−55.9637	0.19	0.021	5.11	21.6	2	1.0	34.8	3	1.5	0.04	0.03	–	0
LCS-CL J234144-5419.5	355.4358	−54.3252	0.60	0.037	3.74	11.2	2	0.1	–	–	–	0.00	0.00	–	-
LCS-CL J234150-5734.4	355.4614	−57.5746	0.72	0.039	4.53	21.1	3	0.3	–	–	–	0.02	0.00	–	-
LCS-CL J234152-5214.2	355.4703	−52.2373	0.55	0.035	3.48	10.6	2	0.3	16.0	3	0.6	0.00	0.01	–	-
LCS-CL J234155-5706.3	355.4823	−57.1065	0.47	0.033	3.88	21.4	3	0.9	42.8	4	3.0	0.00	0.01	–	-
LCS-CL J234156-5308.8	355.4865	−53.1470	0.51	0.033	4.89	28.4	3	1.2	54.0	4	2.8	0.00	0.04	–	2
LCS-CL J234159-5508.3	355.4968	−55.1384	0.70	0.039	4.01	13.7	2	0.4	–	–	–	0.03	0.01	–	-
LCS-CL J234207-5619.4	355.5326	−56.3236	0.43	0.032	3.98	21.9	3	2.8	27.9	3	3.6	0.00	0.07	–	-
LCS-CL J234220-5728.0	355.5854	−57.4671	0.49	0.033	3.72	21.0	3	4.0	35.1	4	6.9	0.00	0.18	–	-
LCS-CL J234220-5734.0	355.5870	−57.5668	0.47	0.032	3.40	21.5	3	1.5	27.4	3	2.0	0.16	0.03	–	-
LCS-CL J234222-5732.6	355.5949	−57.5446	0.59	0.036	4.23	10.2	2	1.1	–	–	–	0.00	0.09	–	-
LCS-CL J234225-5144.9	355.6042	−51.7494	0.17	0.021	3.90	13.0	2	0.6	23.3	3	1.2	0.05	0.05	1	-
LCS-CL J234230-5555.8	355.6267	−55.9303	0.44	0.032	3.64	17.1	3	3.1	28.7	4	4.7	0.34	0.12	1	-
LCS-CL J234231-5621.1	355.6309	−56.3532	0.43	0.032	3.95	35.2	4	7.1	55.4	5	11.9	0.08	0.08	1	-
LCS-CL J234232-5703.6	355.6341	−57.0613	0.74	0.039	3.28	17.4	3	1.5	–	–	–	0.00	0.02	–	-
LCS-CL J234242-5725.9	355.6781	−57.4324	0.71	0.042	3.21	10.7	2	0.5	–	–	–	0.00	0.06	–	-
LCS-CL J234243-5222.4	355.6804	−52.3744	0.60	0.036	3.74	12.9	2	0.4	–	–	–	0.00	0.04	–	-
LCS-CL J234314-5318.7	355.8122	−53.3118	0.35	0.038	3.19	12.3	2	0.0	16.1	3	0.1	0.00	0.01	–	-
LCS-CL J234321-5626.0	355.8377	−56.4338	0.57	0.038	3.19	11.5	2	1.8	–	–	–	0.02	0.07	1	-
LCS-CL J234322-5702.7	355.8448	−57.0451	0.63	0.039	4.21	21.4	3	0.8	–	–	–	0.00	0.00	1	-
LCS-CL J234327-5605.3	355.8655	−56.0890	0.49	0.034	3.73	13.0	3	3.8	20.9	3	5.9	0.27	0.33	–	-
LCS-CL J234328-5659.5	355.8672	−56.9923	0.58	0.036	4.06	16.9	3	2.8	–	–	–	0.05	0.22	1	-
LCS-CL J234336-5148.3	355.9003	−51.8064	0.20	0.021	3.92	10.3	2	0.5	38.2	4	1.9	0.11	0.05	–	-
LCS-CL J234341-5651.3	355.9247	−56.8551	0.49	0.034	3.54	12.2	2	0.5	24.4	3	1.4	0.00	0.01	1	-
LCS-CL J234353-5651.2	355.9719	−56.8547	0.61	0.036	5.60	23.9	3	0.1	–	–	–	0.00	0.00	–	-
LCS-CL J234410-5638.0	356.0454	−56.6333	0.52	0.037	3.19	16.0	2	0.1	21.2	3	0.1	0.00	0.00	–	-
LCS-CL J234417-5653.7	356.0717	−56.8962	0.51	0.033	4.54	23.6	2	0.4	39.4	4	0.6	0.00	0.00	–	-
LCS-CL J234438-5312.9	356.1624	−53.2162	0.50	0.034	3.57	12.4	2	0.2	19.7	3	0.4	0.02	0.00	–	-
LCS-CL J234448-5617.1	356.2023	−56.2864	0.61	0.035	5.40	38.7	3	1.6	–	–	–	0.08	0.01	–	-
LCS-CL J234505-5249.4	356.2711	−52.8237	0.28	0.024	3.69	10.1	2	0.9	15.6	3	1.7	0.01	0.04	–	-
LCS-CL J234520-5415.4	356.3372	−54.2574	0.59	0.036	3.80	12.0	2	0.2	–	–	–	0.00	0.00	–	-
LCS-CL J234529-5139.6	356.3742	−51.6600	0.18	0.022	3.64	15.1	2	1.5	28.1	3	2.8	0.20	0.05	–	-
LCS-CL J234538-5249.5	356.4124	−52.8252	0.17	0.021	3.61	10.1	2	4.3	27.4	4	13.4	0.28	0.44	–	-
LCS-CL J234548-5402.8	356.4527	−54.0479	0.60	0.035	5.84	29.7	3	0.3	–	–	–	0.00	0.01	–	-
LCS-CL J234552-5524.3	356.4685	−55.4060	0.40	0.034	3.52	13.9	2	0.3	19.2	3	0.5	0.00	0.01	1	-
LCS-CL J234601-5208.6	356.5061	−52.1438	0.65	0.040	3.33	11.2	2	1.3	–	–	–	0.00	0.10	1	-
LCS-CL J234605-5539.1	356.5234	−55.6529	0.37	0.034	3.24	14.2	3	4.4	20.4	3	6.0	0.27	0.27	1	-
LCS-CL J234622-5456.9	356.5943	−54.9497	0.56	0.035	3.96	12.9	2	0.7	–	–	–	0.00	0.01	–	-
LCS-CL J234700-5724.2	356.7524	−57.4037	0.49	0.033	3.56	13.3	2	0.1	24.4	3	0.3	0.00	0.01	–	-
LCS-CL J234721-5204.6	356.8402	−52.0782	0.65	0.036	4.48	20.8	3	1.6	–	–	–	0.00	0.09	–	-
LCS-CL J234805-5601.4	357.0230	−56.0239	0.39	0.036	4.38	23.8	3	1.5	40.3	4	2.6	0.01	0.06	–	-
LCS-CL J234814-5438.9	357.0600	−54.6488	0.68	0.039	3.74	10.7	2	0.7	–	–	–	0.00	0.01	1	-
LCS-CL J234854-5349.4	357.2273	−53.8242	0.27	0.024	3.93	11.3	2	0.8	21.9	3	1.6	0.00	0.11	–	-
LCS-CL J234914-5700.2	357.3098	−57.0044	0.47	0.034	3.24	18.0	3	5.3	24.1	4	7.0	0.41	0.37	1	-
LCS-CL J234917-5455.3	357.3221	−54.9226	0.75	0.041	3.32	13.3	2	0.9	–	–	–	0.00	0.00	–	2
LCS-CL J234935-5516.3	357.3979	−55.2719	0.39	0.046	3.65	11.7	2	0.2	14.3	2	0.2	0.00	0.01	–	-
LCS-CL J234943-5403.8	357.4301	−54.0644	0.50	0.033	3.54	10.7	2	0.1	13.3	2	0.1	0.00	0.01	–	-
LCS-CL J235022-5433.8	357.5952	−54.5645	0.51	0.034	4.52	11.8	2	1.0	24.7	3	2.8	0.00	0.01	–	-

TABLE 5 — *Continued*

ID	R.A.	Dec	z	δz	Sigma	λ	$\delta\lambda$	$\Delta\lambda$	$\lambda(0.2L_\star)$	$\delta\lambda(0.2L_\star)$	$\Delta\lambda(0.2L_\star)$	Mask 200 kpc	Mask 500 kpc	Edge of Tile	Previous ID
LCS-CL J235033-5650.2	357.6396	−56.8376	0.68	0.038	4.28	14.3	3	2.4	–	–	–	0.00	0.19	–	-
LCS-CL J235040-5622.0	357.6700	−56.3675	0.42	0.033	3.40	14.4	2	1.5	15.0	3	1.7	0.00	0.04	–	-
LCS-CL J235111-5633.4	357.7981	−56.5579	0.60	0.038	3.66	11.2	2	2.2	–	–	–	0.09	0.13	–	-
LCS-CL J235138-5452.9	357.9086	−54.8817	0.33	0.024	6.12	36.0	3	0.9	68.4	4	1.8	0.00	0.01	–	2,3,8
LCS-CL J235327-5448.4	358.3634	−54.8081	0.39	0.032	3.83	30.9	4	14.6	42.9	5	19.9	0.48	0.36	1	-
LCS-CL J235529-5714.3	358.8744	−57.2391	0.46	0.032	3.96	21.0	2	0.2	30.0	3	0.3	0.00	0.01	–	-
LCS-CL J235556-5736.1	358.9848	−57.6020	0.47	0.033	3.77	16.5	3	3.2	23.1	4	5.0	0.06	0.15	1	-

NOTE. — Galaxy Clusters selected above 3.1 σ with $\lambda(0.4L_\star)$ greater than 10 and z ≤ 0.75 in the 23 h field. We report the cluster ID, the BCG position, red-sequence redshift and uncertainty and detection significance. For richnesses derived to $0.4L_\star$ and $0.2L_\star$ (for z < 0.55) we include the optical richness (λ), richness uncertainty and the amount the richness was boosted to account for masking. Additionally, we report the fraction of area masked within 200 and 500 kpc, flag the system if it is located on the edge of a tile, and note if the cluster has a previous identification. The reported richness uncertainty is the uncertainty estimate from the richness algorithm (see Equation 3 of Rykoff et al. (2012)) added in quadrature with a Poisson uncertainty from masked-area compensation. The previous identification column designates a counterpart using the criterion of §6. Tags correspond to the following works:
0 ACO (Abell et al. 1989)
1 REFLEX (Böhringer et al. 2004),
2 Southern Cosmology Survey (Menanteau et al. 2009, 2010),
3 SPT-SZ Survey (Vanderlinde et al. 2010; Reichardt et al. 2012),
4 ACT (Marriage et al. 2011),
5 XMM-BCS (Šuhada et al. 2012),
6 *PLANCK* (Planck Collaboration et al. 2013)
7 Vikhlinin et al. (1998)
8 Buckley-Geer et al. (2011).

TABLE 6
OPTICALLY-SELECTED GALAXY CLUSTERS LOCATED IN THE 5 H BCS FIELD

ID	R.A.	Dec	z	δz	Sigma	λ	$\delta\lambda$	$\Delta\lambda$	$\lambda(0.2L_\star)$	$\delta\lambda(0.2L_\star)$	$\Delta\lambda(0.2L_\star)$	Mask 200 kpc	Mask 500 kpc	Edge of Tile	Previous ID
LCS-CL J050624-5423.5	76.6001	−54.3925	0.50	0.033	4.56	11.8	2	0.5	12.9	2	0.5	0.00	0.03	–	-
LCS-CL J050715-5145.6	76.8148	−51.7607	0.64	0.037	3.63	14.5	3	2.4	–	–	–	0.00	0.10	1	-
LCS-CL J050728-5431.4	76.8682	−54.5246	0.45	0.033	3.64	11.1	2	1.9	17.8	3	3.0	0.31	0.17	1	-
LCS-CL J050735-5218.0	76.8994	−52.3001	0.43	0.031	4.84	11.2	2	0.5	19.5	3	1.0	0.00	0.05	–	-
LCS-CL J050736-5119.8	76.9020	−51.3314	0.62	0.040	3.39	17.8	3	2.1	–	–	–	0.00	0.01	1	-
LCS-CL J050805-5217.6	77.0214	−52.2947	0.61	0.036	3.66	12.1	2	0.7	–	–	–	0.00	0.06	–	-
LCS-CL J050806-5248.4	77.0285	−52.8081	0.69	0.039	3.66	23.8	3	0.6	–	–	–	0.02	0.00	–	-
LCS-CL J050813-5213.4	77.0571	−52.2241	0.39	0.035	3.58	11.8	2	1.6	11.5	2	1.5	0.17	0.09	–	-
LCS-CL J050818-5400.3	77.0770	−54.0063	0.74	0.039	3.45	18.7	3	0.2	–	–	–	0.00	0.00	–	-
LCS-CL J050820-5423.0	77.0873	−54.3848	0.60	0.037	3.94	12.7	2	0.3	–	–	–	0.00	0.03	–	-
LCS-CL J050821-5227.1	77.0907	−52.4520	0.60	0.035	5.44	36.8	3	1.9	–	–	–	0.00	0.02	–	-
LCS-CL J050830-5204.2	77.1260	−52.0708	0.56	0.035	4.46	12.5	2	0.7	–	–	–	0.01	0.01	1	-
LCS-CL J050831-5111.2	77.1318	−51.1871	0.48	0.033	5.61	39.5	3	6.5	71.0	5	12.2	0.00	0.07	–	-
LCS-CL J050833-5310.1	77.1386	−53.1688	0.43	0.032	3.54	10.3	2	0.5	12.9	3	0.7	0.00	0.04	–	-
LCS-CL J050833-5221.0	77.1386	−52.3515	0.47	0.034	4.09	12.8	2	0.3	17.9	3	0.4	0.00	0.01	–	-
LCS-CL J050834-5356.4	77.1455	−53.9409	0.75	0.038	3.28	17.1	3	1.6	–	–	–	0.00	0.00	–	-
LCS-CL J050845-5316.6	77.1884	−53.2775	0.34	0.025	3.31	10.0	2	2.9	16.4	3	4.8	0.18	0.35	1	-
LCS-CL J050846-5123.1	77.1946	−51.3866	0.44	0.032	3.52	11.3	2	0.5	16.3	3	0.6	0.01	0.05	–	-
LCS-CL J050854-5130.8	77.2252	−51.5134	0.68	0.038	3.39	13.3	3	1.7	–	–	–	0.00	0.04	1	2
LCS-CL J050857-5358.6	77.2380	−53.9771	0.67	0.037	3.70	32.9	4	4.9	–	–	–	0.34	0.16	–	2
LCS-CL J050902-5245.5	77.2610	−52.7599	0.66	0.038	3.52	18.0	3	1.0	–	–	–	0.00	0.01	–	-
LCS-CL J050906-5228.4	77.2776	−52.4748	0.59	0.035	3.64	16.1	3	0.9	–	–	–	0.09	0.05	–	-
LCS-CL J050907-5056.7	77.2814	−50.9462	0.47	0.033	4.51	22.2	2	0.6	39.2	4	1.6	0.00	0.01	–	-
LCS-CL J050912-5116.2	77.3039	−51.2709	0.45	0.032	3.69	10.5	2	0.1	13.1	2	0.2	0.00	0.00	–	-
LCS-CL J050913-5402.2	77.3067	−54.0373	0.71	0.040	3.58	21.0	3	0.5	–	–	–	0.00	0.02	–	-
LCS-CL J050914-5007.7	77.3119	−50.1296	0.43	0.032	3.88	11.8	2	0.2	21.1	3	0.4	0.00	0.03	–	-
LCS-CL J050916-5206.9	77.3178	−52.1156	0.64	0.037	3.43	30.4	4	5.1	–	–	–	0.01	0.05	1	2
LCS-CL J050917-5223.3	77.3235	−52.3887	0.61	0.038	3.27	10.9	2	0.3	–	–	–	0.00	0.00	–	2
LCS-CL J050919-5422.2	77.3333	−54.3700	0.47	0.033	4.08	13.6	2	0.5	22.5	3	0.9	0.01	0.04	–	-
LCS-CL J050921-5342.2	77.3393	−53.7036	0.47	0.032	5.13	49.1	5	16.1	83.2	7	24.4	0.52	0.40	–	3,4
LCS-CL J050921-5219.4	77.3412	−52.3240	0.69	0.038	3.62	20.1	3	0.8	–	–	–	0.00	0.01	–	-
LCS-CL J050926-5233.9	77.3587	−52.5652	0.64	0.039	3.64	10.5	2	0.2	–	–	–	0.00	0.01	–	-
LCS-CL J050927-5454.8	77.3665	−54.9145	0.58	0.035	3.97	14.2	2	0.9	–	–	–	0.00	0.05	1	-
LCS-CL J050928-5132.2	77.3691	−51.5369	0.62	0.036	3.73	10.2	2	0.2	–	–	–	0.00	0.01	–	-
LCS-CL J050929-5406.6	77.3718	−54.1103	0.72	0.039	3.30	17.2	3	0.5	–	–	–	0.00	0.03	–	-
LCS-CL J050932-5225.6	77.3844	−52.4272	0.75	0.041	3.56	17.8	3	1.7	–	–	–	0.15	0.15	–	-
LCS-CL J050932-5347.0	77.3872	−53.7849	0.45	0.034	3.50	19.0	2	1.7	20.2	3	1.8	0.00	0.08	–	-
LCS-CL J050937-5145.5	77.4082	−51.7599	0.61	0.035	3.98	17.7	2	0.7	–	–	–	0.00	0.04	–	-
LCS-CL J050941-5141.3	77.4215	−51.6894	0.65	0.036	3.88	42.1	4	1.5	–	–	–	0.00	0.01	–	-
LCS-CL J050945-5239.8	77.4388	−52.6647	0.62	0.036	3.33	18.1	3	2.9	–	–	–	0.00	0.13	–	-
LCS-CL J050947-5456.7	77.4460	−54.9466	0.58	0.035	4.05	15.1	2	1.3	–	–	–	0.00	0.02	1	-
LCS-CL J050949-5227.3	77.4570	−52.4554	0.64	0.037	3.49	12.6	2	0.8	–	–	–	0.01	0.05	–	-
LCS-CL J051001-5535.0	77.5053	−55.5844	0.35	0.025	4.79	11.9	2	4.0	21.0	3	6.4	0.39	0.39	–	-
LCS-CL J051002-5117.8	77.5093	−51.2975	0.49	0.034	3.29	13.2	2	1.5	15.8	3	1.8	0.17	0.16	–	-
LCS-CL J051005-5519.7	77.5242	−55.3288	0.39	0.032	3.92	17.2	2	1.2	29.4	3	2.2	0.06	0.10	–	-
LCS-CL J051015-5237.4	77.5644	−52.6245	0.32	0.027	3.26	12.1	3	3.4	13.1	3	3.6	0.09	0.31	–	-

TABLE 6 — *Continued*

ID	R.A.	Dec	z	δz	Sigma	λ	$\delta\lambda$	$\Delta\lambda$	$\lambda(0.2L_\star)$	$\delta\lambda(0.2L_\star)$	$\Delta\lambda(0.2L_\star)$	Mask 200 kpc	Mask 500 kpc	Edge of Tile	Previous ID
LCS-CL J051020-5433.9	77.5856	−54.5664	0.43	0.032	4.40	15.1	2	1.1	21.8	3	1.8	0.00	0.03	–	-
LCS-CL J051024-5445.0	77.6009	−54.7512	0.44	0.031	4.81	23.1	3	1.9	54.0	5	5.0	0.00	0.14	–	2
LCS-CL J051025-5302.7	77.6050	−53.0459	0.70	0.038	3.77	18.8	3	1.4	–	–	–	0.04	0.11	1	-
LCS-CL J051026-5520.0	77.6108	−55.3334	0.43	0.070	3.52	10.2	2	0.2	18.6	3	0.4	0.00	0.01	–	-
LCS-CL J051033-5616.0	77.6393	−56.2671	0.74	0.038	3.79	18.0	3	0.4	–	–	–	0.00	0.00	–	-
LCS-CL J051035-5202.2	77.6467	−52.0368	0.75	0.039	3.56	17.1	3	0.6	–	–	–	0.02	0.01	–	-
LCS-CL J051036-5124.4	77.6505	−51.4073	0.47	0.032	5.36	23.0	3	2.8	41.0	4	5.7	0.06	0.07	–	-
LCS-CL J051043-5426.7	77.6796	−54.4463	0.60	0.036	3.87	17.2	2	0.8	–	–	–	0.00	0.05	–	-
LCS-CL J051043-5240.0	77.6806	−52.6679	0.60	0.036	4.16	17.0	3	2.0	–	–	–	0.00	0.10	1	-
LCS-CL J051046-5108.9	77.6936	−51.1487	0.62	0.038	3.46	14.2	2	0.4	–	–	–	0.00	0.01	–	-
LCS-CL J051052-5135.1	77.7173	−51.5854	0.58	0.035	3.48	10.1	2	0.7	–	–	–	0.00	0.12	1	-
LCS-CL J051052-4859.1	77.7196	−48.9854	0.62	0.036	4.13	16.3	3	4.6	–	–	–	0.16	0.27	–	-
LCS-CL J051056-5438.7	77.7364	−54.6455	0.58	0.036	4.46	14.2	2	1.3	–	–	–	0.00	0.12	–	-
LCS-CL J051057-5457.4	77.7400	−54.9572	0.59	0.036	3.85	18.8	3	0.8	–	–	–	0.00	0.04	–	-
LCS-CL J051059-5209.3	77.7461	−52.1558	0.57	0.035	3.83	12.2	2	0.7	–	–	–	0.00	0.01	1	-
LCS-CL J051103-5100.8	77.7626	−51.0139	0.50	0.033	3.93	18.3	3	3.5	36.8	4	6.5	0.21	0.15	1	-
LCS-CL J051109-5531.3	77.7905	−55.5218	0.60	0.036	3.60	11.0	2	1.0	–	–	–	0.03	0.04	–	-
LCS-CL J051114-4906.4	77.8088	−49.1075	0.68	0.038	3.49	12.8	2	1.3	–	–	–	0.00	0.02	1	-
LCS-CL J051115-5153.1	77.8165	−51.8862	0.70	0.037	4.36	25.8	3	0.7	–	–	–	0.00	0.05	1	-
LCS-CL J051120-5107.3	77.8350	−51.1223	0.49	0.033	4.61	19.1	3	1.1	25.5	3	1.5	0.13	0.06	1	-
LCS-CL J051121-5110.6	77.8403	−51.1775	0.49	0.033	3.79	18.2	3	0.8	35.4	4	2.0	0.00	0.01	1	-
LCS-CL J051122-5126.6	77.8437	−51.4441	0.50	0.034	4.27	25.3	3	2.5	33.3	4	3.2	0.01	0.05	1	-
LCS-CL J051126-5129.4	77.8611	−51.4909	0.68	0.038	3.68	25.1	3	3.8	–	–	–	0.00	0.19	1	-
LCS-CL J051131-5014.9	77.8793	−50.2500	0.55	0.034	4.08	23.1	3	4.4	46.3	5	10.1	0.01	0.13	1	-
LCS-CL J051132-4842.3	77.8862	−48.7054	0.65	0.037	3.88	12.7	2	1.0	–	–	–	0.00	0.12	–	-
LCS-CL J051133-5426.8	77.8909	−54.4474	0.75	0.039	3.64	12.7	2	0.3	–	–	–	0.05	0.02	–	-
LCS-CL J051136-5013.1	77.9020	−50.2184	0.66	0.038	3.84	20.0	3	0.9	–	–	–	0.07	0.03	1	-
LCS-CL J051138-5123.8	77.9098	−51.3982	0.55	0.034	4.55	17.0	2	0.4	22.5	3	0.6	0.00	0.01	–	-
LCS-CL J051139-5253.4	77.9126	−52.8904	0.62	0.036	3.70	10.3	2	0.1	–	–	–	0.00	0.01	–	-
LCS-CL J051139-5204.2	77.9127	−52.0714	0.62	0.039	3.27	12.1	2	2.3	–	–	–	0.19	0.27	1	-
LCS-CL J051144-5114.2	77.9343	−51.2380	0.52	0.033	4.04	16.1	2	0.7	28.4	4	1.4	0.00	0.06	–	2
LCS-CL J051144-5305.0	77.9354	−53.0841	0.44	0.031	4.01	11.8	2	1.7	21.5	3	2.9	0.07	0.15	–	-
LCS-CL J051145-5530.5	77.9405	−55.5089	0.57	0.034	5.06	15.6	2	0.9	–	–	–	0.01	0.05	–	-
LCS-CL J051149-5117.9	77.9564	−51.2990	0.60	0.036	3.65	14.7	2	0.7	–	–	–	0.00	0.00	–	-
LCS-CL J051150-5422.5	77.9615	−54.3761	0.57	0.039	3.38	11.0	2	1.0	–	–	–	0.07	0.13	–	-
LCS-CL J051156-5137.5	77.9856	−51.6266	0.44	0.032	3.98	13.9	2	0.9	25.8	4	2.0	0.04	0.10	–	-
LCS-CL J051158-5453.2	77.9956	−54.8869	0.50	0.033	4.07	10.3	2	0.6	12.1	2	0.8	0.00	0.11	–	-
LCS-CL J051204-5109.3	78.0167	−51.1560	0.56	0.035	3.29	11.4	2	1.1	–	–	–	0.12	0.16	–	-
LCS-CL J051204-5542.0	78.0206	−55.7009	0.47	0.035	3.25	13.9	3	3.0	21.0	3	4.1	0.32	0.22	1	-
LCS-CL J051207-5142.0	78.0302	−51.7013	0.52	0.033	5.15	27.8	3	0.9	40.4	4	1.6	0.00	0.01	–	2
LCS-CL J051207-5027.3	78.0324	−50.4558	0.50	0.034	3.37	17.0	3	2.4	43.5	5	8.1	0.00	0.09	–	-
LCS-CL J051211-5419.5	78.0472	−54.3262	0.62	0.038	3.60	11.4	2	0.8	–	–	–	0.00	0.09	–	-
LCS-CL J051215-4945.6	78.0628	−49.7611	0.65	0.040	3.52	10.4	2	2.1	–	–	–	0.32	0.28	–	-
LCS-CL J051224-5536.3	78.1015	−55.6061	0.41	0.032	3.47	11.9	2	0.7	21.9	3	1.6	0.07	0.03	–	-
LCS-CL J051226-5021.0	78.1123	−50.3514	0.50	0.036	3.33	14.1	3	1.1	27.5	4	2.2	0.00	0.09	–	-
LCS-CL J051231-5139.9	78.1321	−51.6651	0.57	0.035	4.29	20.7	3	1.9	–	–	–	0.00	0.10	–	2
LCS-CL J051235-5000.1	78.1495	−50.0021	0.38	0.032	5.23	17.2	2	0.7	30.6	3	1.3	0.00	0.04	–	-

TABLE 6 — *Continued*

ID	R.A.	Dec	z	δz	Sigma	λ	$\delta\lambda$	$\Delta\lambda$	$\lambda(0.2L_\star)$	$\delta\lambda(0.2L_\star)$	$\Delta\lambda(0.2L_\star)$	Mask 200 kpc	Mask 500 kpc	Edge of Tile	Previous ID
LCS-CL J051236-4837.2	78.1528	−48.6215	0.29	0.026	3.93	15.6	2	0.7	22.0	3	1.1	0.00	0.05	–	-
LCS-CL J051238-5013.5	78.1620	−50.2261	0.75	0.039	3.54	18.1	3	1.2	–	–	–	0.00	0.04	–	-
LCS-CL J051239-5041.1	78.1633	−50.6857	0.47	0.033	3.94	14.6	2	0.4	24.0	3	0.7	0.00	0.00	–	-
LCS-CL J051240-5223.1	78.1692	−52.3855	0.58	0.035	3.63	10.3	2	0.2	–	–	–	0.00	0.03	–	-
LCS-CL J051241-5431.1	78.1730	−54.5186	0.26	0.023	4.32	10.9	2	1.4	20.3	3	2.6	0.05	0.17	1	-
LCS-CL J051241-4949.5	78.1739	−49.8251	0.47	0.033	4.75	11.0	2	0.6	17.4	3	0.9	0.04	0.02	–	-
LCS-CL J051247-5514.5	78.1968	−55.2425	0.39	0.032	3.92	13.1	2	0.5	24.7	3	1.3	0.00	0.01	–	-
LCS-CL J051247-5526.4	78.1990	−55.4402	0.47	0.033	4.00	17.3	2	0.2	33.8	4	0.8	0.00	0.00	–	-
LCS-CL J051250-4919.8	78.2086	−49.3306	0.23	0.023	3.39	13.4	2	1.8	16.3	3	2.1	0.00	0.14	–	-
LCS-CL J051259-4849.8	78.2462	−48.8316	0.52	0.033	4.76	18.2	2	1.8	25.7	3	2.8	0.00	0.15	–	-
LCS-CL J051305-5022.6	78.2714	−50.3781	0.50	0.034	3.65	21.5	3	2.1	33.4	4	3.3	0.06	0.12	–	-
LCS-CL J051309-5143.7	78.2903	−51.7293	0.62	0.036	4.13	24.2	3	0.9	–	–	–	0.00	0.01	–	-
LCS-CL J051310-5352.6	78.2926	−53.8771	0.63	0.037	3.53	12.9	3	2.7	–	–	–	0.00	0.28	1	-
LCS-CL J051311-5355.7	78.2986	−53.9298	0.60	0.036	3.30	13.3	3	1.9	–	–	–	0.02	0.10	1	-
LCS-CL J051321-5118.3	78.3381	−51.3051	0.67	0.037	3.36	10.4	2	0.1	–	–	–	0.00	0.01	–	-
LCS-CL J051324-5126.4	78.3541	−51.4405	0.54	0.034	5.86	19.5	3	2.8	35.6	4	5.8	0.04	0.13	–	-
LCS-CL J051340-5230.6	78.4168	−52.5109	0.26	0.024	4.30	16.3	3	2.2	24.4	3	2.9	0.28	0.07	–	-
LCS-CL J051341-5207.2	78.4242	−52.1211	0.75	0.039	3.75	19.8	3	1.8	–	–	–	0.00	0.12	1	-
LCS-CL J051346-5529.5	78.4457	−55.4929	0.47	0.033	4.75	30.0	3	3.3	47.4	4	5.3	0.00	0.07	1	-
LCS-CL J051351-4957.0	78.4654	−49.9504	0.58	0.035	4.28	12.2	2	0.3	–	–	–	0.00	0.00	–	-
LCS-CL J051402-5142.3	78.5119	−51.7061	0.54	0.034	4.39	21.4	3	3.6	60.8	5	9.0	0.40	0.10	–	-
LCS-CL J051422-5238.8	78.5940	−52.6477	0.55	0.035	3.81	11.9	2	2.9	15.8	3	4.0	0.14	0.16	1	-
LCS-CL J051426-5219.7	78.6104	−52.3294	0.51	0.034	4.13	10.3	2	2.3	14.3	3	3.5	0.00	0.25	1	-
LCS-CL J051430-5056.6	78.6282	−50.9445	0.51	0.033	4.33	14.2	2	0.6	19.8	3	0.9	0.00	0.06	–	-
LCS-CL J051431-5407.4	78.6300	−54.1245	0.68	0.044	3.58	10.2	2	3.9	–	–	–	0.46	0.36	–	-
LCS-CL J051431-5301.7	78.6309	−53.0285	0.53	0.034	4.32	13.3	2	2.6	17.2	3	3.3	0.26	0.24	1	-
LCS-CL J051436-5233.4	78.6506	−52.5578	0.31	0.025	3.86	12.5	3	7.6	20.2	4	11.7	0.92	0.63	1	-
LCS-CL J051436-5254.3	78.6510	−52.9065	0.47	0.033	3.49	15.8	2	0.8	21.4	3	1.1	0.00	0.06	1	-
LCS-CL J051439-4903.4	78.6643	−49.0570	0.13	0.022	6.96	40.6	3	4.0	91.9	5	6.8	0.13	0.08	–	1
LCS-CL J051440-5100.4	78.6699	−51.0077	0.55	0.034	4.56	15.1	2	0.9	20.4	3	1.3	0.00	0.02	–	-
LCS-CL J051444-5217.0	78.6840	−52.2835	0.42	0.031	3.55	14.4	3	6.2	23.4	4	9.7	0.40	0.49	1	-
LCS-CL J051457-5159.1	78.7398	−51.9852	0.53	0.034	3.82	11.1	2	1.1	12.8	2	1.3	0.04	0.11	1	-
LCS-CL J051457-5143.7	78.7411	−51.7291	0.73	0.038	4.49	26.7	3	1.4	–	–	–	0.00	0.01	1	2
LCS-CL J051459-4855.0	78.7466	−48.9167	0.53	0.034	3.73	10.3	2	0.4	19.0	3	0.8	0.02	0.05	–	-
LCS-CL J051511-5145.6	78.7961	−51.7603	0.56	0.035	3.61	11.9	2	0.3	–	–	–	0.00	0.00	–	-
LCS-CL J051515-5136.7	78.8133	−51.6131	0.61	0.038	3.47	18.0	3	2.7	–	–	–	0.17	0.23	–	-
LCS-CL J051515-5043.3	78.8163	−50.7232	0.50	0.036	3.38	15.9	2	0.6	22.8	3	1.0	0.00	0.00	1	-
LCS-CL J051524-4933.2	78.8514	−49.5538	0.38	0.031	3.91	11.2	2	0.6	15.8	2	1.0	0.00	0.03	–	-
LCS-CL J051524-5130.6	78.8539	−51.5115	0.51	0.036	3.27	10.4	2	1.9	9.4	2	1.8	0.34	0.11	1	-
LCS-CL J051527-4858.4	78.8643	−48.9742	0.56	0.035	4.16	10.1	2	0.4	–	–	–	0.00	0.04	–	-
LCS-CL J051527-5252.5	78.8650	−52.8755	0.27	0.024	3.42	13.2	2	0.4	13.2	2	0.3	0.00	0.04	–	-
LCS-CL J051549-5329.6	78.9542	−53.4939	0.50	0.033	3.51	14.3	2	1.8	18.9	3	2.3	0.20	0.12	–	-
LCS-CL J051558-5439.1	78.9952	−54.6519	0.68	0.039	3.76	26.8	3	0.7	–	–	–	0.00	0.02	–	2
LCS-CL J051602-4943.7	79.0109	−49.7284	0.70	0.041	3.18	10.4	2	1.3	–	–	–	0.00	0.17	–	-
LCS-CL J051607-4855.1	79.0311	−48.9193	0.59	0.035	5.31	31.2	3	2.8	–	–	–	0.00	0.08	–	-
LCS-CL J051619-5421.9	79.0822	−54.3656	0.29	0.024	3.65	16.0	3	2.3	33.1	4	4.7	0.19	0.13	–	-
LCS-CL J051631-5315.6	79.1297	−53.2613	0.56	0.036	3.98	11.4	2	1.4	–	–	–	0.19	0.06	–	-

TABLE 6 — *Continued*

ID	R.A.	Dec	z	δz	Sigma	λ	$\delta\lambda$	$\Delta\lambda$	$\lambda(0.2L_\star)$	$\delta\lambda(0.2L_\star)$	$\Delta\lambda(0.2L_\star)$	Mask 200 kpc	Mask 500 kpc	Edge of Tile	Previous ID
LCS-CL J051637-5430.0	79.1558	−54.5005	0.28	0.023	6.51	56.6	5	18.5	137.4	7	27.7	0.56	0.39	1	0,1,2,3,4,6
LCS-CL J051643-5528.2	79.1804	−55.4713	0.47	0.033	4.04	12.1	2	0.4	23.6	3	1.0	0.00	0.04	–	-
LCS-CL J051649-4959.3	79.2050	−49.9883	0.49	0.034	3.27	12.3	2	1.4	12.9	2	1.4	0.00	0.09	–	-
LCS-CL J051659-5422.1	79.2499	−54.3683	0.23	0.022	3.73	12.2	2	1.0	19.9	3	1.7	0.03	0.08	–	-
LCS-CL J051707-5438.2	79.2813	−54.6379	0.43	0.032	3.95	12.2	2	1.6	18.5	3	2.5	0.00	0.12	–	-
LCS-CL J051722-4917.7	79.3452	−49.2951	0.48	0.033	4.38	11.2	1	0.2	16.8	2	0.3	0.00	0.00	–	-
LCS-CL J051723-5325.5	79.3473	−53.4252	0.37	0.031	6.10	29.2	3	1.2	51.7	4	2.5	0.08	0.03	–	-
LCS-CL J051757-5514.5	79.4905	−55.2427	0.45	0.032	3.80	12.1	2	0.3	17.1	3	0.5	0.01	0.02	–	-
LCS-CL J051759-5326.4	79.4990	−53.4406	0.39	0.033	3.66	12.9	2	3.1	19.3	3	4.2	0.22	0.19	1	-
LCS-CL J051804-4833.1	79.5194	−48.5522	0.44	0.032	4.07	19.3	2	0.7	28.1	3	1.1	0.13	0.03	–	-
LCS-CL J051804-5356.8	79.5205	−53.9478	0.64	0.039	3.42	14.5	3	3.5	–	–	–	0.15	0.23	1	-
LCS-CL J051813-5327.2	79.5544	−53.4548	0.62	0.037	3.52	11.9	2	2.9	–	–	–	0.31	0.24	1	-
LCS-CL J051817-5229.0	79.5734	−52.4835	0.29	0.024	3.24	11.0	2	0.4	13.2	2	0.5	0.00	0.00	1	-
LCS-CL J051819-4900.6	79.5824	−49.0110	0.58	0.036	4.46	19.8	3	0.7	–	–	–	0.00	0.04	–	-
LCS-CL J051824-4841.9	79.6004	−48.6984	0.43	0.033	3.99	19.1	3	0.3	25.7	3	0.5	0.00	0.00	–	-
LCS-CL J051833-5343.8	79.6385	−53.7304	0.61	0.036	3.40	11.2	2	1.7	–	–	–	0.12	0.18	–	-
LCS-CL J051838-4842.2	79.6624	−48.7047	0.24	0.025	3.30	14.1	2	0.2	23.6	3	0.4	0.00	0.01	–	-
LCS-CL J051839-5435.0	79.6666	−54.5849	0.52	0.035	4.24	14.9	2	0.5	16.0	3	0.6	0.00	0.06	–	-
LCS-CL J051849-5240.0	79.7063	−52.6673	0.73	0.040	3.16	14.2	3	0.3	–	–	–	0.00	0.01	1	-
LCS-CL J051849-4856.9	79.7071	−48.9487	0.22	0.024	3.27	10.7	2	1.2	19.2	3	2.1	0.05	0.14	–	-
LCS-CL J051916-5008.9	79.8193	−50.1493	0.49	0.034	3.62	13.1	2	1.1	14.5	3	1.2	0.00	0.08	1	-
LCS-CL J051917-5243.4	79.8216	−52.7249	0.72	0.039	3.44	11.7	2	0.5	–	–	–	0.02	0.01	–	-
LCS-CL J051917-4857.2	79.8223	−48.9536	0.58	0.036	4.09	20.4	2	2.1	–	–	–	0.02	0.11	1	-
LCS-CL J051917-4845.7	79.8228	−48.7619	0.23	0.022	3.37	14.9	2	0.9	34.5	4	2.1	0.00	0.07	1	-
LCS-CL J051918-5441.4	79.8263	−54.6906	0.31	0.024	4.98	15.3	2	1.1	25.5	3	2.0	0.00	0.09	–	-
LCS-CL J051926-5310.9	79.8620	−53.1824	0.67	0.040	3.38	11.3	2	0.6	–	–	–	0.00	0.02	–	-
LCS-CL J051934-5022.4	79.8920	−50.3740	0.56	0.036	4.19	12.9	2	0.6	–	–	–	0.00	0.04	–	-
LCS-CL J051939-5128.9	79.9161	−51.4820	0.75	0.039	3.77	16.4	3	1.5	–	–	–	0.02	0.09	1	-
LCS-CL J051940-4857.5	79.9188	−48.9589	0.30	0.026	3.39	10.1	2	1.6	18.4	3	2.7	0.20	0.17	–	-
LCS-CL J051940-4829.0	79.9206	−48.4845	0.51	0.034	3.81	18.1	3	5.8	22.3	4	7.2	0.00	0.33	1	-
LCS-CL J051947-5454.0	79.9478	−54.9013	0.30	0.027	4.67	10.1	1	0.2	21.0	3	0.4	0.00	0.03	–	-
LCS-CL J051959-5359.5	79.9964	−53.9925	0.64	0.038	3.76	11.9	2	0.1	–	–	–	0.00	0.00	–	-
LCS-CL J052000-5448.1	80.0008	−54.8027	0.40	0.032	4.11	15.8	2	0.8	20.7	3	1.1	0.00	0.09	–	-
LCS-CL J052000-5435.8	80.0030	−54.5975	0.40	0.032	4.13	17.9	2	0.9	22.4	3	1.2	0.00	0.03	–	-
LCS-CL J052016-5346.8	80.0676	−53.7811	0.22	0.023	4.16	18.3	2	1.1	25.9	3	1.7	0.00	0.09	–	-
LCS-CL J052016-5355.7	80.0677	−53.9291	0.62	0.036	4.01	13.0	2	1.9	–	–	–	0.00	0.09	1	-
LCS-CL J052018-5043.7	80.0790	−50.7291	0.65	0.038	4.13	17.2	3	0.0	–	–	–	0.00	0.00	–	-
LCS-CL J052023-5028.8	80.0997	−50.4815	0.60	0.036	3.88	15.9	2	0.3	–	–	–	0.00	0.01	–	-
LCS-CL J052029-5448.7	80.1210	−54.8120	0.43	0.032	4.32	11.8	2	0.1	21.7	3	0.3	0.00	0.00	–	-
LCS-CL J052029-5449.9	80.1234	−54.8318	0.54	0.034	4.43	24.5	3	0.6	31.5	4	0.7	0.02	0.00	–	-
LCS-CL J052030-5036.9	80.1273	−50.6164	0.68	0.042	3.42	19.8	3	2.0	–	–	–	0.01	0.07	–	-
LCS-CL J052034-5136.1	80.1456	−51.6025	0.62	0.036	3.38	10.2	2	0.9	–	–	–	0.00	0.02	–	-
LCS-CL J052037-5043.2	80.1555	−50.7206	0.56	0.035	3.43	10.0	2	0.3	–	–	–	0.00	0.04	–	-
LCS-CL J052037-5521.1	80.1557	−55.3527	0.23	0.022	3.91	22.7	2	0.9	38.0	3	1.6	0.00	0.05	–	-
LCS-CL J052041-5055.3	80.1713	−50.9224	0.69	0.041	3.45	21.4	3	3.2	–	–	–	0.03	0.09	1	-
LCS-CL J052048-5200.0	80.2006	−52.0008	0.69	0.038	3.79	12.6	2	1.0	–	–	–	0.00	0.08	–	-
LCS-CL J052052-5033.8	80.2184	−50.5636	0.63	0.037	3.96	26.7	3	3.4	–	–	–	0.01	0.14	–	-

TABLE 6 — *Continued*

ID	R.A.	Dec	z	δz	Sigma	λ	$\delta\lambda$	$\Delta\lambda$	$\lambda(0.2L_\star)$	$\delta\lambda(0.2L_\star)$	$\Delta\lambda(0.2L_\star)$	Mask 200 kpc	Mask 500 kpc	Edge of Tile	Previous ID
LCS-CL J052110-4957.8	80.2919	−49.9636	0.23	0.023	4.47	15.9	2	1.6	39.3	4	4.8	0.00	0.06	–	-
LCS-CL J052110-5031.0	80.2940	−50.5179	0.63	0.036	4.09	12.6	2	1.1	–	–	–	0.12	0.13	–	-
LCS-CL J052114-5104.3	80.3107	−51.0718	0.70	0.038	5.60	61.8	4	3.4	–	–	–	0.00	0.06	–	2,3
LCS-CL J052115-5030.3	80.3149	−50.5050	0.25	0.023	3.94	16.7	2	1.1	25.8	3	1.7	0.00	0.05	–	-
LCS-CL J052120-5508.0	80.3351	−55.1335	0.45	0.033	3.47	12.2	2	2.7	21.0	3	4.9	0.02	0.26	1	-
LCS-CL J052124-5451.4	80.3511	−54.8578	0.54	0.036	3.37	16.2	3	2.0	22.9	4	2.8	0.21	0.15	–	-
LCS-CL J052125-5024.1	80.3551	−50.4023	0.73	0.039	4.14	14.7	3	0.4	–	–	–	0.00	0.02	–	-
LCS-CL J052138-5108.7	80.4115	−51.1464	0.72	0.039	3.68	13.1	2	0.4	–	–	–	0.00	0.06	–	-
LCS-CL J052140-5051.2	80.4186	−50.8541	0.71	0.038	4.49	26.4	3	2.9	–	–	–	0.00	0.01	–	-
LCS-CL J052146-5351.2	80.4435	−53.8534	0.71	0.038	3.35	21.7	3	4.0	–	–	–	0.09	0.12	1	-
LCS-CL J052155-5106.0	80.4806	−51.1006	0.70	0.039	3.60	15.7	2	0.3	–	–	–	0.00	0.02	–	-
LCS-CL J052158-5458.2	80.4944	−54.9715	0.50	0.034	3.38	11.6	2	2.2	16.1	3	2.9	0.34	0.13	1	-
LCS-CL J052158-4830.7	80.4951	−48.5121	0.48	0.033	4.00	11.3	2	1.2	10.4	2	1.0	0.00	0.08	1	-
LCS-CL J052159-5140.4	80.4984	−51.6741	0.58	0.035	5.23	20.0	3	1.1	–	–	–	0.00	0.07	–	-
LCS-CL J052200-5027.0	80.5034	−50.4502	0.56	0.034	6.03	64.0	4	4.8	–	–	–	0.06	0.20	–	2,3
LCS-CL J052206-5436.8	80.5286	−54.6141	0.59	0.037	3.81	12.4	2	0.4	–	–	–	0.00	0.05	1	-
LCS-CL J052213-5544.8	80.5563	−55.7473	0.15	0.020	3.88	11.7	2	1.8	15.8	2	2.6	0.06	0.10	1	-
LCS-CL J052224-5041.9	80.6032	−50.6991	0.57	0.034	4.68	24.0	3	2.6	–	–	–	0.00	0.01	1	-
LCS-CL J052231-5107.3	80.6330	−51.1231	0.57	0.037	3.92	13.9	3	1.8	–	–	–	0.00	0.15	1	-
LCS-CL J052234-5122.9	80.6421	−51.3827	0.52	0.035	3.85	13.8	2	1.4	15.0	3	1.4	0.04	0.16	1	-
LCS-CL J052241-5507.3	80.6720	−55.1217	0.27	0.025	3.83	11.0	2	1.8	13.3	2	2.1	0.05	0.17	1	-
LCS-CL J052241-5112.3	80.6744	−51.2060	0.64	0.037	3.97	18.3	3	1.2	–	–	–	0.06	0.06	1	-
LCS-CL J052244-5014.1	80.6869	−50.2351	0.56	0.036	3.11	10.3	2	0.6	–	–	–	0.00	0.05	1	-
LCS-CL J052244-5454.6	80.6870	−54.9107	0.73	0.039	3.98	17.1	3	0.7	–	–	–	0.02	0.01	–	-
LCS-CL J052254-5103.8	80.7275	−51.0641	0.55	0.035	3.89	10.8	2	1.2	15.6	3	1.8	0.00	0.15	–	-
LCS-CL J052304-5116.9	80.7678	−51.2818	0.53	0.034	3.56	16.4	3	7.1	26.3	4	11.6	0.38	0.39	–	-
LCS-CL J052306-5558.3	80.7781	−55.9731	0.44	0.032	4.02	12.7	2	1.0	14.4	3	1.1	0.00	0.09	–	-
LCS-CL J052310-5150.5	80.7934	−51.8431	0.67	0.039	3.99	11.7	2	1.3	–	–	–	0.00	0.03	–	-
LCS-CL J052328-5137.3	80.8675	−51.6225	0.50	0.033	4.46	13.0	2	0.6	19.8	3	1.1	0.00	0.03	–	-
LCS-CL J052335-5116.8	80.8998	−51.2807	0.44	0.032	5.80	23.1	3	3.1	40.8	4	6.7	0.00	0.04	–	-
LCS-CL J052344-5451.5	80.9345	−54.8588	0.51	0.034	3.60	10.0	2	1.1	12.7	2	1.4	0.02	0.13	–	-
LCS-CL J052350-5436.0	80.9604	−54.6012	0.74	0.039	3.30	11.4	2	0.2	–	–	–	0.01	0.01	–	-
LCS-CL J052409-5143.1	81.0381	−51.7189	0.71	0.039	3.15	15.9	3	0.8	–	–	–	0.01	0.01	–	-
LCS-CL J052414-5100.3	81.0612	−51.0059	0.24	0.023	5.08	25.2	2	1.4	41.2	4	2.6	0.00	0.04	–	-
LCS-CL J052420-5214.2	81.0861	−52.2370	0.72	0.041	3.39	14.8	3	1.4	–	–	–	0.00	0.01	–	-
LCS-CL J052425-5150.5	81.1079	−51.8426	0.75	0.039	3.48	14.9	3	1.3	–	–	–	0.00	0.06	–	-
LCS-CL J052431-5523.6	81.1293	−55.3948	0.20	0.026	3.82	16.9	2	1.6	23.1	3	2.2	0.10	0.13	–	-
LCS-CL J052442-5550.5	81.1761	−55.8428	0.20	0.022	5.12	38.1	3	5.7	56.5	5	8.3	0.23	0.18	–	-
LCS-CL J052444-5340.1	81.1834	−53.6691	0.25	0.023	3.95	15.6	2	0.7	26.0	3	1.2	0.01	0.04	–	-
LCS-CL J052502-5144.1	81.2614	−51.7352	0.24	0.024	3.70	10.8	2	0.7	12.2	2	0.8	0.00	0.08	–	-
LCS-CL J052503-5444.1	81.2631	−54.7357	0.69	0.043	3.69	19.4	3	2.7	–	–	–	0.00	0.04	–	-
LCS-CL J052505-5439.0	81.2745	−54.6507	0.50	0.035	3.56	11.4	2	3.8	15.2	3	5.4	0.24	0.34	–	-
LCS-CL J052506-5111.8	81.2779	−51.1973	0.29	0.024	3.87	11.9	2	0.5	18.9	3	1.0	0.00	0.03	–	-
LCS-CL J052509-5459.4	81.2912	−54.9913	0.73	0.041	3.18	11.8	2	1.7	–	–	–	0.18	0.16	–	-
LCS-CL J052510-5517.4	81.2929	−55.2912	0.15	0.020	4.84	25.1	3	2.9	52.3	4	6.6	0.16	0.09	–	0
LCS-CL J052516-5134.1	81.3178	−51.5684	0.22	0.023	4.98	21.6	3	1.5	40.3	4	2.9	0.15	0.06	–	-
LCS-CL J052537-5312.6	81.4059	−53.2107	0.37	0.038	3.99	13.6	2	0.3	22.9	3	0.6	0.00	0.01	–	-

TABLE 6 — *Continued*

ID	R.A.	Dec	z	δz	Sigma	λ	$\delta\lambda$	$\Delta\lambda$	$\lambda(0.2L_\star)$	$\delta\lambda(0.2L_\star)$	$\Delta\lambda(0.2L_\star)$	Mask 200 kpc	Mask 500 kpc	Edge of Tile	Previous ID
LCS-CL J052539-5612.6	81.4131	−56.2115	0.13	0.025	3.85	19.8	3	3.1	41.2	4	7.6	0.11	0.13	1	0,2
LCS-CL J052552-5458.6	81.4672	−54.9775	0.63	0.039	3.74	27.2	4	13.1	–	–	–	0.35	0.56	1	-
LCS-CL J052613-5258.4	81.5564	−52.9743	0.71	0.040	3.46	10.4	3	3.2	–	–	–	0.31	0.35	1	-
LCS-CL J052616-5531.3	81.5677	−55.5227	0.50	0.033	3.93	11.2	2	0.3	14.0	2	0.5	0.00	0.01	–	-
LCS-CL J052620-5527.8	81.5841	−55.4645	0.45	0.034	3.36	12.2	2	2.3	19.2	3	3.9	0.00	0.22	–	-
LCS-CL J052621-5102.7	81.5878	−51.0463	0.59	0.041	3.53	14.3	2	1.5	–	–	–	0.10	0.12	1	-
LCS-CL J052627-5156.0	81.6147	−51.9345	0.29	0.027	3.41	12.5	2	1.0	25.0	3	2.2	0.09	0.08	–	-
LCS-CL J052636-4955.0	81.6536	−49.9169	0.56	0.037	3.94	10.7	2	0.9	–	–	–	0.14	0.12	1	-
LCS-CL J052643-4942.5	81.6818	−49.7093	0.50	0.033	4.51	18.8	3	5.2	32.1	4	9.3	0.26	0.30	1	-
LCS-CL J052656-5208.4	81.7349	−52.1413	0.20	0.021	5.10	12.0	2	1.6	15.8	3	2.1	0.09	0.05	–	-
LCS-CL J052703-5325.4	81.7630	−53.4245	0.43	0.032	4.76	14.2	2	0.9	25.9	3	1.6	0.16	0.05	–	-
LCS-CL J052709-5536.4	81.7888	−55.6075	0.38	0.033	3.50	12.7	2	0.6	23.7	3	1.3	0.05	0.06	–	-
LCS-CL J052714-5436.6	81.8096	−54.6111	0.49	0.033	4.77	17.8	2	2.2	27.0	3	3.5	0.00	0.10	–	-
LCS-CL J052722-5128.4	81.8452	−51.4740	0.66	0.040	3.29	10.6	2	1.0	–	–	–	0.00	0.10	1	-
LCS-CL J052735-5214.0	81.8973	−52.2349	0.74	0.040	3.32	13.2	2	0.3	–	–	–	0.00	0.00	–	-
LCS-CL J052739-5201.4	81.9158	−52.0249	0.74	0.039	3.74	21.0	3	0.7	–	–	–	0.00	0.01	–	-
LCS-CL J052744-5318.5	81.9366	−53.3088	0.49	0.033	3.53	14.9	3	4.2	24.5	4	6.6	0.31	0.30	1	-
LCS-CL J052752-5359.4	81.9669	−53.9912	0.57	0.036	4.88	11.2	2	0.6	–	–	–	0.02	0.02	–	-
LCS-CL J052753-5339.4	81.9730	−53.6576	0.61	0.036	4.84	18.0	2	0.3	–	–	–	0.00	0.00	–	-
LCS-CL J052808-5308.5	82.0367	−53.1425	0.69	0.039	3.24	17.5	3	1.5	–	–	–	0.04	0.04	–	-
LCS-CL J052810-5148.6	82.0444	−51.8110	0.69	0.037	4.52	27.0	3	2.8	–	–	–	0.00	0.06	–	2
LCS-CL J052812-5518.5	82.0518	−55.3086	0.68	0.044	3.35	10.1	2	1.0	–	–	–	0.14	0.07	–	-
LCS-CL J052816-5443.5	82.0692	−54.7261	0.46	0.033	3.62	12.1	2	0.2	16.7	3	0.3	0.00	0.00	–	-
LCS-CL J052841-5421.0	82.1735	−54.3516	0.50	0.033	4.94	12.0	2	0.2	23.5	3	0.4	0.00	0.02	–	-
LCS-CL J052841-5206.0	82.1736	−52.1011	0.26	0.022	3.25	16.9	3	6.0	32.0	4	10.5	0.57	0.36	1	-
LCS-CL J052849-5146.9	82.2053	−51.7819	0.74	0.039	3.35	12.7	2	0.6	–	–	–	0.05	0.06	–	-
LCS-CL J052850-5300.2	82.2112	−53.0046	0.49	0.033	4.12	11.3	2	0.3	23.7	3	0.8	0.00	0.04	–	-
LCS-CL J052852-5218.6	82.2183	−52.3106	0.32	0.025	3.35	10.0	2	0.5	22.1	3	1.1	0.00	0.05	–	-
LCS-CL J052915-5453.9	82.3134	−54.8987	0.62	0.039	3.19	13.0	2	0.9	–	–	–	0.00	0.04	–	-
LCS-CL J052922-5210.4	82.3427	−52.1745	0.25	0.026	3.24	10.1	2	1.0	21.7	3	2.3	0.06	0.12	–	-
LCS-CL J052932-5327.2	82.3844	−53.4538	0.58	0.035	3.62	11.0	2	0.4	–	–	–	0.00	0.01	–	-
LCS-CL J052948-5007.5	82.4527	−50.1259	0.62	0.038	3.56	27.6	4	7.4	–	–	–	0.04	0.21	1	-
LCS-CL J052951-5516.1	82.4659	−55.2699	0.65	0.037	4.54	20.4	3	2.3	–	–	–	0.00	0.07	1	2
LCS-CL J052956-5211.5	82.4856	−52.1917	0.27	0.023	3.32	12.9	2	1.2	30.6	4	3.1	0.00	0.10	1	-
LCS-CL J052957-5409.6	82.4898	−54.1611	0.72	0.038	3.45	19.0	4	7.4	–	–	–	0.13	0.41	1	-
LCS-CL J053007-4957.0	82.5314	−49.9506	0.17	0.021	5.31	11.3	2	0.9	20.6	3	2.0	0.00	0.07	1	-
LCS-CL J053014-5104.3	82.5595	−51.0721	0.55	0.034	4.20	11.3	2	0.9	15.3	3	1.2	0.00	0.09	–	-
LCS-CL J053018-5201.4	82.5761	−52.0244	0.46	0.032	3.97	13.6	2	1.1	28.3	4	2.2	0.00	0.05	–	-
LCS-CL J053022-5208.9	82.5945	−52.1484	0.25	0.023	4.71	14.7	2	1.4	36.4	4	4.0	0.00	0.05	1	-
LCS-CL J053024-5337.2	82.6034	−53.6202	0.70	0.040	3.75	12.4	3	3.6	–	–	–	0.24	0.32	–	-
LCS-CL J053029-5340.7	82.6211	−53.6790	0.56	0.035	4.49	11.9	2	1.2	–	–	–	0.00	0.02	–	-
LCS-CL J053036-5213.4	82.6526	−52.2236	0.68	0.039	3.22	12.7	3	1.8	–	–	–	0.00	0.18	–	-
LCS-CL J053048-5129.8	82.7035	−51.4981	0.69	0.039	3.58	11.7	2	0.5	–	–	–	0.00	0.00	1	-
LCS-CL J053052-5520.9	82.7182	−55.3490	0.69	0.038	3.71	13.4	2	0.2	–	–	–	0.00	0.01	–	2
LCS-CL J053108-5111.9	82.7843	−51.1988	0.58	0.035	4.08	16.8	2	1.6	–	–	–	0.20	0.10	–	-
LCS-CL J053108-5310.5	82.7849	−53.1766	0.75	0.039	3.92	12.0	2	0.8	–	–	–	0.00	0.06	–	-
LCS-CL J053119-5001.2	82.8295	−50.0207	0.27	0.024	3.87	11.1	2	2.6	17.1	3	4.3	0.17	0.18	–	-

TABLE 6 — *Continued*

ID	R.A.	Dec	z	δz	Sigma	λ	$\delta\lambda$	$\Delta\lambda$	$\lambda(0.2L_\star)$	$\delta\lambda(0.2L_\star)$	$\Delta\lambda(0.2L_\star)$	Mask 200 kpc	Mask 500 kpc	Edge of Tile	Previous ID
LCS-CL J053126-5522.9	82.8611	−55.3822	0.74	0.039	3.47	10.1	2	0.5	–	–	–	0.06	0.02	–	-
LCS-CL J053132-4953.1	82.8872	−49.8852	0.69	0.042	3.48	12.7	3	1.5	–	–	–	0.09	0.08	–	-
LCS-CL J053137-5100.2	82.9071	−51.0038	0.44	0.034	4.07	12.8	2	2.3	17.2	3	3.0	0.13	0.20	–	-
LCS-CL J053143-5202.1	82.9295	−52.0354	0.69	0.038	4.14	22.1	3	0.2	–	–	–	0.00	0.00	–	-
LCS-CL J053154-5156.3	82.9761	−51.9393	0.74	0.038	3.63	31.7	4	1.9	–	–	–	0.00	0.06	–	-
LCS-CL J053154-5520.5	82.9787	−55.3420	0.26	0.023	4.38	45.9	4	2.8	106.3	5	4.5	0.02	0.05	–	2,6
LCS-CL J053203-5000.7	83.0163	−50.0127	0.19	0.021	4.08	12.4	2	1.5	24.4	3	3.4	0.00	0.08	–	-
LCS-CL J053205-5217.0	83.0220	−52.2836	0.49	0.034	4.39	10.4	2	0.8	20.9	3	2.3	0.00	0.04	–	-
LCS-CL J053208-5102.4	83.0373	−51.0412	0.58	0.035	3.82	12.8	2	1.4	–	–	–	0.07	0.14	–	-
LCS-CL J053221-5323.1	83.0902	−53.3863	0.63	0.038	3.70	14.2	3	1.1	–	–	–	0.06	0.10	–	-
LCS-CL J053224-5131.6	83.1002	−51.5278	0.56	0.034	4.28	10.6	2	0.9	–	–	–	0.13	0.07	–	-
LCS-CL J053227-5302.4	83.1160	−53.0408	0.75	0.039	3.70	10.8	3	2.4	–	–	–	0.39	0.24	–	-
LCS-CL J053237-5013.3	83.1571	−50.2225	0.37	0.036	4.26	11.0	2	0.3	20.1	3	0.7	0.00	0.00	–	-
LCS-CL J053243-5244.6	83.1829	−52.7441	0.27	0.024	3.83	17.8	2	1.0	26.3	3	1.5	0.00	0.03	–	-
LCS-CL J053251-5255.0	83.2127	−52.9175	0.63	0.036	3.72	11.1	2	0.5	–	–	–	0.00	0.02	–	-
LCS-CL J053258-5331.0	83.2435	−53.5180	0.29	0.023	4.40	14.7	2	0.8	28.9	3	1.6	0.00	0.04	–	-
LCS-CL J053331-4949.9	83.3797	−49.8319	0.59	0.037	4.04	12.0	3	3.4	–	–	–	0.00	0.27	1	-
LCS-CL J053335-5218.3	83.3990	−52.3057	0.47	0.032	3.76	14.4	2	1.0	21.5	3	1.6	0.00	0.06	1	-
LCS-CL J053339-5353.2	83.4128	−53.8879	0.28	0.024	4.71	18.2	3	3.1	38.4	4	7.0	0.12	0.15	1	-
LCS-CL J053345-5257.6	83.4385	−52.9616	0.58	0.035	3.57	12.5	2	1.1	–	–	–	0.05	0.08	1	-
LCS-CL J053354-5219.0	83.4756	−52.3172	0.75	0.038	3.27	17.1	3	0.3	–	–	–	0.00	0.00	1	-
LCS-CL J053418-5222.1	83.5755	−52.3697	0.48	0.033	3.52	10.8	2	1.6	12.1	3	1.7	0.11	0.22	–	-
LCS-CL J053426-5328.2	83.6087	−53.4702	0.62	0.036	3.91	11.0	2	1.1	–	–	–	0.00	0.09	–	-
LCS-CL J053427-5202.0	83.6135	−52.0337	0.48	0.033	4.71	18.7	3	1.9	34.2	4	4.3	0.00	0.10	–	-
LCS-CL J053500-5217.8	83.7508	−52.2979	0.50	0.034	4.36	11.8	2	0.9	12.9	2	0.9	0.00	0.09	–	-
LCS-CL J053501-5320.6	83.7554	−53.3448	0.53	0.034	4.80	16.0	3	3.5	25.5	4	5.2	0.25	0.34	–	2
LCS-CL J053516-5224.8	83.8194	−52.4146	0.23	0.022	3.57	10.6	2	0.5	11.6	2	0.6	0.00	0.04	–	-
LCS-CL J053524-5226.7	83.8512	−52.4457	0.70	0.040	3.70	17.3	3	0.8	–	–	–	0.00	0.07	–	-
LCS-CL J053531-5050.7	83.8810	−50.8456	0.58	0.035	4.25	12.5	2	1.2	–	–	–	0.00	0.04	–	-
LCS-CL J053544-5229.2	83.9335	−52.4875	0.40	0.034	3.72	11.8	2	0.3	15.9	3	0.5	0.00	0.01	–	-
LCS-CL J053605-5338.7	84.0220	−53.6463	0.61	0.036	4.08	14.0	2	1.0	–	–	–	0.06	0.13	–	-
LCS-CL J053608-5157.8	84.0363	−51.9638	0.47	0.032	3.86	10.4	2	1.2	24.2	4	3.0	0.00	0.15	–	-
LCS-CL J053617-5155.1	84.0716	−51.9190	0.57	0.035	4.27	14.9	2	0.4	–	–	–	0.00	0.01	–	-
LCS-CL J053637-5142.2	84.1566	−51.7050	0.29	0.024	4.12	15.2	2	1.7	23.9	3	3.3	0.00	0.09	–	-
LCS-CL J053658-5302.4	84.2434	−53.0406	0.49	0.033	4.80	12.3	2	1.7	21.5	3	2.9	0.21	0.09	–	-
LCS-CL J053739-5041.1	84.4138	−50.6858	0.73	0.040	3.55	11.1	2	0.7	–	–	–	0.00	0.08	–	-
LCS-CL J053806-4949.3	84.5260	−49.8231	0.69	0.039	3.31	16.0	3	1.0	–	–	–	0.02	0.08	–	-
LCS-CL J053812-5040.9	84.5522	−50.6819	0.26	0.024	3.45	12.1	3	4.7	23.1	4	8.6	0.40	0.39	–	-
LCS-CL J053822-5009.3	84.5958	−50.1566	0.40	0.040	4.77	14.0	2	1.3	15.1	3	1.5	0.07	0.10	–	-
LCS-CL J053823-5028.4	84.5964	−50.4747	0.75	0.038	3.23	10.2	2	0.1	–	–	–	0.00	0.00	–	-
LCS-CL J053825-5305.6	84.6059	−53.0948	0.71	0.039	3.19	14.2	3	1.2	–	–	–	0.08	0.11	–	-
LCS-CL J053827-5338.2	84.6152	−53.6375	0.66	0.042	3.75	15.8	2	0.6	–	–	–	0.00	0.04	–	-
LCS-CL J053849-5345.9	84.7049	−53.7663	0.38	0.031	3.94	16.7	2	2.0	33.6	4	3.5	0.21	0.05	–	-
LCS-CL J053850-5341.5	84.7099	−53.6918	0.41	0.032	3.85	27.3	3	0.8	39.2	4	1.1	0.00	0.01	–	-
LCS-CL J053855-5324.5	84.7296	−53.4099	0.22	0.022	5.37	11.7	2	1.4	29.8	3	3.6	0.17	0.11	–	-
LCS-CL J053903-5336.9	84.7657	−53.6161	0.64	0.038	4.51	16.8	2	0.1	–	–	–	0.00	0.00	–	-
LCS-CL J053938-5056.1	84.9119	−50.9359	0.39	0.031	4.65	16.4	2	2.2	35.1	4	5.9	0.00	0.08	–	-

TABLE 6 — *Continued*

ID	R.A.	Dec	z	δz	Sigma	λ	$\delta\lambda$	$\Delta\lambda$	$\lambda(0.2L_\star)$	$\delta\lambda(0.2L_\star)$	$\Delta\lambda(0.2L_\star)$	Mask 200 kpc	Mask 500 kpc	Edge of Tile	Previous ID
LCS-CL J053949-5352.8	84.9550	−53.8810	0.50	0.033	4.37	20.0	3	2.1	33.1	4	3.5	0.00	0.08	1	-
LCS-CL J054016-5346.3	85.0669	−53.7730	0.19	0.023	3.93	10.2	2	1.1	12.1	2	1.3	0.12	0.10	–	-
LCS-CL J054044-5147.2	85.1864	−51.7877	0.55	0.035	4.53	11.8	2	1.5	15.7	3	2.0	0.19	0.16	–	-
LCS-CL J054052-5328.9	85.2196	−53.4824	0.71	0.040	3.96	10.2	2	0.2	–	–	–	0.00	0.01	–	-
LCS-CL J054056-5311.8	85.2364	−53.1979	0.44	0.033	3.92	10.2	2	3.0	14.1	3	4.3	0.14	0.39	–	-
LCS-CL J054101-5253.9	85.2576	−52.8999	0.63	0.037	4.15	14.3	2	0.5	–	–	–	0.00	0.02	–	-
LCS-CL J054109-5133.9	85.2906	−51.5660	0.63	0.036	3.77	21.9	3	1.3	–	–	–	0.00	0.00	1	-
LCS-CL J054111-5209.7	85.2972	−52.1618	0.75	0.038	3.34	10.1	2	0.6	–	–	–	0.00	0.08	–	-
LCS-CL J054126-5252.7	85.3590	−52.8787	0.68	0.038	3.29	13.8	2	0.4	–	–	–	0.00	0.01	1	-
LCS-CL J054126-5143.2	85.3605	−51.7215	0.37	0.031	4.30	11.9	2	1.3	33.1	4	3.5	0.20	0.08	1	-
LCS-CL J054159-5036.8	85.4975	−50.6139	0.44	0.033	3.50	10.2	2	1.2	23.8	3	3.4	0.00	0.08	–	-
LCS-CL J054203-5301.0	85.5162	−53.0178	0.64	0.041	3.58	11.0	2	1.3	–	–	–	0.16	0.08	–	-
LCS-CL J054204-5343.2	85.5174	−53.7207	0.56	0.035	4.79	13.5	2	1.8	–	–	–	0.00	0.12	1	-
LCS-CL J054209-5104.8	85.5382	−51.0803	0.65	0.039	3.67	11.4	2	0.3	–	–	–	0.00	0.02	–	-
LCS-CL J054219-5057.6	85.5829	−50.9615	0.38	0.032	4.24	12.4	2	0.4	25.5	3	1.0	0.00	0.00	–	-
LCS-CL J054252-5238.8	85.7179	−52.6474	0.52	0.034	5.18	19.5	2	0.4	34.8	4	1.2	0.00	0.00	–	-
LCS-CL J054320-5208.8	85.8339	−52.1467	0.58	0.036	3.43	12.3	2	1.0	–	–	–	0.00	0.09	–	-
LCS-CL J054322-5219.8	85.8447	−52.3315	0.51	0.034	4.90	20.7	2	1.1	34.4	4	2.0	0.00	0.06	–	-
LCS-CL J054332-5056.8	85.8834	−50.9477	0.44	0.031	6.40	52.0	4	5.3	85.0	5	8.5	0.02	0.12	–	2
LCS-CL J054334-5357.7	85.8949	−53.9624	0.33	0.024	4.57	15.1	3	2.0	38.3	4	5.7	0.15	0.09	–	-
LCS-CL J054335-5437.4	85.8984	−54.6246	0.38	0.033	3.94	10.8	2	0.4	18.2	3	0.8	0.00	0.02	–	-
LCS-CL J054345-5149.6	85.9403	−51.8278	0.50	0.033	4.18	27.5	3	3.2	51.0	5	5.3	0.23	0.04	–	-
LCS-CL J054348-5038.7	85.9539	−50.6454	0.33	0.026	3.69	12.7	2	1.3	14.2	2	1.3	0.18	0.11	–	-
LCS-CL J054350-5236.0	85.9602	−52.6009	0.69	0.038	4.04	11.7	2	0.6	–	–	–	0.06	0.06	–	-
LCS-CL J054351-5112.4	85.9635	−51.2071	0.33	0.024	5.58	20.7	2	1.8	43.2	4	3.4	0.09	0.12	–	2
LCS-CL J054358-5313.8	85.9925	−53.2304	0.29	0.023	5.28	17.0	2	0.9	34.5	4	2.3	0.00	0.05	–	2
LCS-CL J054402-5103.5	86.0088	−51.0583	0.33	0.030	3.40	10.7	2	0.9	22.2	3	2.1	0.00	0.02	–	-
LCS-CL J054405-5024.5	86.0229	−50.4099	0.31	0.024	3.83	15.5	2	0.9	18.3	3	1.4	0.00	0.02	–	-
LCS-CL J054408-5050.7	86.0337	−50.8458	0.30	0.028	4.01	12.0	2	0.9	14.9	3	1.2	0.00	0.09	–	-
LCS-CL J054414-5342.1	86.0608	−53.7018	0.52	0.034	3.81	12.6	2	0.8	17.5	3	1.0	0.01	0.08	–	-
LCS-CL J054451-5047.2	86.2128	−50.7876	0.22	0.023	3.21	11.3	2	1.7	19.3	3	3.3	0.00	0.13	1	-
LCS-CL J054458-5046.7	86.2435	−50.7790	0.66	0.039	3.37	10.8	2	0.5	–	–	–	0.00	0.02	–	-
LCS-CL J054501-5458.7	86.2580	−54.9792	0.40	0.032	4.44	10.3	2	0.3	20.3	3	0.8	0.00	0.03	–	-
LCS-CL J054508-5105.2	86.2853	−51.0868	0.74	0.039	4.63	15.0	3	0.4	–	–	–	0.00	0.00	1	-
LCS-CL J054510-5450.0	86.2937	−54.8337	0.16	0.021	4.71	11.5	2	1.1	20.4	3	2.0	0.08	0.09	–	-
LCS-CL J054516-5022.1	86.3172	−50.3699	0.32	0.023	4.88	10.1	2	0.5	23.6	3	1.6	0.00	0.04	–	-
LCS-CL J054520-5047.2	86.3334	−50.7882	0.22	0.022	3.87	10.9	2	1.2	18.9	3	2.4	0.06	0.11	–	-
LCS-CL J054526-5120.0	86.3615	−51.3342	0.68	0.040	3.86	17.6	3	1.1	–	–	–	0.00	0.11	–	-
LCS-CL J054539-4956.0	86.4162	−49.9347	0.72	0.039	3.50	13.1	3	0.5	–	–	–	0.00	0.02	–	-
LCS-CL J054555-5122.1	86.4812	−51.3698	0.75	0.040	3.40	14.0	3	0.7	–	–	–	0.00	0.06	–	-
LCS-CL J054556-5448.4	86.4848	−54.8078	0.39	0.039	3.11	11.8	2	1.1	15.2	3	1.4	0.04	0.12	1	-
LCS-CL J054556-5132.3	86.4864	−51.5400	0.70	0.039	4.50	14.8	3	1.2	–	–	–	0.00	0.04	–	-
LCS-CL J054603-5148.9	86.5128	−51.8166	0.56	0.035	3.43	11.3	2	1.0	–	–	–	0.00	0.09	–	-
LCS-CL J054610-5338.2	86.5428	−53.6369	0.43	0.032	4.05	11.9	2	0.8	19.6	3	1.4	0.00	0.09	–	-
LCS-CL J054619-5200.0	86.5833	−52.0010	0.63	0.038	3.94	12.0	2	0.1	–	–	–	0.00	0.00	–	-
LCS-CL J054653-5550.4	86.7244	−55.8409	0.50	0.035	3.56	10.1	2	3.2	15.2	3	4.7	0.39	0.22	1	-
LCS-CL J054654-5142.5	86.7261	−51.7097	0.34	0.025	3.45	12.8	2	1.4	15.1	3	1.6	0.00	0.07	–	-

TABLE 6 — *Continued*

ID	R.A.	Dec	z	δz	Sigma	λ	$\delta\lambda$	$\Delta\lambda$	$\lambda(0.2L_\star)$	$\delta\lambda(0.2L_\star)$	$\Delta\lambda(0.2L_\star)$	Mask 200 kpc	Mask 500 kpc	Edge of Tile	Previous ID
LCS-CL J054654-5125.3	86.7291	−51.4219	0.33	0.024	4.50	20.4	2	1.0	31.7	3	1.6	0.00	0.05	–	-
LCS-CL J054710-5112.0	86.7940	−51.2013	0.28	0.024	3.83	32.8	3	6.9	53.2	5	12.1	0.00	0.12	–	-
LCS-CL J054712-5559.5	86.8001	−55.9932	0.61	0.036	4.03	11.4	2	0.9	–	–	–	0.19	0.07	–	-
LCS-CL J054712-5552.1	86.8016	−55.8696	0.72	0.043	3.30	16.4	3	2.7	–	–	–	0.21	0.16	–	-
LCS-CL J054717-5604.6	86.8248	−56.0768	0.75	0.041	3.30	13.4	3	1.2	–	–	–	0.02	0.02	–	-
LCS-CL J054720-4957.2	86.8344	−49.9548	0.41	0.034	3.42	13.5	2	2.0	21.3	3	3.2	0.05	0.25	–	-
LCS-CL J054721-5549.0	86.8383	−55.8183	0.67	0.037	5.40	44.0	4	6.6	–	–	–	0.11	0.23	–	2
LCS-CL J054726-5248.0	86.8624	−52.8012	0.44	0.032	4.58	15.3	2	0.6	21.6	3	0.9	0.00	0.00	–	-
LCS-CL J054727-5617.5	86.8656	−56.2929	0.57	0.036	3.99	14.4	2	2.2	–	–	–	0.00	0.09	1	-
LCS-CL J054742-5548.5	86.9259	−55.8099	0.50	0.033	4.34	20.7	3	2.6	45.5	5	5.7	0.16	0.12	–	2
LCS-CL J054744-5047.2	86.9371	−50.7879	0.31	0.025	4.15	14.2	2	0.3	16.4	2	0.3	0.00	0.00	–	-
LCS-CL J054747-5614.7	86.9468	−56.2450	0.67	0.037	4.47	26.7	3	3.7	–	–	–	0.09	0.20	–	-
LCS-CL J054759-5008.4	86.9973	−50.1413	0.34	0.038	3.78	12.0	2	1.9	23.2	3	3.5	0.26	0.05	1	-
LCS-CL J054808-5004.6	87.0363	−50.0770	0.68	0.043	3.39	10.8	2	0.7	–	–	–	0.00	0.06	1	-
LCS-CL J054809-5039.8	87.0379	−50.6650	0.58	0.035	4.04	13.0	2	1.0	–	–	–	0.19	0.07	1	-
LCS-CL J054811-5556.0	87.0472	−55.9337	0.61	0.038	3.81	18.0	3	2.4	–	–	–	0.00	0.10	–	2
LCS-CL J054825-5151.4	87.1044	−51.8569	0.51	0.034	3.79	13.3	2	0.5	19.2	3	0.7	0.00	0.05	–	-
LCS-CL J054835-4952.8	87.1468	−49.8812	0.42	0.033	3.76	10.0	2	0.5	11.5	2	0.6	0.00	0.03	–	-
LCS-CL J054839-5157.8	87.1651	−51.9645	0.52	0.034	3.26	14.2	2	1.1	24.5	4	1.9	0.02	0.09	1	-
LCS-CL J054841-5348.1	87.1715	−53.8021	0.40	0.031	3.72	14.5	2	0.3	16.8	3	0.4	0.00	0.00	–	-
LCS-CL J054844-5155.0	87.1839	−51.9178	0.56	0.036	4.13	16.7	2	1.1	–	–	–	0.00	0.11	1	-
LCS-CL J054853-5155.1	87.2222	−51.9199	0.38	0.043	3.72	11.8	2	1.2	15.2	3	1.5	0.04	0.09	1	-
LCS-CL J054914-5550.7	87.3124	−55.8455	0.69	0.042	3.50	10.1	2	0.3	–	–	–	0.00	0.02	–	-
LCS-CL J054923-5135.5	87.3494	−51.5931	0.27	0.026	4.59	11.4	2	0.8	16.8	3	1.3	0.00	0.11	–	-
LCS-CL J054924-5006.2	87.3519	−50.1049	0.59	0.036	4.12	18.5	2	0.6	–	–	–	0.00	0.01	–	-
LCS-CL J054933-5227.0	87.3905	−52.4517	0.44	0.032	3.99	17.6	2	1.0	22.1	3	1.2	0.00	0.06	–	2
LCS-CL J054947-5009.6	87.4495	−50.1601	0.73	0.040	3.57	18.1	3	3.1	–	–	–	0.28	0.21	–	-
LCS-CL J054953-5355.9	87.4711	−53.9326	0.44	0.032	3.47	17.0	3	5.5	21.5	4	6.8	0.18	0.37	1	-
LCS-CL J055007-5043.0	87.5316	−50.7183	0.66	0.040	3.44	12.1	2	0.1	–	–	–	0.00	0.02	–	-
LCS-CL J055008-5441.3	87.5344	−54.6889	0.53	0.037	3.18	30.9	4	7.7	52.2	5	13.5	0.04	0.14	1	-
LCS-CL J055019-5019.6	87.5813	−50.3269	0.66	0.037	4.28	39.7	4	1.0	–	–	–	0.00	0.01	–	-
LCS-CL J055023-5052.0	87.5998	−50.8667	0.29	0.025	3.74	16.0	3	5.0	32.2	4	10.3	0.14	0.40	1	-
LCS-CL J055034-5012.8	87.6426	−50.2149	0.60	0.036	3.96	16.0	2	1.7	–	–	–	0.18	0.06	–	-
LCS-CL J055043-5019.5	87.6812	−50.3257	0.63	0.036	3.53	11.2	2	1.6	–	–	–	0.19	0.13	–	-
LCS-CL J055104-5223.4	87.7702	−52.3913	0.73	0.040	3.80	18.6	3	0.9	–	–	–	0.00	0.01	–	-
LCS-CL J055129-5557.8	87.8746	−55.9640	0.49	0.034	3.31	10.9	2	1.0	14.7	3	1.4	0.00	0.08	–	-
LCS-CL J055146-5217.1	87.9446	−52.2853	0.70	0.038	3.63	19.3	3	0.7	–	–	–	0.00	0.06	–	-
LCS-CL J055147-5531.5	87.9496	−55.5260	0.49	0.033	4.60	12.0	2	0.8	16.8	3	1.3	0.04	0.08	–	-
LCS-CL J055227-5617.9	88.1136	−56.2999	0.40	0.039	3.44	17.4	3	4.3	19.3	3	5.0	0.00	0.21	1	-
LCS-CL J055412-5552.8	88.5529	−55.8805	0.44	0.032	3.56	13.3	2	2.8	21.8	3	5.1	0.00	0.14	–	-

NOTE. — The same as Table 5, except for clusters selected in the 5 h field.